

Adaptive Droop Control Based Power Flow Regulation and Optimization in Multi-terminal High Voltage DC System

by

Yuanshi Zhang

M.A.Sc., The University of Harbin Institute of Technology, 2015

A THESIS SUBMITTED IN PARTIAL FULFILLMENT OF
THE REQUIREMENTS FOR THE DEGREE OF

DOCTOR OF PHILOSOPHY

in

The College of Graduate Studies

(Electrical Engineering)

THE UNIVERSITY OF BRITISH COLUMBIA
(Okanagan)

April 2021

© Yuanshi Zhang, 2021

The following individuals certify that they have read, and recommend to the College of Graduate Studies for acceptance, a thesis/dissertation entitled:

Adaptive Droop Control Based Power Flow Regulation and Optimization in Multi-terminal High Voltage DC System

submitted by Yuanshi Zhang in partial fulfillment of the requirements of

the degree of Doctor of Philosophy

Liwei Wang

Supervisor

Morad Abdelaziz

Supervisory Committee Member

Wilson Eberle

Supervisory Committee Member

Mahmudur Fatmi

University Examiner

Xiao-Ping Zhang

External Examiner

Abstract

Minimization of the total transmission loss of an interconnected AC-DC grid plays an important role in the economic operation of the AC-DC grid. Different from the conventional AC grid where the transmission loss is usually minimized by reactive power regulation, the transmission loss of a meshed AC-DC grid can be optimized by adjusting the active power exchange between the AC and DC grids. Additionally, smaller DC voltage deviation after grid disturbances is very desirable since it can bring less impact to the operations of AC-DC grid. This thesis firstly presents two improved sequential power flow algorithms for modular multilevel converters (MMCs) based AC-DC grid under DC power-voltage droop control. An optimization algorithm is then proposed to minimize the total loss of the AC-DC grid and the overall DC voltage deviation after the change of operating conditions. Adaptive droop control is used in the proposed optimization algorithm in which the power references are control variables solved from the optimal AC-DC power flow.

Active power sharing and voltage regulation are two of the major control challenges in the operation of the voltage source converter based multi-terminal high-voltage DC (VSC-MTDC) system. Conventional droop control methods for power-sharing in an MTDC grid lead to voltage deviation from the nominal value. Moreover, the power-sharing is inaccurate in the droop-controlled MTDC system. This thesis proposes two novel autonomous control methods to regulate average DC voltage and share the power burden proportionally, using the adaptive droop control strategy. The proposed Method I utilizes DC grid lossy model with the local voltage droop control (LVDC) strategy, while the proposed Method II adopts a modified common voltage droop control (MCVDC) based on DC grid lossless model.

The regulation of active power flowing through one or multiple DC lines plays an important role to guarantee secure and economic operations of MTDC grids. This thesis proposes a new method to regulate DC line power flow based on the adaptive DC voltage droop control strategy in which the voltage references of the voltage droop controllers vary autonomously at post-contingencies. The main advantage of the proposed method is that it can avoid installation of extra equipment and thus the associated losses and costs in the power-converter-based power flow control methods. The proposed control approach does not require solving online global AC-DC power flow equations, leading to autonomous control.

Lay Summary

MTDC network is a promising technology to integrate large-scale renewable energy sources into conventional AC grid. An MTDC grid, enabled by the voltage source converter VSC technology, provides numerous advantages over the traditional point-to-point high voltage direct current HVDC systems. In order to determine the steady-state operating points and to plan future expansion of an AC-MTDC grid, the power flow of the AC-MTDC grid is required to be solved accurately and efficiently. One of the ultimate aims of this thesis is to develop an improved sequential power flow method that is more accurate and efficient than the existing methods. At the same time, the proposed improved power flow method can also realize some optimization targets, so as to guarantee safe and economic operation of the AC-MTDC system. On the other hand, active power sharing and voltage regulation are two of the major control challenges in the operation of the voltage source converter based multi-terminal high-voltage DC (VSC-MTDC) system. The existing control methods to control DC voltage and power sharing need tradeoff between the two control targets and heavily rely on communication system. Thus, the other ultimate goal of this thesis is to propose an autonomous control strategy to realize average DC voltage regulation and power sharing without any tradeoff.

Preface

Most of the chapters presented in this thesis have been or will be published in scientific journals or conference publications. I have derived the formulas, developed simulation models, performed case studies, analyzed results, and prepared the first draft. My supervisor has provided guidance on my research works and revised my publications. Other co-authors have assisted me to prepare simulation models and experimental results. The chapters presented in this thesis are based on the research works conducted throughout my doctorate program as listed below.

Chapter 1 presents the basic introduction and background of my research topics.

Chapter 2:

- **Yuanshi Zhang**, Xuekun Meng, Amin Shotorbani, and Liwei Wang, “Minimization of AC-DC Grid Transmission Loss and DC Voltage Deviation Using Adaptive Droop Control and Improved AC-DC Power Flow Algorithm”, published in *IEEE Transactions on Power Systems*, vol. 36, no. 1, pp. 744-756, Jan. 2021.

Chapter 3:

- **Yuanshi Zhang**, Liwei Wang, and Wei Li, “Autonomous DC Line Power Flow Regulation Using Adaptive Droop Control in HVDC Grid,” published in *IEEE Transactions on Power Delivery*, doi: 10.1109/TPWRD.2020.3044978.

Chapter 4:

- **Yuanshi Zhang**, Liwei Wang and Wei Li, “Autonomous Controls of Average Voltage and Converter Power Sharing in MTDC Grid”, submitted to *IEEE Transactions on Power System*.
- **Yuanshi Zhang**, Amin Shotorbani, Liwei Wang, and Wei Li, “Distributed Voltage Regulation and Automatic Power Sharing in Multi-Terminal HVDC Grids”, published in *IEEE Transactions on Power Systems*, vol. 35, no. 5, 2020.
- **Yuanshi Zhang**, Amin M. Shotorbani, Liwei Wang and Wei Li, “A Combined Hierarchical and Autonomous DC Grid Control for Proportional Power Sharing with Minimized Voltage Variation and Transmission Loss”, submitted to *IEEE Transactions on Power Delivery*.

Table of Contents

Abstract	iii
Lay Summary	iv
Preface	v
Table of Contents	vi
List of Tables	x
List of Figures	xi
Acknowledgements	xiii
Dedication	xiv
1 Introduction	1
1.1 Motivation	1
1.2 Literature Review	2
1.2.1 Minimization of AC-DC Grid Transmission Loss and DC Voltage Deviation Using Adaptive Droop Control	2
1.2.2 DC Voltage Control and Power Sharing of the MTDC system.....	3
1.2.3 DC Line Power Flow Control.....	5
1.3 Research Objectives and Anticipated Impact.....	6
2 Minimization of AC-DC Grid Transmission Loss and DC Voltage Deviation Using Adaptive Droop Control and Improved AC-DC Power Flow Algorithm	8
2.1 Preliminary Methods	10
2.1.1 Method I.....	10
2.1.2 Method II	12
2.2 Proposed Sequential AC-DC Power Flow	13
2.2.1 Method III	14
2.2.1.1 Elimination of SBI/DBI.....	14
2.2.1.2 DC Grid Pre-calculation	14
2.2.1.3 Convergence Condition.....	16
2.2.2 Method IV.....	16
2.3 Minimization of Total AC-DC Grid Transmission Loss and DC Voltage Variation	17
2.3.1 Hierarchical Control Scheme	17

2.3.2	Minimization of Total Loss of AC-DC Grid	18
2.3.3	Minimization of DC Voltage Deviation	21
2.3.4	Linear Scalarization	21
2.3.5	Degree of Freedom	22
2.4	Case Studies	22
2.4.1	Case A: Static Power Flow Results	24
2.4.1.1	Base Case.....	24
2.4.1.2	Droop Control Mode	25
2.4.2	Case B: Power Flow Results after the Contingencies.....	26
2.4.2.1	Power Variation.....	26
2.4.2.2	Converter Outage.....	26
2.4.3	Case C: Minimization of AC-DC Grid Total Loss	28
2.4.4	Case D: Minimization of DC Voltage Variation	28
2.4.5	Case E: Minimization of DC Voltage Variation and AC-DC Grid Transmission Loss	29
2.4.6	Case F: Dynamic Simulation	29
2.4.6.1	Minimization of MTDC System Loss	31
2.4.6.2	Minimization of DC Voltage Variation.....	32
2.4.6.3	Minimization of MTDC System Loss and Voltage Variation.....	32
2.5	Summary	33
3	Autonomous DC Line Power Flow Regulation Using Adaptive Droop Control in HVDC Grid.....	35
3.1	Analytical Modeling of VSC-HVDC Grid.....	35
3.2	Autonomous DC Line Power Flow Regulation	37
3.2.1	Linearized Model of VSC-HVDC Grid in Voltage Droop Control.....	37
3.2.2	Power Reference Variations under Various Contingencies.....	38
3.2.3	DC Line Power Flow Regulation Algorithm	39
3.2.3.1	One DC Line Power Regulation.....	40
3.2.3.2	One DC Line Power Regulation.....	40
3.2.3.3	One DC Line Power Regulation.....	41
3.2.4	DC Line Power Flow Regulation Algorithm.....	41
3.2.5	Discussion.....	42

3.3	Case Studies	44
3.3.1	Static Simulation Results	46
3.3.2	Single DC Line Power Regulation under Variation of Offshore Wind Farm Generation	48
3.3.3	Multiple DC Line Power Regulation under Converter Outage	49
3.3.4	Multiple DC Line Power Regulation under Converter Outage	51
3.3.5	Disconnection of One DC Line.....	52
3.4	Summary	53
4	Converter Power Sharing and Average Voltage Regulation in MTDC System	55
4.1	Autonomous Controls of Average Voltage and Converter Power Sharing in MTDC Grid 55	
4.1.1	Steady-State Operation of MTDC System.....	55
4.1.2	Autonomous Controls of Average Voltage Regulation and Proportional Power Sharing 57	
4.1.2.1	Proposed Method I.....	57
4.1.2.2	Proposed Method II	61
4.1.2.3	Control Scheme Diagram	63
4.1.2.4	Discussion.....	64
4.1.3	Case Studies	66
4.1.3.1	System Configuration	66
4.1.3.2	Case A : Variation of OWF Generation	68
4.1.3.3	Case B: GSVSC Outage	70
4.1.3.4	Case C: $N - 2$ Contingency	71
4.1.4	Summary	72
4.2	A Combined Hierarchical and Autonomous DC Grid Control for Proportional Power Sharing	73
4.2.1	Autonomous Power-Sharing Control in MTDC.....	74
4.2.1.1	Open-Loop Autonomous Power Sharing Control	74
4.2.1.2	Feedback-Control-Based Autonomous Power Sharing.....	78
4.2.2	Autonomous Power-Sharing Control in MTDC.....	79
4.2.2.1	Hierarchical Control Framework.....	79
4.2.2.2	Optimization Targets	79
4.2.3	Case Studies	82

4.2.3.1	Autonomous Power Sharing Control.....	82
4.2.3.2	Hierarchical Power Sharing Control with Minimized Voltage Variation and Transmission Loss	84
4.2.1	Summary	85
5	Concluding Chapter	87
5.1	Conclusion.....	87
5.2	Future Work	89
	Bibliography	91

List of Tables

Table 2.1 MTDC Grid Parameter For Base Case (in P.U.)	23
Table 2.2 DC Transmission Line Parameter For Base Case (in P.U.).....	24
Table 2.3 Converter Loss Coefficients (in P.U.)	24
Table 2.4 Calculation Results of Base Case (in P.U.)	24
Table 2.5 Power Reference of the Droop Controlled MMCs (in P.U.)	25
Table 2.6 Calculation Results for MTDC Grid under Droop Control (in P.U.)	25
Table 2.7 Calculation Results after Power Variation (in P.U.).....	26
Table 2.8 Calculation Results after Converter Outage (in P.U.)	27
Table 2.9 Comparison of Power Flow Accuracy	27
Table 2.10 Comparison of Computational Times.....	28
Table 2.11 DC Line Parameters.....	30
Table 2.12 Parameters of MMC Stations.....	30
Table 2.13 Optimal Results of Different Scenarios	32
Table 3.1 DC Transmission Line length.....	45
Table 3.2 DC Line Data [35]	45
Table 3.3 VSC Parameters.....	45
Table 3.4 DC Power Flow Solution.....	46
Table 3.5 DC Line Powers of two Scenarios.....	48
Table 3.6 DC Line Current and Power Limits.....	52
Table 4.1 DC Cable Length	67
Table 4.2 DC Cable Parameter	67
Table 4.3 VSC Station Parameter	67
Table 4.4 Converter Loss Coefficients (in P.U.) [33].....	68
Table 4.5 Comparison of Methods I and II under Power Variation	70
Table 4.6 Comparison of Methods I and II under Converter Outage	71
Table 4.7 Comparison of Methods I and II under N-2 Contingency	72
Table 4.8 Proportional Power Sharing Results of Autonomous Controls	84

List of Figures

Figure 2-1	Flow chart of the sequential AC-DC power flow [12], [14].	12
Figure 2-2	Flow chart of the AC-DC power flow [13].	13
Figure 2-3	Flow chart of the Method III.	15
Figure 2-4	Flow chart of the Method IV.	17
Figure 2-5	The hierarchical control structure.	18
Figure 2-6	Configuration of MTDC network with MMC stations.	23
Figure 2-7	Comparison of total losses with and without optimization algorithm.	28
Figure 2-8	Comparison of DC voltage variations with and without optimization algorithm.	29
Figure 2-9	Five-terminal MTDC system.	30
Figure 2-10	DC powers and DC grid loss.	31
Figure 2-11	DC voltages and voltage variation.	32
Figure 2-12	The relationships of MTDC system loss and DC voltage variation with respect to w	33
Figure 3-1	Four-terminal HVDC grid with dummy DC generators.	39
Figure 3-2	Hierarchical diagram of autonomous DC line power regulation.	42
Figure 3-3	Five-terminal HVDC grid.	46
Figure 3-4	DC line power flow results with and without the proposed line flow regulation method.	47
Figure 3-5	DC line powers under VSC-3 power variation.	49
Figure 3-6	DC powers and voltages of VSCs under VSC-3 power variation.	49
Figure 3-7	DC line powers under converter outage.	50
Figure 3-8	DC powers and voltages of VSCs under converter outage.	50
Figure 3-9	DC line powers under power increase of VSC-5.	51
Figure 3-10	DC powers and voltages under power increase of VSC-5.	52
Figure 3-11	DC line powers under disconnection of line 3-4.	53
Figure 3-12	DC powers and voltages under disconnection of line 3-4.	53
Figure 4-1	Control scheme diagram of the proposed autonomous control strategy.	64
Figure 4-2	Single line diagram of the test system.	66

Figure 4-3 DC powers, voltages and average voltage of VSCs when VSC-5 power increases under the proposed Method I.	69
Figure 4-4 DC powers, voltages and average voltage of VSCs when VSC-5 power increases under the proposed Method II.	69
Figure 4-5 DC powers, voltages and average voltage of VSCs when VSC-2 is forced outage under the proposed Method II.	70
Figure 4-6 DC powers, voltages and average voltage of VSCs following N-2 contingency under the proposed Method II.	72
Figure 4-7 Combined control framework for an MTDC system.	73
Figure 4-8 Autonomous control framework.	79
Figure 4-9 Five-terminal MTDC system.	82
Figure 4-10 DC power of the droop-controlled VSCs under outage of VSC-2.....	83
Figure 4-11 DC voltage of VSCs under outage of VSC-2.....	84
Figure 4-12 Relationships of DC-grid loss and DC voltage variation with w	85

Acknowledgements

Many thanks to my supervisor, Dr. Liwei Wang, for providing valuable guidance and great help throughout my doctoral program. I really appreciate for the valuable comments and constructive suggestions from the external examiner Dr. Xiao-ping Zhang and my committee members Dr. Morad Abdelaziz and Dr. Wilson Eberle. I would also like to thank Amin M. Shotorbani, William Han, Xuekun Meng, and Henry Li for the support and help in my everyday life. Particular thanks are attributed to my parents, who have supported me throughout my years of growing up, both morally and financially.

Dedication

To my parents

1 Introduction

1.1 Motivation

Sustainable energy future calls for the development of large-scale onshore and offshore wind power generation. Offshore wind farms are growing rapidly due to the advantages of less wind variation and space restriction. Generally, offshore wind farms are located far away from the main AC grid. High voltage multi-terminal DC (MTDC) network, also known as DC grid, is a promising technology to integrate large-scale renewable energy sources especially offshore wind farms into conventional AC grid. A DC grid, enabled by the voltage source converter (VSC) technology, provides numerous advantages over the traditional point-to-point high voltage direct current (HVDC) systems such as improved efficiency, increased reliability, and reduced number of converter stations [1]–[3]. In addition, newer power converter technology, i.e., modular multilevel converters (MMCs) have been replacing the conventional two- or three-level converter technologies for HVDC applications due to their distinguished merits in terms of performance, scalability and controllability [4]–[6].

The use of an MTDC grid brings challenges for converter control strategies. The traditional master-slave control for the converter stations has one DC slack bus to regulate the DC grid voltage which is vulnerable to DC-grid faults. The stability of the DC grid can be greatly improved by applying P-V or I-V droop control since several converters in a droop control mode can function as distributed DC slack buses [7]–[11]. However, conventional droop control methods for power-sharing in a multi-terminal high voltage DC (MTDC) grid lead to voltage deviation from the nominal value. Moreover, the power-sharing is inaccurate in the droop-controlled MTDC system. Thus, it is essential to guarantee desirable power sharing and regulate the DC voltage profile following unscheduled contingencies.

In order to determine the steady-state operating points and to plan future expansion of an AC-MTDC grid, the power flow of the AC-MTDC grid is required to be solved accurately. There are mainly two types of power flow algorithm for AC-MTDC grid, i.e., the sequential [12]–[14] and the unified power flow methods [15]–[17]. The advantage of the sequential power flow approach is that it is convenient to incorporate the DC power flow algorithm into an existing AC power flow software package such as PSS/E. In [18] and [19], the power flow algorithms for islanded

microgrids are proposed. The sequential power flow algorithms were proposed for AC-MTDC grid with master slave control in [12] and power voltage droop control schemes in [13] and [14]. However, the sequential power flow methods in [12] and [14] involve an additional iteration step, the so-called DC slack bus or droop bus iteration (SBI/DBI), which increases computational burden. In [13], DC grid power flow is only implemented once at the beginning of AC-DC power flow algorithm and is not incorporated in the overall iteration loop, leading to slightly inaccurate power flow results. Thereby, one of the ultimate aims of this thesis is to develop an improved sequential power flow method that is more accurate and efficient than the existing methods.

1.2 Literature Review

1.2.1 Minimization of AC-DC Grid Transmission Loss and DC Voltage Deviation Using Adaptive Droop Control

For an interconnected AC-DC grid, it is important to reduce the grid transmission loss and the operational costs. The transmission loss of the AC-DC grid is different from that of the conventional AC system in which the transmission loss is usually optimized by managing the reactive power distribution. For an AC-DC grid, the total transmission loss can be minimized by adjusting the active power exchange through the VSC converters of the AC-DC grid. In [18] and [19], the DC grid transmission loss is minimized, as the objective function of the optimal power flow employing Karush–Kuhn–Tucker (KKT) condition. In [20], an evolutionary strategy called covariance matrix adaptation (CMA) is applied to solve the optimal DC power flow and give the DC voltage droop control strategy the necessary voltage references. However, the AC network transmission loss and the converter loss are not considered in [18]–[20]. The nonlinearity of the optimal power flow (OPF) model for AC-MTDC system is handled by adopting interior point methods [21] and semidefinite programming relaxation methods [22]. In [23], the multi-objective optimal operation of AC-MTDC grid is formulated as a corrective security-constrained optimal power flow problem and is solved using the non-dominated sorting genetic algorithm. In [24] and [25], two open-source OPF software for hybrid AC/DC systems are proposed, focusing on point-to-point, radial and meshed MTDC networks respectively. In [26], two distributed approaches on the decomposition of a hybrid AC–DC grid are proposed. In [27], an iterative solution algorithm is proposed for the optimal AC–DC power flow with discrete control devices. As the control mode

for MTDC systems in [21]–[27] is the traditional master-slave (P-V) control, the optimal power flow for AC-MTDC grids is realized by adjusting the active and reactive powers of the generators as well as transformer tapping.

DC power voltage droop control is used for the DC grid which can enhance the reliability of the DC grid since multiple VSCs simultaneously contribute to DC voltage regulation. Moreover, adaptive droop control scheme shows superior maneuverability and flexibility compared to the master-slave control. The optimal AC-DC power flow is realized by the adaptive droop control scheme where only the power references are the control variables. In this approach, the transmission loss of the AC-DC grid can be optimized by adjusting the active power exchange between the AC and DC grids. In addition, the proposed adaptive droop control method is different from the conventional adaptive droop control method in [28] and [29], where the droop slopes/coefficients are adjusted to realize desirable power sharing. It is noted that adapting the droop slopes/coefficients may influence the stability of the MTDC system. On the other hand, the proposed adaptive droop control method only updates the active power references of the droop controlled converters. Therefore, the adaptive droop control method can realize the optimization targets without the negative impact on the stability of the AC-DC grid.

In case of the changing system operating conditions in the DC grid, such as converter outage or DC active power fluctuation, smaller DC voltage variation can bring less impact to the operations of the AC-DC grid. In [30] and [31], an optimization algorithm is developed taking DC voltage deviation and desirable power sharing into consideration. In [32], a two-stage solution approach for solving the problem of multi-objective optimal power flow is proposed for AC-MTDC systems coordinating the economy, voltage deviation and environmental benefits. However, the transmission loss of the AC-MTDC system is not taking into account in [30]–[32]. Additionally, it will be desirable to consider the two optimization objectives, i.e., the minimized AC-DC grid total transmission loss and the DC voltage variation simultaneously.

1.2.2 DC Voltage Control and Power Sharing of the MTDC system

In the MTDC grid, the VSC stations use one of the three main control schemes: constant power mode, constant DC voltage mode, and the droop control mode. In the constant DC voltage control mode, when a converter outage occurs in the voltage control station (i.e. the DC slack bus), the stability of the MTDC grid is deteriorated significantly [8]. In this case, the droop control scheme

seems more reliable than the constant DC voltage control mode since the droop-controlled buses share the function of the DC slack bus, greatly alleviating the impact of converter outage [8], [33].

The droop control mode is also employed to share the power demand among the stations, by modifying the output DC voltage with respect to the output DC current or power of the station. In order to eliminate the circulating currents and share the power demand, variants of droop control [28], [34], [35] and the virtual output impedance scheme [36] were proposed.

The use of only local voltage in the feedback loop cannot yield a unique solution for power flow of the MTDC grid [28]. To tackle the challenge, a common signal feedback scheme was introduced by communicating a common voltage to entire stations. The average DC voltage is usually employed as the common feedback signal for MTDC grid. In [31], a common voltage feedback signal is used to remove the voltage dependence of the power sharing after an outage. In [35], a pilot voltage droop was introduced and the methodology for designing the droop gains was proposed. In [28], an adaptive droop gain was used to avoid post-contingency saturation of the VSCs by sharing the power mismatch based on the available headroom of a converter.

However, all variants of droop controls result in the deviation of the voltage from the nominal value in the steady state. Although a smaller droop gain yields less deviation, the stability of MTDC grid may deteriorate [31], [37]. In this regard, an important research objective is to mitigate the DC voltage deviation [37]. For the MTDC grid integrating the offshore wind farms with relatively high power rating and long transmission distance, the DC voltages of the stations may be significantly different from each other [14], [34]. Establishing a stable DC voltage controller is critically important for balancing the power exchange among the converter stations. A large voltage deviation in a droop-controlled MTDC grid can also have an undesirable impact on the voltage controller of the AC-side system [38].

On the other hand, the system operators need to regulate the average voltage of the DC buses, especially for an MTDC grid with large power flow and long transmission distance [13], [39]. When the droop control strategy is adopted, it is important to maintain the average DC voltage of the VSC stations constant [17]. In analogy to frequency in the AC system, the DC average voltage acts as the common feedback of the DC system and represents the overall DC voltage level [28], [39]. Controlling the DC average voltage to the reference value can effectively avoid the DC voltages approaching their limits, which can improve the operating condition especially after the

contingencies. If the voltages exceed their upper limit after transients, it may activate protective equipment, e.g., dump resistors. Similarly, large voltage drop may generate challenges for the control systems and restrict the capability of voltage controller of the AC system [37]. Therefore, in a droop-controlled MTDC grid, voltage deviations from the reference value should be mitigated while the average voltage needs to be regulated.

Another challenge operating the MTDC grid is to automatically share the power demands among the converter stations after transients, in order to minimize the influence on the adjoining AC system. In [31], the droop coefficients are adapted to achieve proportional power sharing after converter outage. However, the average DC voltage is not regulated in [28] and [31]. Moreover, varying the droop coefficients may influence small signal stability of the system [40], [41].

The secondary controller can have either a centralized or a distributed architecture. In a centralized controller, the failure of the communication network or the control center can reduce the reliability of the MTDC grid and may cause instability [42]–[44]. In contrast, a distributed controller eliminates the dependency of the MTDC grid on the control center.

1.2.3 DC Line Power Flow Control

The DC line power flow control is identified as an active research area [45]–[56]. The state-of-the-art DC line power flow control approaches are based on power converter hardware equipment. Three types of DC line power flow control devices have been proposed, i.e. the variable series resistors [45], [47], the DC-DC converters [46], [48]–[50] and the series voltage sources [51]–[56]. In the first method, series variable resistors are inserted in an HVDC grid to change the resistances of the DC lines directly. The main disadvantage of this method is the high power losses due to the inserted resistors [45]. In the second method, a DC-DC converter is utilized to change the DC voltage at one end of a DC line. However, a DC-DC converter needs to withstand the high DC voltage rating, resulting in high capital cost [46], [48]. In the last method, an equivalent voltage source with several different topologies is inserted into a DC line. This method has less power loss and lower voltage rating compared to the other two methods [45], [51]–[56]. However, it still needs additional power electronic devices installed in the HVDC grid, which causes extra costs and power losses.

In this thesis, a new DC line power flow control method is proposed based on analytical models [34], [57] of an HVDC grid, from which the DC line voltage difference is derived for the configuration of the voltage references in the adaptive droop controls [28], [58]. In [34], an analytical expression for accurate estimation of power distribution in an HVDC grid is proposed. It can evaluate the impact of DC line voltage drops on the power distribution of MTDC grids after contingencies. In [57], an analytical model is proposed to estimate the DC voltage variations, power distributions, and power losses under converter outage and overloading conditions based on the bisection algorithm and superposition principle. However, the analytical models in [34] and [57] didn't discuss the scenario of HVDC grid topology change, i.e., disconnecting or adding DC lines. This thesis proposes an improved analytical model to estimate the system performance involving grid topology change. Adaptive droop control methods are widely used for power-sharing control [28], [59], [60], limiting DC voltage deviation [61], and minimizing system transmission loss in the HVDC grid [19]. However, the adaptive droop control methods were not applied to DC line power flow regulation applications.

1.3 Research Objectives and Anticipated Impact

Based on the motivation represented in Subsection 1.1, the objectives of the thesis are discussed as the following.

Objective 1: Propose improved sequential power flow algorithms for modular multilevel converters (MMCs) based AC-MTDC grid under DC power-voltage droop control. An optimization algorithm is then developed to minimize the total loss of the AC-DC grid and the overall DC voltage deviation after the change of operating conditions.

Objective 2: Propose a new method to regulate DC line power flow based on the adaptive DC voltage droop control strategy in which the voltage references of the voltage droop controllers vary autonomously at post-contingencies. The main advantage of the proposed method is that it can avoid installation of extra equipment and thus the associated losses and costs in the power-converter-based power flow control methods.

Objective 3: Propose novel autonomous control methods to regulate average DC voltage and share the power burden proportionally, using the adaptive droop control strategy.

In the Objective 1, the improved power flow algorithms for the AC-MTDC system are developed. To improve the calculation efficiency and to realize autonomous control without communication, a linearized model for the MTDC system is developed from the power flow algorithms. Then, the Objective 2 adopts the linearized model to regulate the DC line power flow of the MTDC system. Lastly, the Objective 3 uses the power flow algorithms studied in Objective 1 and the linearized model proposed in Objective 2 to realize hierarchical control and autonomous control respectively for power sharing and DC voltage regulation of the MTDC system.

To sum up, the first goal of this thesis is to develop an improved sequential power flow method that is more accurate and efficient than the existing methods. At the same time, the proposed improved power flow method can also realize some optimization targets, such as minimization of transmission loss and DC voltage deviation. The second goal of this thesis is to develop an autonomous line flow control method without using of additional power electronics devices. The last goal of this thesis is to propose an autonomous control strategy to realize average DC voltage regulation and power sharing simultaneously.

2 Minimization of AC-DC Grid Transmission Loss and DC Voltage Deviation Using Adaptive Droop Control and Improved AC-DC Power Flow Algorithm

Nomenclature

Abbreviations

MTDC	Multi-terminal high-voltage DC
VSC	Voltage-source converter
HVDC	High voltage direct current
MMCs	Modular multilevel converters
SBI	Slack bus iteration
DBI	Droop bus iteration
KKT	Karush–Kuhn–Tucker
CMA	Covariance matrix adaptation
OPF	Optimal power flow
PCCs	Points of the common coupling

Variables, Parameters, Functions and Vectors

$P_{dc,i}/P_{c,i}$	DC/converter power
$P_{loss,i}/P_{comp,i}$	Converter/Complex equivalent impedance loss
$P_{s,i} + jQ_{s,i}$	Complex power injection at PCC bus
$U_{s,i} \angle \delta_{s,i} / U_{c,i} \angle \delta_{c,i}$	AC-/converter-bus voltage
$P_{dc,i} / P_i^*$	Actual/ reference DC power
$V_{dc,i} / V_{dc,i}^*$	Actual/reference DC voltage
k_i	Droop coefficient
G_{ij}	Conductance between terminals i and j
$I_{c,i} / I_{dc,i}$	Converter/DC current

$a/b_{ac,i}/c_{ac,i}/b_{dc,i}/c_{dc,i}$	Coefficients of converter loss formula
i_d/i_q	Actual d/q axis current of inner current controller
i_d^*/i_q^*	Reference d/q axis current of inner current controller
L	Total loss of AC-DC grid
A/D	AC/DC grid's transmission loss
$\mathbf{f}_1, \mathbf{f}_2, \mathbf{f}_3$	Equality constraints of optimal AC-DC power flow
\mathbf{g}	Inequality constraints of optimal AC-DC power flow
F	Lagrange function
λ	Lagrange multiplier
w	Weighting factor

This chapter presents improved sequential power flow methods¹ to minimize transmission loss and DC voltage deviation based on adaptive droop control method. The total transmission loss includes the AC grid transmission line loss and DC grid transmission line/cable loss.

Minimization of the total transmission loss of an interconnected AC-DC grid plays an important role for the economic operation of the AC-DC grid. Different from the conventional AC grid where the transmission loss is usually minimized by reactive power regulation, the transmission loss of a meshed AC-DC grid can be optimized by adjusting the active power exchange between the AC and DC grids. Additionally, smaller DC voltage deviation after grid disturbances is very desirable since it can bring less impact to the operations of AC-DC grid. This section firstly presents two improved sequential power flow algorithms for modular multilevel converters (MMCs) based AC-DC grid under DC power-voltage droop control. An optimization algorithm is then proposed to minimize the total loss of the AC-DC grid and the overall DC voltage deviation after the change of operating conditions. Adaptive droop control is used in the proposed optimization algorithm in

¹ **Yuanshi Zhang**, Xuekun Meng, Amin Shotorbani, and Liwei Wang, "Minimization of AC-DC Grid Transmission Loss and DC Voltage Deviation Using Adaptive Droop Control and Improved AC-DC Power Flow Algorithm", published in *IEEE Transactions on Power Systems*, vol. 36, no. 1, pp. 744-756, Jan. 2021.

which the power references are control variables solved from the optimal AC-DC power flow. The proposed algorithm is verified in an AC-DC grid consisting of a six-terminal DC grid connected to the IEEE 39-bus AC grid and a classical five-terminal AC-MTDC system.

2.1 Preliminary Methods

In this subsection, two types of conventional sequential power flow algorithms are introduced as preliminary methods.

2.1.1 Method I

The sequential AC-DC power flow methods for master-slave control [12] and DC voltage droop control [14] are briefly introduced, as shown in Figure 2-1. In this algorithm, AC and DC power flows are implemented iteratively. Firstly, the initial active power injection to the AC grid at PCCs of DC slack bus or droop buses is estimated. For DC slack bus, its power injection is estimated to be the negative summation of the active power injections from other buses [12], while the estimation of power injection at PCC for DC droop buses is assumed to be the negative values of power reference [14]. The power reference is set according to the normal operating points. However, under unpredicted disturbances such as converter outage or wind power variation, the actual power of droop buses may deviate greatly from the power reference. Therefore, the overall iterations may increase due to the large deviation of initial power estimation for droop buses during contingencies.

The AC power flow, the converter power and losses, and the DC power flow are solved sequentially. After calculating the DC power flow, the converter power of the DC slack or droop buses can be calculated as

$$P_{c,i} = P_{dc,i} - P_{loss,i} \quad (2.1)$$

where $P_{dc,i}$, $P_{loss,i}$ and $P_{c,i}$ are DC power, converter loss and converter power respectively.

However, $P_{loss,i}$ in (2.1) is the function of the converter current, which is yet unknown. Therefore, an additional iteration loop, i.e., SBI or DBI, is required to calculate the $P_{c,i}$, as shown in Figure 2-2.

The active and reactive power injections of the converter at PCC and converter bus can be given by [12]

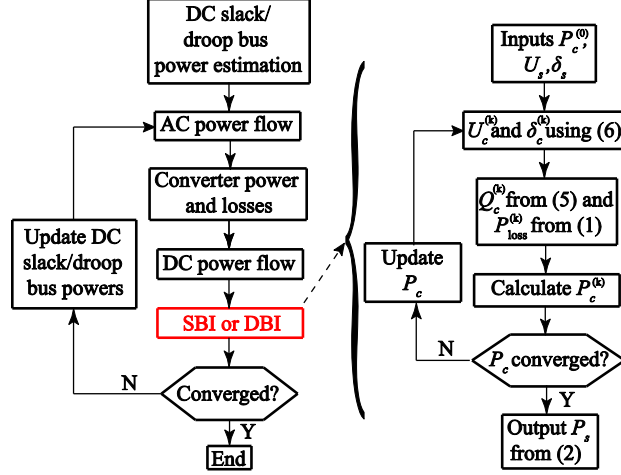


Figure 2-1 Flow chart of the sequential AC-DC power flow [12], [14].

2.1.2 Method II

The power flow algorithm proposed in [13] can effectively represent and solve the load flow problems of the AC-DC grid, as shown in Figure. 2-2, with different types of droop controls, i.e. V-P droop, V-I droop, and droop control with dead-band. But the power flow result is slightly inaccurate due to the use of converter DC-side power instead of AC-side active power at the PCC in the droop equation as

$$P_{dc,i} - P_i^* + k_i(V_{dc,i} - V_{dc,i}^*) = 0 \quad (2.7)$$

where $P_{dc,i}$ and P_i^* are actual DC power and power reference respectively; $V_{dc,i}$ and $V_{dc,i}^*$ are actual DC voltage and voltage reference respectively. For DC nodes in droop control mode, the droop coefficient k_i in (2.7) is positive while for active power controlled nodes, k_i equals zero. In [13], DC power flow is calculated first with the generalized DC power flow equation as

$$P_{dc,i} = V_{dc,i} \left(\sum_{j=1}^N G_{ij} V_{dc,j} \right) \quad (2.8)$$

where G_{ij} indicates the total conductance between terminals i and j . The DC grid power flow can be solved by combining (2.7) and (2.8). Then, AC grid power flow, converter loss calculation are implemented sequentially as shown in Figure 2-2. The convergence of the overall iteration loop is checked by the value of the active power injection at PCC.

In the accurate formula of droop control equation [28], $P_{dc,i}$ in (2.7) should be substituted by $P_{s,i}$. Then, the accurate form of generalized droop control equation is given by

$$P_{s,i} - P_i^* + k_i(V_{dc,i} - V_{dc,i}^*) = 0 \quad (2.9)$$

The relationship of $P_{s,i}$ and $P_{dc,i}$ can be given by

$$P_{s,i} = P_{dc,i} - P_{loss,i} - P_{comp,i} \quad (2.10)$$

where $P_{loss,i}$ and $P_{comp,i}$ are converter loss and complex equivalent impedance loss respectively.

It can be seen from (2.10) that, $P_{loss,i}$ and $P_{comp,i}$ are neglected in the DC power flow calculation in [13]. However, $P_{loss,i}$ and $P_{comp,i}$ accounts for a small proportion of $P_{s,i}$. Thereby, the computational results of Method II (especially DC grid power) are slightly inaccurate.

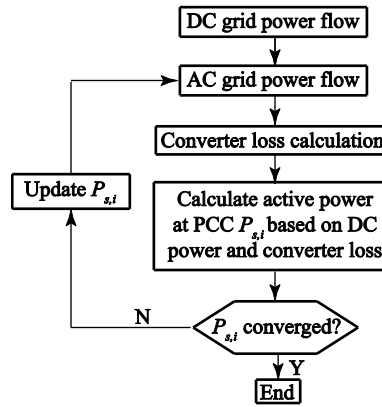


Figure 2-2 Flow chart of the AC-DC power flow [13].

2.2 Proposed Sequential AC-DC Power Flow

In this subsection, two improved AC/DC power flow algorithms are proposed, as shown in Figures 2-3 and 2-4 respectively. The proposed algorithms eliminate SBI/DBI iterations and reduce overall iteration numbers by using more accurate estimation power injection at PCC for DC droop buses compared to Method I. In addition, it is more accurate than Method II since $P_{loss,i}$ and $P_{comp,i}$ are included in the generalized droop control equation.

2.2.1 Method III

2.2.1.1 Elimination of SBI/DBI

In the proposed method (Method III) shown in Figure 2-3, the SBI/DBI iteration loop in Figure 2-1 is eliminated. According to power balance and neglecting the converter loss, the converter current $I_{c,i}$ can be calculated by DC current $I_{dc,i}$ as

$$I_{c,i} = I_{dc,i} \frac{2}{3m|\cos(\varphi)|} \quad (2.11)$$

where $\cos(\varphi)$ is the power factor; m is the RMS value of AC voltage modulation index.

The converter loss can be represented by a function of converter current as [12], [16]

$$P_{loss,i} = a + b_{ac,i} * I_{c,i} + c_{ac,i} * I_{c,i}^2 \quad (2.12)$$

where a , $b_{ac,i}$ and $c_{ac,i}$ are constant, linear, quadratic coefficients of $I_{c,i}$ for the i^{th} converter.

After calculating DC power flow in Figure 2-3, the DC current is known. From (2.11), it can be seen that, the converter current can be represented by the DC current. As converter loss is the function of the converter current in (2.12), it can also be calculated using DC current by substituting (2.11) into (2.12) as

$$P_{loss,i} = a + b_{dc,i} * I_{dc,i} + c_{dc,i} * I_{dc,i}^2 \quad (2.13)$$

where a , $b_{dc,i}$ and $c_{dc,i}$ are constant, linear, quadratic coefficients of $I_{dc,i}$. $b_{dc,i}$ and $c_{dc,i}$ can be derived from $b_{ac,i}$ and $c_{ac,i}$ respectively by combining (2.11)–(2.13).

Therefore, as the converter loss can be obtained from the known DC current by (2.13), the SBI/DBI step formulated as (2.6) can be eliminated.

2.2.1.2 DC Grid Pre-calculation

In the proposed Method III, the first step is called DC grid pre-calculation, which is further illustrated in Figure 2-3. This step is required because DC grid power flow is calculated by combining (2.8), (2.9) and (2.10), but $P_{loss,i}$ and $P_{comp,i}$ in (2.10) is yet unknown at the beginning and needed to be calculated. At the first overall iteration, the sum of $P_{loss,i}$ and $P_{comp,i}$ is estimated

to be 1.5% of $P_{dc,i}$ for the i^{th} converter. If the active power flows from DC grid to AC grid for DC bus i , $P_{s,i} = 0.985P_{dc,i}$; otherwise, $P_{s,i} = 1.015P_{dc,i}$. Thus, (2.9) can be rewritten as either (2.14) or (2.15), depending on the direction of active power injection

$$0.985P_{dc,i} - P_i^* + k_i(V_{dc,i} - V_{dc,i}^*) = 0 \quad (2.14)$$

$$1.015P_{dc,i} - P_i^* + k_i(V_{dc,i} - V_{dc,i}^*) = 0 \quad (2.15)$$

It is noted that the bold letters represent the phasor and the non-bold letters denote the magnitude of the phasor. When the overall iteration number is larger than one, $P_{loss,i}$ and $P_{comp,i}$ are pre-calculated from the result of AC and DC grid power flow from the last iteration. $P_{s,i}$, $Q_{s,i}$, and $U_{s,i}$ are known from the result of AC grid power flow. Then, the converter current $I_{c,i}$ can be calculated by

$$I_{c,i} = \frac{P_{s,i} - jQ_{s,i}}{U_{s,i}^*} \quad (2.16)$$

The complex equivalent impedance loss $P_{comp,i}$ is calculated by

$$P_{comp,i} = \text{real}(1/(G_{c,i} + jB_{c,i}))|I_{c,i}|^2 \quad (2.17)$$

Thus, $P_{comp,i}$ can be calculated by (2.16) and (2.17). $P_{loss,i}$ is obtained by (2.13); $I_{dc,i}$ in (2.13) can be obtained from the result of DC grid power flow.

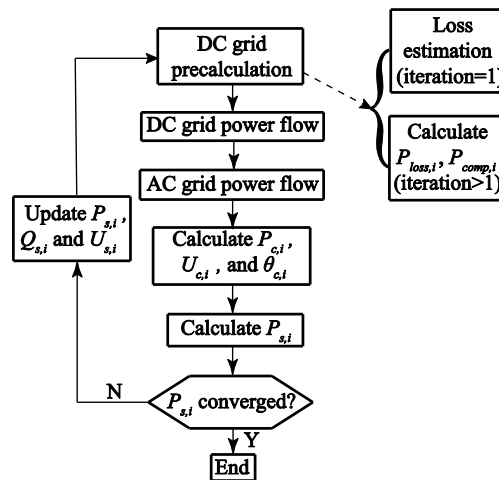


Figure 2-3 Flow chart of the Method III.

2.2.1.3 Convergence Condition

After calculating DC and AC grid power flow, the converter power $P_{c,i}$ is calculated by

$$P_{c,i} = P_{dc,i} - P_{loss,i} \quad (2.18)$$

$U_{c,i}$ is calculated by

$$U_{c,i} = U_{s,i} - I_{c,i}/(G_{c,i} + jB_{c,i}) \quad (2.19)$$

Finally, the new $P_{s,i}$ can be calculated by (2.2). The convergence of the overall iteration is checked by

$$\| [P_{s,i}^{new} - P_{s,i}^{old}]_m \|_{\infty} < \varepsilon \quad (2.20)$$

where $P_{s,i}^{new}$ and $P_{s,i}^{old}$ are the values of $P_{s,i}$ in new and the last iterations respectively; m is the number of DC buses connected to AC-grid; ε is the maximum allowable error.

2.2.2 Method IV

In this subsection, an improved AC-DC power flow algorithm, i.e., Method IV is proposed based on Method III as shown in Figure 2-4. The main difference between Methods III and IV is the approach to calculate $P_{s,i}$, which is used as the convergence condition of the overall iteration. In Method IV, $P_{s,i}$ in the third step is calculated from the results of the DC power flow ($I_{dc,i}$ and $P_{dc,i}$), using (2.10)–(2.13) and (2.17), while in Method III, $P_{s,i}$ is computed based on the results of AC grid power flow using (2.2). Therefore, AC power flow can be excluded from the overall iteration loop in Method IV. Thus, the computational efficiency is greatly enhanced with straightforward implementation in commercial power system simulation packages. It is noted that Method IV involves minor approximation because the power balance equation (2.11) is used to calculate $P_{s,i}$ for the convergence condition. However, this minor approximation produces negligible calculation error, compared to Method III, as will be shown in the case studies in Subsection 2.4. It is also noted that the calculation of the AC current in (2.11) requires the power factor, which is estimated in the first-round DC power flow iteration and is assumed to be constant for the subsequent AC-DC power flow calculation. Since the converter loss only accounts for around 1% of the total converter power, $P_{s,i}$, the deviation of power factor is very small and will lead to minor errors to the AC-DC power flow. Here, the estimation of the power factor is

described. As shown in Figure 2-4, the converter loss is estimated in the first step of Method IV. $P_{s,i}$ and $P_{c,i}$ are estimated after the DC power flow calculation in the second step in Figure 2-4. For the converter q-axis control in the outer control loop, either the AC-side reactive power $Q_{s,i}$ or the AC-side voltage $U_{s,i}$ is controlled. If $Q_{s,i}$ is controlled, we can easily calculate the power factor, $\cos(\varphi)$. On the other hand, if $U_{s,i}$ is controlled, $U_{c,i}$ and $(\delta_{s,i} - \delta_{c,i})$ can be solved by combining (2.2) and (2.4). Then, $I_{c,i}$ can be obtained by (19). Finally, the power factor can be calculated since $P_{s,i}$, $U_{s,i}$ and $I_{c,i}$ are all known.

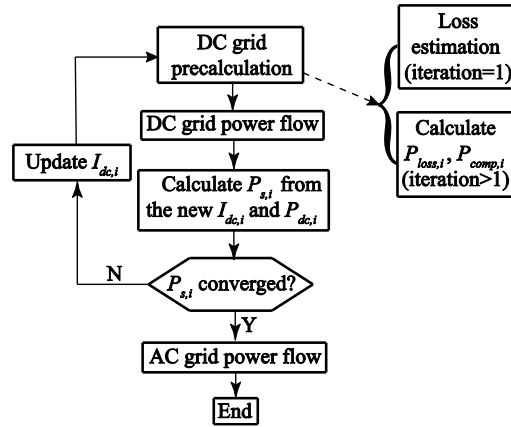


Figure 2-4 Flow chart of the Method IV.

2.3 Minimization of Total AC-DC Grid Transmission Loss and DC Voltage Variation

In this subsection, an optimization algorithm is proposed based on the proposed sequential power flow algorithms in Subsection 2.2. Two optimal targets are considered in the proposed optimization algorithm. The optimal targets are realized by using adaptive droop control strategy in which the active power references of the droop-controlled MMCs are adjusted adaptively.

2.3.1 Hierarchical Control Scheme

The overall hierarchical control structure is shown in Figure 2-5. In the secondary control layer, the steady state measurement and the contingency information are collected. After solving the AC-DC grid optimal power flow algorithm, the targeted state variables are known. Then, the power references \mathbf{P}^* of the MMCs in droop control mode are set to be adaptive based on the results of

optimal power flow. Thereafter, the adaptive power P^* are transmitted to the droop controlled MMCs in the primary layer via communication system.

In the primary control layer, the dq -axis current control is employed. Thus, we can control the P and Q of each MMC station independently. For d -axis, the control objectives can be either P (Switch 1 in Figure 2-5) or DC voltage droop (Switch 2 in Figure 2-5), while either Q (Switch 3 in Figure 2-5) or AC voltage magnitude (Switch 4 in Figure 2-5) is controlled for the q -axis. It is noted that only power reference P_i^* is adaptive and the droop coefficient k_i is kept constant to void any impact on the stability of the AC-DC grid.

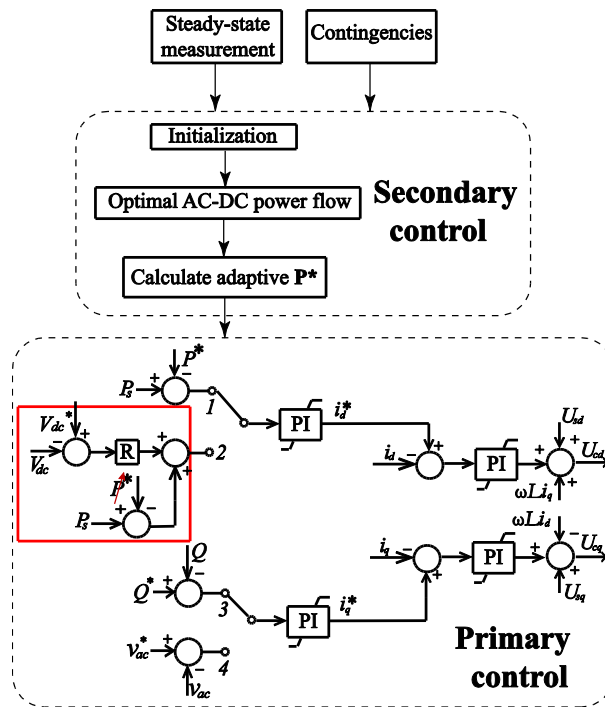


Figure 2-5 The hierarchical control structure.

2.3.2 Minimization of Total Loss of AC-DC Grid

Adjusting the active power transmitted to the AC grid from the droop controlled DC buses is an important measure to change the power flow distribution of the AC-DC grid. The mathematical model of the optimization problem to minimize the total loss of AC-DC grid is formulated as

$$\begin{cases} \min L(\boldsymbol{\delta}_s, \mathbf{U}_s, \mathbf{V}_{dc}) = A(\boldsymbol{\delta}_s, \mathbf{U}_s) + D(\mathbf{V}_{dc}) \\ s. t. \mathbf{f}_1(\boldsymbol{\delta}_s, \mathbf{U}_s, \mathbf{V}_{dc}) = \mathbf{P}_s(\mathbf{V}_{dc}) - \mathbf{P}_s(\boldsymbol{\delta}_s, \mathbf{U}_s) = \mathbf{0} \\ \mathbf{f}_2(\mathbf{V}_{dc}) = \mathbf{P}_s(\mathbf{V}_{dc}) - \mathbf{P}^* = \mathbf{0} \\ \mathbf{f}_3(\boldsymbol{\delta}_s, \mathbf{U}_s) = \mathbf{0} \\ \mathbf{g}(\boldsymbol{\delta}_s, \mathbf{U}_s, \mathbf{V}_{dc}) \leq \mathbf{0} \end{cases} \quad (2.21)$$

where $\boldsymbol{\delta}_s = (\delta_{s,1}, \delta_{s,2}, \dots, \delta_{s,N})^T$ and $\mathbf{U}_s = (U_{s,1}, U_{s,2}, \dots, U_{s,N})^T$ represent the AC node phase angle and voltage vectors respectively; $\mathbf{V}_{dc} = (V_{dc,1}, V_{dc,2}, \dots, V_{dc,n})^T$ is the DC voltage vector; $A(\boldsymbol{\delta}_s, \mathbf{U}_s)$ and $D(\mathbf{V}_{dc})$ are the transmission losses of the AC and DC grids respectively; $C(\mathbf{V}_{dc})$ stands for the converter loss and complex equivalent impedance loss; $L(\boldsymbol{\delta}_s, \mathbf{U}_s, \mathbf{V}_{dc})$ is the total loss of the interconnected AC-DC system; $\mathbf{f}_1(\boldsymbol{\delta}_s, \mathbf{U}_s, \mathbf{V}_{dc})$ is the function for the PCC nodes and imposes both DC power flow equation $\mathbf{P}_s(\mathbf{V}_{dc})$ and AC power flow equation $\mathbf{P}_s(\boldsymbol{\delta}_s, \mathbf{U}_s)$; $\mathbf{f}_2(\mathbf{V}_{dc})$ includes both DC nodes in active power control mode and DC nodes without connecting to AC grid; $\mathbf{f}_3(\boldsymbol{\delta}_s, \mathbf{U}_s)$ represents the function for AC nodes that are not connected to DC grid; $\mathbf{g}(\boldsymbol{\delta}_s, \mathbf{U}_s, \mathbf{V}_{dc})$ stands for all the inequality constraints including DC cable capacity constraints, convert limits and DC voltage limits.

The transmission losses of AC and DC grid are given by

$$A(\boldsymbol{\delta}_s, \mathbf{U}_s) = \sum_{i=1}^N U_{s,i} \sum_{j=i+1}^N U_{s,j} G_{ij} \cos(\delta_{s,i} - \delta_{s,j}) \quad (2.22)$$

$$A(\boldsymbol{\delta}_s, \mathbf{U}_s) = \sum_{i=1}^N U_{s,i} \sum_{j=i+1}^N U_{s,j} G_{ij} \cos(\delta_{s,i} - \delta_{s,j}) \quad (2.23)$$

If the DC grid has ground admittance, (2.23) is expressed as

$$D(\mathbf{V}_{dc}) = \sum_{i=1}^n \sum_{j=i+1}^n G_{ij} (V_{dc,i} - V_{dc,j})^2 + \sum_{i=1}^n G_{ii} V_{dc,i}^2 \quad (2.24)$$

where G_{ij} indicates the total conductance between terminals i and j ; and G_{ii} represents the sum of all conductance connected between terminal i and the ground.

The Lagrange function of (2.21) can be written as

$$\begin{aligned}
F(\boldsymbol{\delta}_s, \mathbf{U}_s, \mathbf{V}_{dc}) &= A(\boldsymbol{\delta}_s, \mathbf{U}_s) + D(\mathbf{V}_{dc}) + \boldsymbol{\lambda}_1^T \mathbf{f}_1(\boldsymbol{\delta}_s, \mathbf{U}_s, \mathbf{V}_{dc}) + \boldsymbol{\lambda}_2^T \mathbf{f}_2(\mathbf{V}_{dc}) \\
&\quad + \boldsymbol{\lambda}_3^T \mathbf{f}_3(\boldsymbol{\delta}_s, \mathbf{U}_s) + \boldsymbol{\lambda}_4^T \mathbf{g}(\boldsymbol{\delta}_s, \mathbf{U}_s, \mathbf{V}_{dc})
\end{aligned} \tag{2.25}$$

Now let $\boldsymbol{\lambda} = [\boldsymbol{\lambda}_1; \boldsymbol{\lambda}_2; \boldsymbol{\lambda}_3; \boldsymbol{\lambda}_4]$, $\mathbf{f}(\boldsymbol{\delta}_s, \mathbf{U}_s, \mathbf{V}_{dc}) = [\mathbf{f}_1(\boldsymbol{\delta}_s, \mathbf{U}_s, \mathbf{V}_{dc}); \mathbf{f}_2(\mathbf{V}_{dc}); \mathbf{f}_3(\boldsymbol{\delta}_s, \mathbf{U}_s); \mathbf{g}(\boldsymbol{\delta}_s, \mathbf{U}_s, \mathbf{V}_{dc})]$; and \mathbf{x} stand for all the AC-grid state variables $\boldsymbol{\delta}_s$ and \mathbf{U}_s . Then, (25) can be rewritten as

$$F(\mathbf{x}, \mathbf{V}_{dc}) = A(\mathbf{x}) + D(\mathbf{V}_{dc}) + \boldsymbol{\lambda}^T \mathbf{f}(\mathbf{x}, \mathbf{V}_{dc}) \tag{2.26}$$

The formulation of the KKT condition can be given by

$$\left\{ \begin{array}{l}
\frac{\partial F(\mathbf{x}, \mathbf{V}_{dc})}{\partial \mathbf{x}} = \frac{\partial A(\mathbf{x})}{\partial \mathbf{x}} + \boldsymbol{\lambda}^T \frac{\partial \mathbf{f}(\mathbf{x}, \mathbf{V}_{dc})}{\partial \mathbf{x}} = \mathbf{0} \\
\frac{\partial F(\mathbf{x}, \mathbf{V}_{dc})}{\partial \mathbf{V}_{dc}} = \frac{\partial (D(\mathbf{V}_{dc}))}{\partial \mathbf{V}_{dc}} + \boldsymbol{\lambda}^T \frac{\partial \mathbf{f}(\mathbf{x}, \mathbf{V}_{dc})}{\partial \mathbf{V}_{dc}} = \mathbf{0} \\
\mathbf{f}_1(\boldsymbol{\delta}_s, \mathbf{U}_s, \mathbf{V}_{dc}) = \mathbf{0} \\
\mathbf{f}_2(\mathbf{V}_{dc}) = \mathbf{0} \\
\mathbf{f}_3(\boldsymbol{\delta}_s, \mathbf{U}_s) = \mathbf{0} \\
\boldsymbol{\lambda}_4^T \mathbf{g}(\boldsymbol{\delta}_s, \mathbf{U}_s, \mathbf{V}_{dc}) = \mathbf{0} \\
\mathbf{g}(\boldsymbol{\delta}_s, \mathbf{U}_s, \mathbf{V}_{dc}) \leq \mathbf{0} \\
\boldsymbol{\lambda}_4^T \geq \mathbf{0}
\end{array} \right. \tag{2.27}$$

Based on the first equation in (2.27), one can get the expression of $\boldsymbol{\lambda}^T$ as

$$\left\{ \begin{array}{l}
\frac{\partial F(\mathbf{x}, \mathbf{V}_{dc})}{\partial \mathbf{x}} = \frac{\partial A(\mathbf{x})}{\partial \mathbf{x}} + \boldsymbol{\lambda}^T \frac{\partial \mathbf{f}(\mathbf{x}, \mathbf{V}_{dc})}{\partial \mathbf{x}} = \mathbf{0} \\
\frac{\partial F(\mathbf{x}, \mathbf{V}_{dc})}{\partial \mathbf{V}_{dc}} = \frac{\partial (D(\mathbf{V}_{dc}))}{\partial \mathbf{V}_{dc}} + \boldsymbol{\lambda}^T \frac{\partial \mathbf{f}(\mathbf{x}, \mathbf{V}_{dc})}{\partial \mathbf{V}_{dc}} = \mathbf{0} \\
\mathbf{f}_1(\boldsymbol{\delta}_s, \mathbf{U}_s, \mathbf{V}_{dc}) = \mathbf{0} \\
\mathbf{f}_2(\mathbf{V}_{dc}) = \mathbf{0} \\
\mathbf{f}_3(\boldsymbol{\delta}_s, \mathbf{U}_s) = \mathbf{0} \\
\boldsymbol{\lambda}_4^T \mathbf{g}(\boldsymbol{\delta}_s, \mathbf{U}_s, \mathbf{V}_{dc}) = \mathbf{0} \\
\mathbf{g}(\boldsymbol{\delta}_s, \mathbf{U}_s, \mathbf{V}_{dc}) \leq \mathbf{0} \\
\boldsymbol{\lambda}_4^T \geq \mathbf{0}
\end{array} \right. \tag{2.28}$$

Substituting (2.28) into the second equation in (2.27), one can get

$$\frac{\partial (D(\mathbf{V}_{dc}))}{\partial \mathbf{V}_{dc}} - \frac{\partial A(\mathbf{x})}{\partial \mathbf{x}} \left(\frac{\partial \mathbf{f}(\mathbf{x}, \mathbf{V}_{dc})}{\partial \mathbf{x}} \right)^{-1} \frac{\partial \mathbf{f}(\mathbf{x}, \mathbf{V}_{dc})}{\partial \mathbf{V}_{dc}} = \mathbf{0} \tag{2.29}$$

Simplifying (2.29) gives the following equation

$$\frac{\partial((D(\mathbf{V}_{dc}))}{\partial \mathbf{V}_{dc}} - \frac{\partial A(\mathbf{x})}{\partial \mathbf{V}_{dc}} = \mathbf{0} \quad (2.30)$$

The AC-DC grid transmission loss can be minimized by adjusting the active power exchange at the PCCs between AC and DC grids. According to (2.8), the DC node active power is the function of the DC node voltages. Therefore, it is observed from (2.30) that the condition of minimization of the total loss of AC-DC system can be viewed as the equal DC voltage sensitivity rule. To be more specific, when the total grid transmission loss is minimized, the incremental transmission loss of AC grid should be equal to that of the DC grid together with converter loss. After solving the optimal power flow, all the state variables, i.e., δ_s , \mathbf{U}_s and \mathbf{V}_{dc} are known. Then, the adaptive active power references can be solved.

2.3.3 Minimization of DC Voltage Deviation

The optimal objective function is established to minimize the RMS value of total steady-state DC voltage deviation before and after the change of system operating conditions as

$$Obj = \min \sqrt{\sum_{i=1}^n (V_{dc,i}^{post} - V_{dc,i}^{pre})^2 / n} \quad (2.31)$$

where $V_{dc,i}^{post}$ is the DC voltage of bus i after change of system operating condition and $V_{dc,i}^{pre}$ is the voltage before the change. To minimize the DC voltage deviation with KKT condition, the first equation in (2.21) should be substituted by (2.31) while the equality and inequality constraints in (2.21) are the same.

2.3.4 Linear Scalarization

Linear scalarization method is widely used to translate the multi-objective nature of a problem into a standard, single-objective problem. Based on linear scalarization method, we can obtain the single-objective problem as

$$obj = w * \min(P_{loss}) + (1 - w) * \min(V_{variation}) \quad (2.32)$$

where w is the weighting factor; P_{loss} is the per-unit value of the AC-DC grid total loss; and $V_{variation}$ is the per-unit value of the DC voltage variation. It is noted that the weighting factor w is selected by the system operator based on specific AC-DC grid and its configurations, system operating conditions, contingencies, preferred optimization target towards system loss or voltage

derivation. The increase of w leads to reduced total loss but increased DC voltage variation and vice versa. By selecting appropriate value of w , it is desirable that both of the total loss and voltage variation should be less than those under the fixed droop control. The method to obtain the desirable value range of w will be further shown in the case study.

2.3.5 Degree of Freedom

The degree of freedom is the total number of variables subtracted from the number of equality constraints and the equations leading to optimal condition in the proposed optimal AC-DC power flow algorithm. In order to enable an optimal solution of the AC-DC grid power flow problem, the degree of freedom must be greater than or equal to zero. According to (2.8), the DC node active power injection $P_{dc,i}$ is the function of the DC voltage $V_{dc,i}$. In the conventional fixed-parameter droop control strategy, there is only one variable V_{dc} in (2.9). Therefore, the degree of freedom is zero for the conventional AC-DC power flow. But in adaptive droop control method, given the power reference P_i^* to be adjustable, there exist two variables, i.e., $V_{dc,i}$ and P_i^* for every DC nodal equation. In addition, for minimizing the total AC-DC grid transmission loss, one equation is derived from KKT condition for every adaptive-droop-controlled converter node, which leads to N numbers of equations for optimal condition for the MTDC system with N adaptive-droop-controlled converters. Therefore, the total degree of freedom is $2N - N - N = 0$.

2.4 Case Studies

An interconnected AC-DC grid is used as the test system in this subsection to verify the proposed sequential power flow methods and the optimization algorithm in Cases A-D. The AC-DC grid consists of an *IEEE* New England 39-bus AC grid integrated with a six-terminal MTDC grid in which five terminals are equipped with MMCs, as shown in Figure 2-6. In Figure 2-6, the DC nodes 1, 2, 4, 5, and 6 are connected to the AC grid through five MMC stations and the corresponding AC nodes 9, 18, 24, 14, and 36. The DC node 3 does not have an MMC station connecting to the AC grid.

In the base case, the MTDC system is operated in the conventional master-slave control mode. The MMC station connected to DC node 1 is operated in DC voltage control mode while the other four MMC stations are in active power control mode. The MTDC grid parameters and transmission line resistances are given in Tables 2.1 and 2, respectively. The per-unit converter loss coefficients for the DC current are listed in Table 2.3. The MMCs 4 and 5 are with full-bridge sub-modules,

while the other MMCs are with half-bridge sub-modules. The active power flowing from DC to AC is defined as the positive direction. The sequential AC-DC power flow together with the KKT condition are implemented in Matlab 2014b. The case studies are executed on a PC with 2.3 GHz Intel core i5-6300HQ and 8 GB RAM under Microsoft Windows 10 operating system.

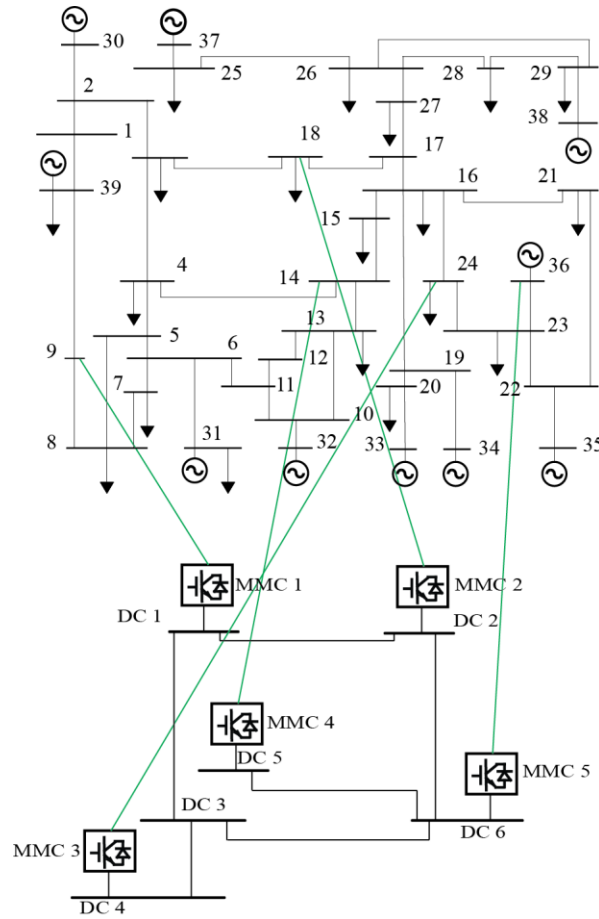


Figure 2-6 Configuration of AC-MTDC network with MMC stations.

Table 2.1 MTDC Grid Parameter For Base Case (in P.U.).

DC Node No.	P_s	Q_s	Control Mode of the Connected MMC	Complex Equivalent Impedance
1	—	—	Slack-V	$0.0009 + 0.2j$
2	2	0.25	P-Q	$0.0009 + 0.2j$
3	—	—	—	—
4	0.8	—	P- U_s	$0.0009 + 0.2j$
5	3.5	0.9	P-Q	$0.0012 + 0.2j$
6	-3.5	-1	P-Q	$0.0012 + 0.2j$

Table 2.2 DC Transmission Line Parameter For Base Case (in P.U.)

DC Line	1-2	1-3	1-5	2-6	3-4	3-6	5-6
R	0.0	0.0	0.0	0.0	0.0	0.0	0.0
	1	1	19	16	1	16	04

Table 2.3 Converter Loss Coefficients (in P.U.)

DC Line	a_{dc}	b_{dc}	c_{dc}
Half-bridge	8.8	4.0	0.4
Full-bridge	00	6.7	0.9
		00	56

$\times 10^4$

2.4.1 Case A: Static Power Flow Results

In this case, the proposed Methods III and IV are compared with the AC-DC power flow approaches in [12] (Method I) and [13] (Method II) under static operation condition. The results of Method I are used as the reference.

2.4.1.1 Base Case

The power flow results under master-slave control (base case) in Table 2.1 are shown in Table 2.4. Only DC-grid power P_{dc} is selected to be shown for brevity. From Table 2.4, it can be seen that there is some difference between the results of Methods I and II. However, the results of the proposed Method III are exactly the same as Method I; and the results of the proposed Method IV are very similar to Method I with minor errors. The computational times of the Methods III and I are 0.4221s and 0.4733s respectively. This is because the proposed Method III eliminates the SBI step, thus reduce the total computation burden by about 10%.

Table 2.4 Calculation Results of Base Case (in P.U.)

DC Node No.	Method I	Method II	Method III	Method IV
1	-2.999	-2.971	-2.999	-2.999
2	2.023	2.000	2.023	2.023
3	0	0	0	0
4	0.813	0.800	0.813	0.813
5	3.565	3.500	3.565	3.563
6	-3.443	-3.500	-3.443	-3.441

2.4.1.2 Droop Control Mode

Now the control strategy of the MTDC system in Figure 2-6 is switched from master-slave control in base case to droop control. MMCs 2 and 4 are operated in active power control mode while all the other three MMC stations are in droop control mode. The power reference (P_i^*) of the droop controlled MMCs is obtained from the power flow results of the base case, as shown in Table 2.5. The droop coefficients for the droop controlled MMCs are all set to be 50. The power flow results of the four methods are shown in Table 2.6. From Table 2.6, it can be observed that the results of the proposed Methods III and IV are accurate while the results of Method II have notable differences with the result of Method I.

Table 2.5 Power Reference of the Droop Controlled MMCs (in P.U.)

MMC No.	1	2	3	4	5
P_i^*	-3.00	2.00	0.80	3.50	-3.50

Table 2.6 Calculation Results for MTDC Grid under Droop Control (in P.U.)

DC Node No.	Method I	Method II	Method III	Method IV
1	-3.462	-3.502	-3.462	-3.462
2	2.023	2.000	2.023	2.023
3	0	0	0	0
4	0.813	0.800	0.813	0.812
5	4.154	4.077	4.154	4.153
6	-3.634	-3.696	-3.634	-3.633

Moreover, the computation times of Methods III and I are 0.5221s and 0.6133s respectively. By eliminating the DBI step, the total computational burden is reduced by about 21%. Compared with the base case, eliminating DBI can save more percentage of computational burden than that of eliminating SBI. This is because as the number of droop nodes increases, the DBI iterative solution becomes more complicated and gives rise to additional computational load to the power flow algorithm. The proposed method is particularly advantageous when there are more droop controlled nodes in the DC grids.

2.4.2 Case B: Power Flow Results after the Contingencies

In Case B, sequential power flow results are compared using two contingencies, i.e. power variation and converter outage. The results of Method I are also used as the reference.

2.4.2.1 Power Variation

The active power at the PCC of DC node 2 is decreased from 2 p.u. to 1 p.u.. The results of Methods I, II and IV are shown in Table 2.7. It is noted that the results of Method III are not shown in Table 2.7 they are identical to Method I.

The overall iterations of the Methods III and I are 4 and 6 respectively. This is because power variation gives rise to large deviation of initial droop bus power estimation when AC grid is calculated first. Thus, Method I needs more iterations to converge compared to the proposed Method III.

From Table 2.7, it is observed that the results of Method II are different from those of Method I, while the results of Methods I and IV are nearly identical. The computational times of Methods I, II and IV are 0.7013s, 0.5965s and 0.4536s respectively, which shows that the proposed Method IV is both accurate and efficient. It is noted that the system operator may need to conduct numerous times of power flows for planning and control purpose. Thus, it is significant to improve the computational efficiency by the improved power flow algorithms.

Table 2.7 Calculation Results after Power Variation (in P.U.)

DC Node No.	Method I	Method II	Method IV
1	-3.067	-3.101	-3.067
2	1.014	1	1.014
3	0	0	0
4	0.813	0.800	0.813
5	4.455	4.370	4.454
6	-3.313	-3.368	-3.312

2.4.2.2 Converter Outage

After MMC-2 is forced into outage, results of Methods I, II and IV are shown in Table 2.7. Now, the overall iterations of Method I increase to 7 while the proposed Method III is still 4. From Table 2.8, we can also see that Method IV is much more accurate than Method II. The computational times of Methods I, II and IV are 0.7924s, 0.6142s and 0.4577s respectively. Compared to Case

B.1), it can be seen that the overall iterations and computational time of Method I increase for large disturbance case, while the computational time for the proposed Method IV is nearly unchanged.

In order to illustrate the advantage of the proposed Method IV over the existing methods, the comparisons of accuracy and computational times of Case B are summarized in Tables 2.9 and 10, respectively. The results of Method I are used as the reference for accuracy comparison. It is observed from Table 2.9 that the results of Method II are inaccurate as $P_{loss,i}$ and $P_{comp,i}$ are neglected in the DC power flow. On the other hand, the results of the proposed Method IV are very close to the reference solutions with the small errors due to the assumption of AC and DC power balance in (11). From Table 2.10, it can be seen that, the computational times of the proposed Method IV are smaller than Methods I and II as the DBI iteration step is eliminated and only DC grid power flow is iterated instead of AC grid power flow in Method IV.

Table 2.8 Calculation Results after Converter Outage (in P.U.)

DC Node No.	Method I	Method II	Method IV
1	-2.675	-2.705	-2.676
2	0	0	0
3	0	0	0
4	0.813	0.800	0.813
5	4.755	4.662	4.752
6	-2.995	-3.044	-2.994

Table 2.9 Comparison of Power Flow Accuracy

DC Node No.	Method II		Method IV	
	Power Variation	Converter Outage	Power Variation	Converter Outage
1	1.11%	1.12%	0	0
2	1.4%	—	0	—
3	—	—	—	—
4	1.63%	1.63%	0	0
5	1.91%	1.96%	0.02%	0.06%
6	1.66%	1.63%	0.03%	0.03%

Table 2.10 Comparison of Computational Times

Computational Time	Method I	Method II	Method IV
Power Variation	0.7013s	0.5965s	0.4536s
Converter Outage	0.7924s	0.6142s	0.4577s

2.4.3 Case C: Minimization of AC-DC Grid Total Loss

In this case, the active power at the PCC of the DC node 2 is increased from 2 p.u. to 3 p.u.. With the loss minimization algorithm proposed in Subsection 2.3.2 (without minimizing the DC voltage variation), the AC-DC grid total loss is minimized to be 0.585 p.u., as shown in Figure 2-7. The computational time of Case C is 4.2237s.

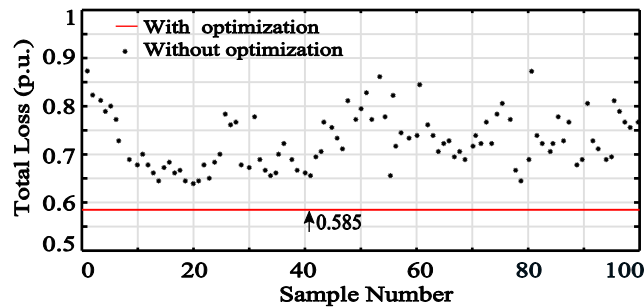


Figure 2-7 Comparison of total losses with and without optimization algorithm.

In Figure 2-7, the black dots represent the AC-DC grid total losses for 100 samples with random values of the power reference P^* used for the three droop controlled MMC stations. It is shown in Figure 2-7 that, without the optimization algorithm, the AC-DC grid total losses are always greater than the total loss obtained using the minimization algorithm shown by the red line.

2.4.4 Case D: Minimization of DC Voltage Variation

In Case *D*, similar to Case *C*, the active power injection at PCC of the DC node 2 is increased from 2 p.u. to 3 p.u.. Meanwhile, applying the optimization algorithm minimizing voltage variation as proposed in Subsection 2.3.3 (without minimizing the AC-DC total loss), the DC nodes voltage variation (2.31) is minimized to 0.0025 p.u., as shown in Figure 2-8. The computational time of Case *D* is 3.9144s.

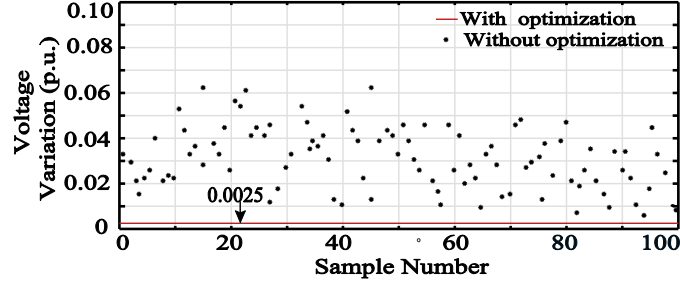


Figure 2-8 Comparison of DC voltage variations with and without optimization algorithm.

The black dots shown in Figure 2-8 represent the DC voltage variations of 100 samples using random values of the P^* for the three droop-control converters. It is observed in Figure 2-8 that, without using the optimization algorithm, the total DC voltage variations are always larger than the optimal value represented by the red line when the optimization algorithm is used.

2.4.5 Case E: Minimization of DC Voltage Variation and AC-DC Grid Transmission Loss

Similar to the previous two cases, the active power injection of the DC node 2 is increased from 2 p.u. to 3 p.u.. The two optimization objectives given in Subsection 2.3, i.e., minimization of AC-DC grid total loss and DC node voltage deviation, are considered simultaneously using linear scalarization in Subsection 2.3.4. By selecting the weighting factor w to be 0.5, the total transmission loss of the AC-DC grid is minimized to be 0.642 p.u. and the DC voltage variation (2.31) to be 0.0124 p.u.. Compared to the previous two cases, which have only one optimization target, the optimal DC voltage variation and total transmission loss in Case *E* are achieved simultaneously but with compromised objective function values. Therefore, Cases *C*, *D* and *E* verify the effectiveness of the proposed optimization algorithm.

2.4.6 Case F: Dynamic Simulation

In this case, a five-terminal MTDC system [34], [42] is implemented using Matlab/Simulink/SimScape Toolbox for EMT-type solutions to verify the proposed adaptive droop control strategy and the optimal power flow algorithms. The MMCs are represented using average value models [62] with the detailed outer power and inner current control loops. As the EMT solver in Matlab/Simulink/SimScape Toolbox represents system components with detailed models and a small simulation time step ($20 \mu\text{s}$), the AC grid is simplified to AC Thevenin equivalent circuits to accelerate the EMT simulation. DC transmission line parameters are given

in Table 2.11. The control modes, rated powers, droop coefficients and power references of MMC stations are given in Table 2.12. The nominal voltage and power of the MTDC system are 400 kV and 600 MW respectively. The MMC-5 is forced outage at $t = 0$ s. Considering the computational delay, the adaptive droop control strategy is activated at $t = 0.5$ s.

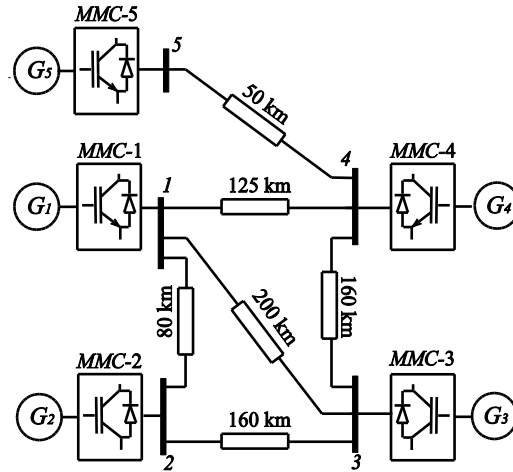


Figure 2-9 Five-terminal MTDC system.

Table 2.11 DC Line Parameters

Parameter	$R(\Omega/km)$	$L(mH/km)$	$C(\mu F/km)$
<i>Value</i>	0.20	0.15	0.27

Table 2.12 Parameters of MMC Stations

MMC Number	1	2	3	4	5
Control Modes	AdaptiveDroop	AdaptiveDroop	P	AdaptiveDroop	P
Rated Powers (MW)	650	650	700	650	750
Droop Coefficients k_i	12.5	25	0	50	0
Power Reference (MW)	-400	-500	550	-600	500

2.4.6.1 Minimization of MTDC System Loss

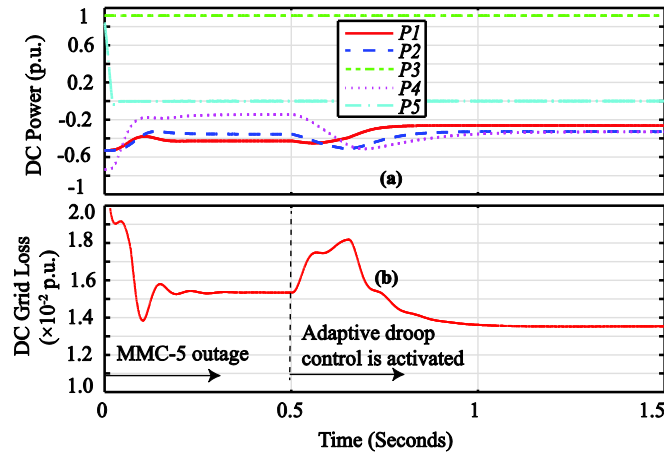


Figure 2-3 DC powers and DC grid loss.

(a) DC powers; (b) MTDC system loss.

In this case, minimization of MTDC system loss is set to be the optimal objective. Figure 2-10 illustrate the DC powers and MTDC loss before and after the adaptive droop control is activated. It is seen in Figure 2-10 (a) that the converter powers are within their rated power limits. It is also observed in Figure 2-10 (b) that the DC transmission loss is minimized from 0.0150 p. u. under fixed droop control to 0.0133 p. u. under adaptive droop control, leading to a loss reduction by 11.3%.

In addition, the influence of MMC control modes on the result of optimal power flow is analyzed by setting three different scenarios. The MMC control modes in Table 2.12 are defined as Scenario I. Scenario II is obtained by changing the control mode of MMC-2 to active power control mode. If both MMCs-2 and 4 are switched to active power control mode, we can get Scenario III. The results of optimal power flow under different scenarios are shown in Table 2.13. It is observed in Table 2.13 that the increased number of adaptive droop controlled MMCs leads to more optimization decision variables and better optimization results, although the computational time of the optimization algorithm will slightly increase.

Table 2.13 Optimal Results of Different Scenarios

	Scenario I	Scenario II	Scenario III
System Loss	0.0133 p. u.	0.0143 p. u	0.0146 p. u.
Calculation Time	0.172s	0.146s	0.113s

2.4.6.2 Minimization of DC Voltage Variation

Applying the optimization algorithm to minimize DC voltage variation, the DC powers and DC voltage variations following MMC-5 outage are shown in Figures 2-11 (a) and (b) respectively. It can be seen from Figure 2-11 that the DC voltage variation is greatly reduced (from 0.022 p.u. to 0.011 p.u.) by the proposed adaptive droop control strategy.

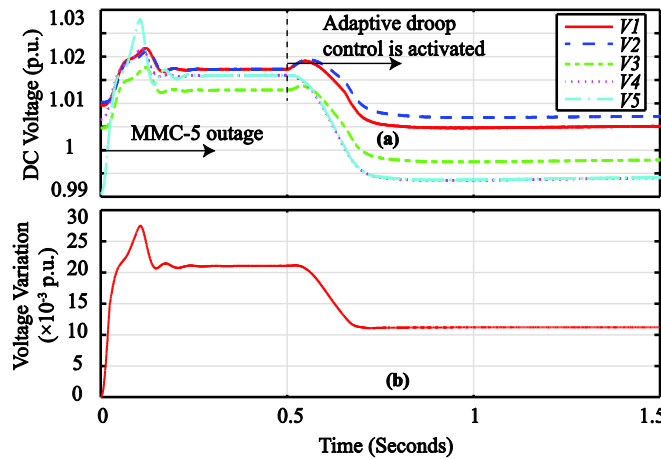


Figure 2-4 DC voltages and voltage variation.

(a) DC voltages; (b) DC voltage variation.

2.4.6.3 Minimization of MTDC System Loss and Voltage Variation

In this subsection, minimization of MTDC system loss and voltage deviation are considered simultaneously using linear scalarization. The relationships of MTDC system loss and DC voltage variation with respect to w are shown in Figures 2-12 (a) and (b). When w increases from zero to one in Figure 2-12 (a), the MTDC system loss initially decreases slowly, then reduces sharply and finally remains nearly unchanged. By contrast, Figure 2-12 (b) depicts the opposite tendency of

DC voltage variation. The red lines in Figures 2-12 (a) and (b) represent the MTDC system loss and DC voltage variation under fixed droop control, respectively. Since the proposed optimal power flow is based on adaptive droop control, the selection of w is made such that the values of both optimal objectives (system loss and DC voltage deviation) under adaptive droop control strategy is smaller than those under fixed droop control. Thus, the desired value range of w can be obtained as

$$0.07 < w < 0.72 \quad (2.33)$$

It is noted that in a specific AC-DC grid, the system operators may define some certain ranges of maximum transmission loss and DC voltage deviation based on system operating conditions. Thus, the desired values of w in (2.33) should be selected accordingly based on the requirements of the two optimal targets.

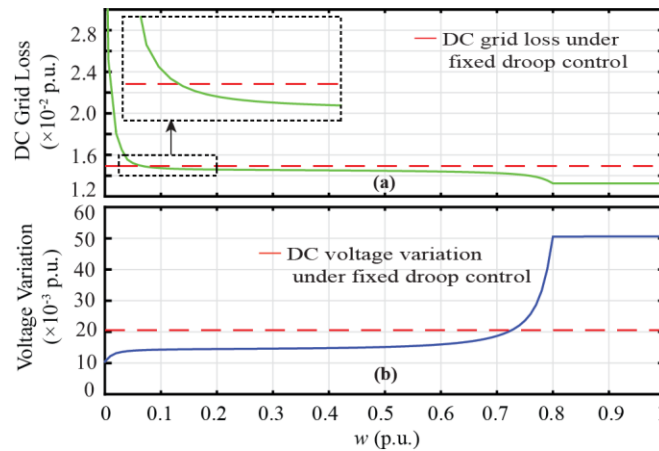


Figure 2-5 The relationships of MTDC system loss and DC voltage variation with respect to w
(a) MTDC system loss; (b) DC voltage variation.

2.5 Summary

This chapter proposes two improved sequential AC-DC power flow algorithms. The second proposed algorithm is based on the first one with higher efficiency and negligible errors. Compared to the conventional sequential power flow methods, it is shown in the results of Case *B* that the proposed algorithms have much less computational burden (Table 2.10) than the existing approaches while maintaining their calculation accuracy (Table 2.9) under two types of system

contingencies in the interconnected AC-DC grid consisting of an *IEEE* New England 39-bus AC grid integrated with a six-terminal MTDC grid.

Additionally, based on the proposed AC-DC power flow methods, an optimization algorithm to minimize the total loss of the AC-DC grid or the DC voltage deviation after the change of operating conditions is proposed. The adaptive droop control strategy is used to achieve the optimization targets by dynamically adjusting the active power references of the droop-controlled MMC stations. The two optimal targets can also be realized together with compromise by employing the linear scalarization method. The results of static and dynamic simulation studies verify the validity and feasibility of the proposed adaptive droop control based optimal power flow method. The static simulations show that two optimal targets, achieved by the proposed adaptive droop control strategy, are smaller than 100 random samples. The dynamic simulations demonstrate that the proposed optimization method can reduce 11.3% of system loss and 50% DC voltage deviation compared with the fixed droop control. The proposed OPF algorithm is based on the adaptive droop control scheme in which the OPF decision variables are the power references of the droop controlled converters. Therefore, the adaptive droop control method can realize the optimization targets without the negative impact on the stability of the AC-DC grid. The proposed improved power flow algorithms for AC-DC sequential power flow approach can also be applied to the unified power flow approach as well as the microgrid. In addition, power sharing accuracy and minimization of operation cost can also be realized by the adaptive droop control method, which we will pursue as the future work.

3 Autonomous DC Line Power Flow Regulation Using Adaptive Droop Control in HVDC Grid

In Section 2, improved AC-DC power flow algorithms were proposed. A linearized model can be developed from the power flow algorithms to improve the calculation efficiency. Based on the linearized model, this chapter proposes a new DC line power flow regulation strategy² based on adaptive droop control for an HVDC grid under various contingencies. The proposed DC line power flow control method does not require any new installation of power converter equipment in an HVDC grid and thus greatly reduces the capital costs and power losses compared to the existing methods. The DC line power regulation is achieved by autonomously adjusting voltage references of the adaptive droop controlled VSCs.

3.1 Analytical Modeling of VSC-HVDC Grid

In this subsection, analytical modeling of a VSC-HVDC grid in steady-state operating condition is introduced under DC voltage droop control scheme. The converter DC power, DC line voltage, and DC line power are formulated based on HVDC grid configuration to facilitate the derivation of the proposed DC line power flow regulation method.

The generalized DC voltage droop control is represented as:

$$P_{c,i} - P_{c,i}^* + R_i(V_i - V_i^*) = 0 \quad (3.1)$$

where $P_{c,i}$ and $P_{c,i}^*$ are the actual and reference values of the power injection to the AC grid from the i^{th} VSC, respectively; V_i and V_i^* are the actual and reference values of the DC pole-to-pole voltage, respectively; R_i is the droop coefficient of the i^{th} VSC, which is defined by

$$R_i = P^r k_i / V^r \quad (3.2)$$

where P^r and V^r are the rated power and rated DC voltage respectively; k_i is the droop coefficient in per unit. It is noted that k_i is positive for a VSC in droop control mode and $k_i = 0$ for a VSC in active power control mode.

² Yuanshi Zhang, Liwei Wang, and Wei Li, "Autonomous DC Line Power Flow Regulation Using Adaptive Droop Control in HVDC Grid," published in *IEEE Transactions on Power Delivery*, doi: 10.1109/TPWRD.2020.3044978.

The relationship between power injections of the AC and HVDC grids through the i^{th} VSC station can be given by

$$P_{c,i} = P_{DC,i} + P_{loss,i} \quad (3.3)$$

where $P_{loss,i}$ is the converter loss; $P_{DC,i}$ is the active power injection to the DC grid.

Given a symmetrical monopolar HVDC grid, $P_{DC,i}$ can be computed by

$$P_{DC,i} = V_i \left(\sum_{j=1}^N g_{ij} V_j \right) \quad (3.4)$$

where N stands for the total number of DC nodes; g_{ij} is self- or mutual-conductance of negative and positive poles between node i and node j .

The vector form of (3.4) can be written as

$$\mathbf{P}_{DC} = \mathbf{V} \otimes (\mathbf{G}\mathbf{V}) \quad (3.5)$$

where $\mathbf{P}_{DC} = [P_{DC,i}]_{N \times 1}$, $\mathbf{V} = [V_i]_{N \times 1}$ and $\mathbf{G} = [g_{ij}]_{N \times N}$. The symbol \otimes is an entry-wise matrix multiplication operator, also known as Hadamard product operator [34].

The active power flowing from DC nodes i to j , i.e., DC line power $P_{L,k}$ is calculated by

$$P_{L,k} = V_i (V_i - V_j) / R_{ij} \quad (3.6)$$

where R_{ij} is the resistance of DC line between nodes i and j .

It is assumed that there are M DC lines and N DC nodes in the HVDC grid. The $M \times N$ matrix \mathbf{T} is defined as incidence matrix [57]. An element of \mathbf{T} , i.e. T_{ij} , takes the value of -1 , 0 or 1 . $T_{ij} = -1$ or 1 means the defined line current of the i^{th} line enters or leaves the node j , while $T_{ij} = 0$ means the i^{th} line is not connected to the node j . Thus, DC line voltage vector \mathbf{U}_L is given by

$$\mathbf{U}_L = \mathbf{T}\mathbf{V} \quad (3.7)$$

If the elements with the value of -1 in \mathbf{T} are all set to be zero, one can get the $M \times N$ leaving node matrix \mathbf{W} . Thereby, DC leaving node voltage \mathbf{U}_W vector is expressed as

$$\mathbf{U}_W = \mathbf{W}\mathbf{V} \quad (3.8)$$

Once \mathbf{U}_L and \mathbf{U}_W are formulated, the vector form of the DC line power in (3.6) can be expressed as

$$\mathbf{P}_L = \mathbf{U}_W \otimes [\text{diag}(\mathbf{Y}_L) \mathbf{U}_L] \quad (3.9)$$

where \mathbf{Y}_L is the DC line conductance column vector, i.e. $\mathbf{Y}_L = [\frac{1}{R_{ij}}]_{M \times 1}$, and *diag* stands for a mathematical operator to transform a vector into a diagonal matrix.

3.2 Autonomous DC Line Power Flow Regulation

In this subsection, an autonomous DC line power flow regulation method is proposed based on adaptive DC voltage droop control. The proposed DC line power flow regulation method can effectively control the power flows in one or multiple DC lines under various contingencies including power variation caused by renewable energy sources, converter outage, and DC grid topology change.

3.2.1 Linearized Model of VSC-HVDC Grid in Voltage Droop Control

It is assumed that the initial steady-state operating point of the i^{th} droop controlled VSC is given by the droop characteristic equation in (3.1). Under contingencies, let the variations of actual power, power reference, and node voltage be $\Delta P_{c,i}$, $\Delta P_{c,i}^*$ and ΔV_i . In order to regulate DC line power, the voltage reference of the i^{th} droop controlled VSC is set to be adaptive. Let the variation of voltage reference be ΔV_i^* . It is noted that ΔV_i^* is calculated at each VSC station locally, which will be elaborated in Subsection 3.2.2.

The post-contingency operating point of the i^{th} droop controlled VSC station can be given by

$$P_{c,i} + \Delta P_{c,i} - P_{c,i}^* - \Delta P_{c,i}^* + R_i (V_i + \Delta V_i - V_i^* - \Delta V_i^*) = 0 \quad (3.10)$$

Subtracting (3.10) from (3.1), one can obtain

$$\Delta P_{c,i} = \Delta P_{c,i}^* + (\Delta V_i^* - \Delta V_i) R_i \quad (3.11)$$

The vector format of (3.11) is expressed as

$$\Delta \mathbf{P}_c = \Delta \mathbf{P}_c^* + \text{diag}(\mathbf{R})(\Delta \mathbf{V}^* - \Delta \mathbf{V}) \quad (3.12)$$

If the variation of converter loss is ignored, the variation of converter power injection to the AC grid is derived from (3.3) as

$$\Delta \mathbf{P}_c = \Delta \mathbf{P}_{DC} \quad (3.13)$$

where $\Delta \mathbf{P}_{DC}$ is the variation of DC side active power.

The relationship between the DC voltage variation $\Delta \mathbf{V}$ and DC power variation $\Delta \mathbf{P}_{DC}$ is given by [34]

$$\Delta \mathbf{P}_{DC} = \mathbf{J} \Delta \mathbf{V} \quad (3.14)$$

where \mathbf{J} is the Jacobian matrix of the HVDC grid and is defined as

$$\mathbf{J} = \frac{\partial \mathbf{P}_{DC}}{\partial \mathbf{V}} \quad (3.15)$$

An element of \mathbf{J} , i.e., J_{ij} , can be written as

$$J_{ij} = \frac{\partial P_{DC,i}}{\partial V_j} \quad (3.16)$$

When $i = j$, a diagonal element of \mathbf{J} , i.e., $J_{i,i}$ is derived from (3.4) as

$$\frac{\partial P_{DC,i}}{\partial V_i} = \sum_{j=1}^N (g_{ij} V_j) + g_{ii} V_i \quad (3.17)$$

When $i \neq j$, an off-diagonal element of \mathbf{J} , i.e., $J_{i,j}$ is derived from (3.4) as

$$\frac{\partial P_i}{\partial V_j} = g_{ij} V_i \quad (3.18)$$

Combining (3.12), (3.13) and (3.14), the DC node voltage variation can be obtained as

$$\Delta \mathbf{V} = (\mathbf{J} + \text{diag}(\mathbf{R}))^{-1} (\Delta \mathbf{P}_c^* + \text{diag}(\mathbf{R}) \Delta \mathbf{V}^*) \quad (3.19)$$

3.2.2 Power Reference Variations under Various Contingencies

The DC node voltage variation $\Delta \mathbf{V}$ due to contingencies in HVDC grid can be calculated by (3.19) given the power reference variation $\Delta \mathbf{P}_c^*$ which depends on a specific type of contingency. Four types of contingencies are considered in this subsection. The first one is power variation of an active power controlled converter. This applies to the case of power fluctuation of renewable energy sources, e.g., offshore wind generation. The second one is outage of an active power controlled VSC. For the first two types of contingencies, $\Delta P_{c,i}^*$ is set to be the power difference of the active power controlled VSC before and after the contingency. The third one is outage of a droop controlled VSC. In this case, the disconnected droop controlled VSC is regarded as active

power controlled converter (i. e. R_i in (3.1) and (3.19) are set to zero). If the initial power of the disconnected converter is P_{initial} and it decreases to zero after converter outage, the power variation $\Delta P_{c,i}^*$ under this scenario is set to $-P_{\text{initial}}$.

The last type of contingency is HVDC grid topology change, i.e. disconnecting or adding DC lines. It is noted that the analytical model proposed in [34] and [57] have not included and discussed this type of contingency. This is because the elements of Jacobian matrix \mathbf{J} in (3.16) can not be directly obtained by (3.17) and (3.18) when HVDC grid topology changes. In this subsection, a new method is proposed to convert the change of DC grid topology to power variations of DC nodes by using dummy DC generators. We take an example of DC line disconnection to elaborate the proposed method. Assume that the DC line 3–4 in Figure 3-1 is disconnected. At the initial steady state, suppose that the power injections from DC line 3–4 to DC nodes 4 and 3 are D_1 and D_2 respectively. Employing the substitution principle, power injections of DC line 3–4 to DC nodes 4 and 3 can be substituted by adding two dummy generators to provide constant power D_1 and D_2 respectively. With this approach, when the DC line 3-4 is disconnected, only the two dummy generators are cut off while the HVDC grid topology does not change. Thus, $\Delta \mathbf{P}_c^*$ should be set to $[0, 0, -D_2, -D_1]^T$. It also noted that in case of adding DC lines, we can also assume that the added lines exist at the initial state according to this approach, in order to keep the DC topology unchanged. Dummy generators are also added at the initial steady state to compensate power injections of the added DC lines.

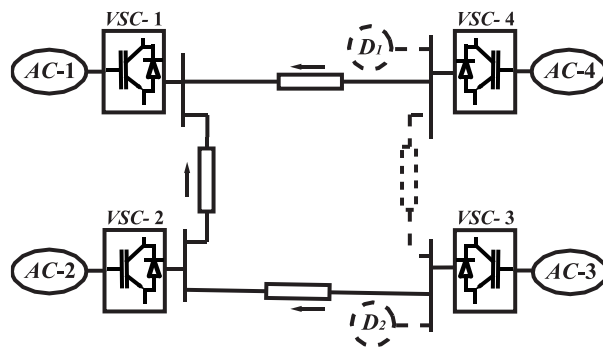


Figure 3-1 Four-terminal HVDC grid with dummy DC generators.

3.2.3 DC Line Power Flow Regulation Algorithm

Following a contingency in the HVDC grid, it is critical that DC line power flows are kept unchanged or are regulated to the targeted values within the operation limits. Furthermore, it is

desirable for the DC lines to share the powers proportionally based on their power ratings. In this subsection, firstly the method of regulating single DC line power is presented. Then, the proposed method is extended to regulate multiple DC line powers simultaneously. Finally, the proportional DC line power sharing algorithm is proposed.

3.2.3.1 One DC Line Power Regulation

The post-contingency operating point of DC line power equation (3.6) can be given by

$$P_{L,k} + \Delta P_{L,k} = (V_i + \Delta V_i)(V_i + \Delta V_i - V_j - \Delta V_j)/R_{ij} \quad (3.20)$$

where $\Delta P_{L,k}$ is the variation of DC line power after and before a contingency; $P_{L,k}$ is the original DC line power before the contingency.

Subtracting (3.20) from (3.6), one can obtain

$$\Delta P_{L,k} = [(2V_i - V_j)\Delta V_i - V_i\Delta V_j + \Delta V_i^2 - \Delta V_i\Delta V_j]/R_{ij} \quad (3.21)$$

In order to simplify the calculation, quadratic variation terms in (3.21) are neglected. Thus, we can obtain a linear equation as

$$\Delta P_{L,k} = [(2V_i - V_j)\Delta V_i - V_i\Delta V_j]/R_{ij} \quad (3.22)$$

Based on (3.19), the voltage variation $\Delta \mathbf{V}$ can be represented by the voltage reference variation $\Delta \mathbf{V}^*$. Furthermore, it is observed from (3.22) that the variation of DC line power $\Delta P_{L,k}$ is a function of voltage variation $\Delta \mathbf{V}$. Therefore, combining (3.19) and (3.22), $\Delta P_{L,k}$ can be regulated by adjusting the DC voltage reference variation $\Delta \mathbf{V}^*$. It is noted that \mathbf{J} and \mathbf{R} in (3.19) along with V_i and V_j in (3.22) are pre-contingency values and can be obtained from an arbitrary steady-state operating condition. Thus, a secondary/centralized controller is not needed. Hence, the proposed control method can autonomously regulate DC line powers.

3.2.3.2 One DC Line Power Regulation

From the DC line power formulation (3.9) in initial steady state, the post-contingency DC line power can be expressed as

$$\mathbf{P}_L + \Delta \mathbf{P}_L = (\mathbf{U}_W + \Delta \mathbf{U}_W) \otimes [\text{diag}(\mathbf{Y}_L)(\mathbf{U}_L + \Delta \mathbf{U}_L)] \quad (3.23)$$

where $\Delta \mathbf{P}_L$ is the DC line power variation vector, $\Delta \mathbf{U}_P$ is the DC leaving node voltage variation vector, and $\Delta \mathbf{U}_L$ is the DC line voltage variation vector.

Subtracting (3.23) from (3.9) and neglecting the quadratic variation terms, one can obtain

$$\Delta \mathbf{P}_L = \mathbf{U}_W \otimes (\text{diag}(\mathbf{Y}_L) \Delta \mathbf{U}_L) + \Delta \mathbf{U}_W \otimes (\text{diag}(\mathbf{Y}_L) \mathbf{U}_L) \quad (3.24)$$

Hence, the DC voltage reference variation vector $\Delta \mathbf{V}^*$ for achieving the DC line power regulation can be calculated by combining (3.7), (3.8), (3.19) and (3.24).

3.2.3.3 One DC Line Power Regulation

After a contingency in the HVDC grid, it is crucial that the designated DC lines share the power burden in a desirable way to avoid DC line overloading. A DC line power limit $P_{L,k}^{max}$ can be obtained from the DC line current limit as

$$P_{L,k}^{max} = I_{L,k}^{max} V^N \quad (3.25)$$

where $I_{L,k}^{max}$ is the DC current limit; V^N is the nominal DC voltage of the HVDC grid.

Now, assume that q is the number of the DC lines, designated to share the active power mismatch proportionally to the DC line power limits. We can get a system of $q - 1$ equations as

$$\begin{bmatrix} \frac{\Delta P_{L,1}}{P_{L,1}^{max}} - \frac{\Delta P_{L,2}}{P_{L,2}^{max}} = \frac{P_{L,2}}{P_{L,2}^{max}} - \frac{P_{L,1}}{P_{L,1}^{max}} \\ \frac{\Delta P_{L,2}}{P_{L,2}^{max}} - \frac{\Delta P_{L,3}}{P_{L,3}^{max}} = \frac{P_{L,3}}{P_{L,3}^{max}} - \frac{P_{L,2}}{P_{L,2}^{max}} \\ \vdots \\ \frac{\Delta P_{L,q-1}}{P_{L,q-1}^{max}} - \frac{\Delta P_{L,q}}{P_{L,q}^{max}} = \frac{P_{L,q}}{P_{L,q}^{max}} - \frac{P_{L,q-1}}{P_{L,q-1}^{max}} \end{bmatrix} \quad (3.26)$$

consequently, the targeted $\Delta \mathbf{V}^*$ to realize proportional DC line power sharing can be obtained by combining (3.24) and (3.26) with (3.7), (3.8), and (3.19).

3.2.4 DC Line Power Flow Regulation Algorithm

In this subsection, the control hierarchy of the proposed DC line power regulation based on adaptive voltage droop control is illustrated in Figure 3-2. The inner current control loop and the outer power control loop are usually used in a VSC's primary control layer, as shown in Figure 3-2. In the inner current control loop in Figure 3-2, i_d and i_d^* are the actual and reference values of the d -axis component AC current; i_q and i_q^* are the actual and reference values of the q -axis component AC current; L is the AC filter inductance; ω is the AC frequency; U_{sd} and U_{sq} are the d -axis and q -axis components of the VSC's AC voltage.

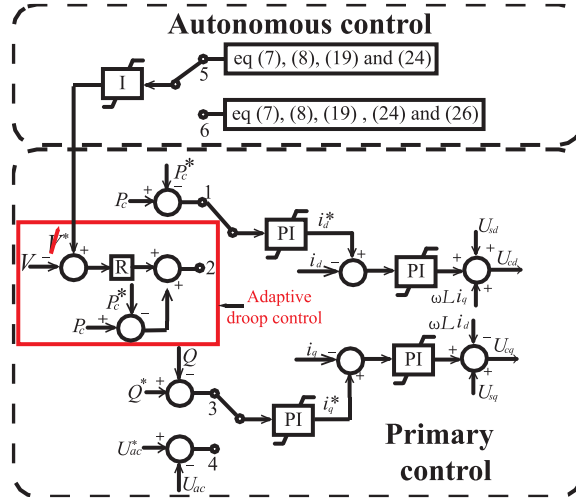


Figure 3-2 Hierarchical diagram of autonomous DC line power regulation.

In Figure 3-2, the outer power control loop regulates the active and reactive power injections into the VSC. The control objective is either active power control (Switch 1 in Figure 3-2) or DC voltage droop control (Switch 2 in Figure 3-2) for the d axis. The voltage reference of droop control in Figure 3-2 is configured to be adaptive to realize DC line power regulation. The adaptive voltage reference V^* is obtained from the proposed autonomous control layer. It is designed to calculate the voltage reference variation ΔV^* based on the DC line power regulation target, i.e., the scheduled DC line power flow control (Switch 5 in Figure 3-2) or the proportional DC line power sharing (Switch 6 in Figure 3-2). It is noted that an integral controller is used in the autonomous control to achieve a smooth change of the voltage reference ΔV^* instead of an abrupt change to avoid large transient.

3.2.5 Discussion

In adaptive droop control mode, each adaptive droop controlled VSC (i.e. the voltage reference V_i^* in (3.1) is adjustable) gives one degree of freedom for control, while each DC line power to be regulated requires one degree of freedom. The system with d number of adaptive droop controlled VSCs and e number of DC line powers to be regulated has $(d - e)$ degree of freedom for control. In order to ensure at least one feasible solution, the system must have the degree of freedom being greater than or equal to zero, i.e., $d \geq e$. It is noted that DC line power regulation can be realized using any combination of adaptive droop controlled VSCs with sufficient degree of freedom, which increases the maneuverability and flexibility of the proposed method.

The minor errors of the proposed DC line power regulation method are due to the following three approximations to simplify the calculations. The first one, which causes the major approximation error, is the linearization in (3.14). The Taylor expansion is given by

$$\Delta \mathbf{P}_{\text{DC}} = \mathbf{J} \Delta \mathbf{V} + \frac{1}{2} \Delta \mathbf{V}^T \mathbf{H} \Delta \mathbf{V} + \varepsilon(\|\Delta \mathbf{V}\|^3) \quad (3.27)$$

Comparing the equations (3.14) and (3.27), it can be seen that the quadratic term related to Hessian matrix \mathbf{H} and also the higher order infinitesimal $\varepsilon(\|\Delta \mathbf{V}\|^3)$ are ignored. This simplification is used in the popular analytical models of the MTDC system in [34] and [57]. The second simplification is resulted from neglecting the variation of converter loss in (3.13). The converter loss of the state-of-the-art MMC HVDC technology is normally 1% of the total transmitted power and mainly depends on converter current [12]. Therefore, the variation of converter losses due to converter operating point change is even smaller than the converter losses. The third simplification is due to neglecting the quadratic variation terms of the voltages in (3.21) and (3.24). The error is only relevant to the DC nodes where DC line power flow control occurs. This error is similar to that of the first simplification since the quadratic voltage terms are ignored in these two simplifications. However, the third simplification is local to the DC nodes under DC line power flow control while the first simplification involves all the DC nodes in the MTDC system. These three simplifications can greatly reduce the computational burden of the proposed DC line power regulation method involving minor errors.

The Jacobian matrices can be updated after line disconnection from the original Jacobian matrix without any line disconnection. It is noted that communication between VSCs is needed to transmit the line disconnection information so that the original Jacobian matrix can be updated accordingly. It is assumed that line L was connected between DC nodes m and n . When line L is disconnected, we only need to update $J_{mm}, J_{nn}, J_{mn}, J_{nm}$ in the original Jacobian matrix \mathbf{J} . The equation to calculate the J_{mm} and J_{nn} is given in (3.17). Thus, the following elements in the Jacobian matrix after line disconnection can be derived as

$$J_{mm.new} = J_{mm.old} - g_{mn}(V_m + V_n) \quad (3.28)$$

$$J_{nn.new} = J_{nn.old} - g_{mn}(V_m + V_n) \quad (3.29)$$

where $J_{mm.old}$ and $J_{nn.old}$ are the original values of J_{mm} and J_{nn} before line disconnection; $J_{mm.new}$ and $J_{nn.new}$ are the values of J_{mm} and J_{nn} after line disconnection, g_{mn} is the mutual

conductance of the DC line connected between the two DC nodes m and n . V_m and V_n are the voltages at DC nodes m and n . It is noted that J_{mn} and J_{nm} are both zero after line disconnection. Therefore, the new Jacobian matrix after line disconnection can be updated from the original Jacobian matrix with little computational burden. Thus, it is feasible for a large system as only four terms in the Jacobian need to be updated.

It is noted that under line disconnection, communication between VSCs is needed. But the communication is very simple since it only needs to transmit the line disconnection information among VSC stations. This is different from the communication required by a centralized controller to compute the global DC power flow. Since the solution of global DC power flow in the secondary control layer is not required, the proposed control approach is still considered as an autonomous one based on primary control.

3.3 Case Studies

A five-terminal MTDC system, as shown in Figure 3-3, is implemented in MATLAB/Simulink Simscape/Specialized Technology Blockset and OPAL-RT RT-LAB libraries to verify the proposed DC line flow regulation method. The test system includes two offshore wind farms and three stiff AC grids represented by ideal voltage sources behind the impedances. The two offshore wind farms are connected to VSCs-3 and 5 operating in active power control mode. While the grid side VSCs-1, 2 and 4 are all in droop control mode. The VSC stations are realized with modular multilevel converters and are represented using average-value models [5], [62]. While the DC transmission lines utilize the distributed parameter line model in ARTEMiS Blockset of RT-LAB. The DC transmission line data and VSC parameters are given in Tables 3.1 and 2 [35] and 3 respectively. The DC line powers of the initial steady state are given in Figure 3-3. It is noted that DC line powers are reported at the sending ends.

The numerical solution from the DC power flow analysis of the initial steady state is given in Table 3.4. The DC voltage in Table 3.4 can be used to calculate the elements in the Jacobian matrix \mathbf{J} in (16). The static simulation of regulating DC line power under DC line disconnection is shown in Case *A*, while the dynamic simulation of DC line disconnection is given in Case *E*. Cases *B* and *C* demonstrate that the proposed autonomous control can regulate DC line powers under variations of power generation and converter outage.

Table 3.1 DC Transmission Line length

Line	1-2	1-3	1-4	1-5	2-3	3-4	4-5
<i>Length (km)</i>	80	200	125	160	160	160	250

Table 3.2 DC Line Data [35]

Parameter	R(Ω/km)	L(mH/km)	C($\mu F/km$)
<i>Value</i>	0.0100	0.1463	0.2662

Table 3.3 VSC Parameters

VSC Station Number	1	2	3	4	5
Rated Power P^r (MW)	650	650	800	650	750
Droop Coefficient R_i (kW/V)	12.7	25.4	0	50.8	0
Power Reference P_i^* (MW)	400	500	-400	600	-500

Table 3.4 DC Power Flow Solution

VSC Station Number	1	2	3	4	5
V_i (kV)	633.3	632.9	633.9	633.4	634.8
$P_{DC,i}$ (MW)	314.4	320.6	-400	263.3	-500

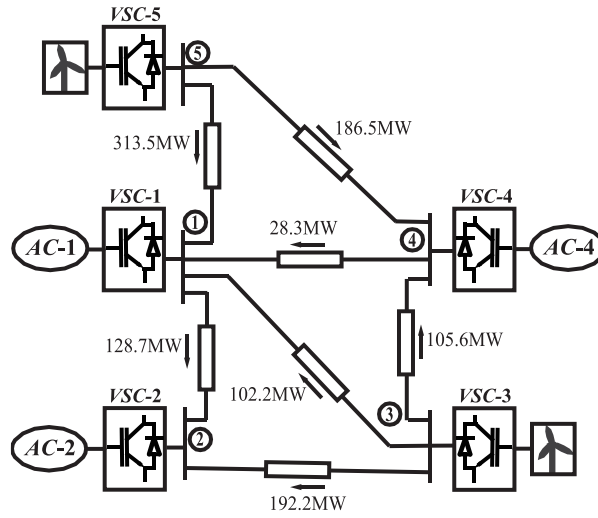


Figure 3-3 Five-terminal HVDC grid.

3.3.1 Static Simulation Results

In Case *A*, the autonomous control strategy is implemented to maintain the power flow of DC line 3–2 constant when DC line 1–3 is disconnected. The configuration of the HVDC grid, after disconnecting DC line 1–3, is illustrated in Figure 3-5. With the parameters listed in Tables 3.1, 2 and 4, the Jacobian matrix can be calculated from (3.17) and (3.18) as

$$J = \begin{bmatrix} 846.7 & -395.8 & 0 & -253.3 & -197.9 \\ -395.6 & 592.9 & -197.8 & 0 & 0 \\ 0 & -198.1 & 396.7 & -198.1 & 0 \\ -253.4 & 0 & -197.9 & 577.5 & -126.7 \\ -198.4 & 0 & 0 & -127.0 & 326.1 \end{bmatrix} \begin{matrix} \text{MW} \\ \text{kV} \end{matrix} \quad (3.30)$$

The dummy generators in Figure 3-4 are set to be $D1 = -102.1$ MW and $D2 = 102.2$ MW. ΔP_c^* in (3.19) is given by

$$\Delta P_c^* = [102.1, 0, -102.2, 0, 0]^T \text{MW} \quad (3.31)$$

At least one VSC is required to operate in the adaptive droop control mode for regulating one DC line power to assure that the system has enough degree of freedom for control. Without loss of generality, the voltage reference V_2^* of VSC-2 is set to be adaptive while VSCs-1 and 4 operate in fixed droop control mode. Combining (3.19) and (3.22), ΔV_2^* is calculated as 59.9 kV. The DC line powers under adaptive and fixed droop control of VSC-2 are given in Figure 3-4 by green and red colors, respectively. Comparing Figure 3-4 with Figure 3-3, it is seen that a significant power increase of DC line 3–2 is observed under fixed droop control after disconnecting DC line 1–3. On the contrary, the line power under adaptive droop control is very close to the original value with a minor error of 2.97%.

It is noted that instead of VSC-2, setting VSC-1 (Scenario I) or VSC-4 (Scenario II) in adaptive droop control mode can also regulate the targeted DC line power. The line powers of Scenarios I and II are given in Table 3.5. From Table 3.5 it can be observed that, the line powers 3–2 in both scenarios are kept nearly identical with small errors. This case study illustrates the effectiveness and flexibility of the proposed control method regulating the targeted DC line power by adapting the voltage reference of a droop controlled VSC.

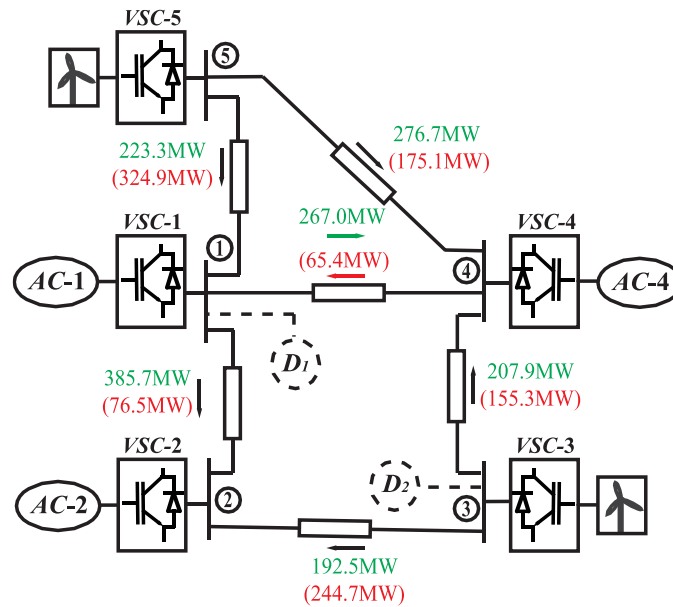


Figure 3-4 DC line power flow results with and without the proposed line flow regulation method.

Table 3.5 DC Line Powers of two Scenarios

DC Line Power (MW)	3-2	1-2	1-4	5-1	3-4	5-4
Scenario I	199.3	343.5	221.6	237.2	200.7	262.8
Scenario II	198.1	206.5	181.0	299.4	201.9	200.7

3.3.2 Single DC Line Power Regulation under Variation of Offshore Wind Farm Generation

Case *B* demonstrates that the proposed autonomous control can regulate DC line power under varying power generation. In this case, the power generation of the offshore wind farm connected to VSC-3 changes from -400 MW to -600 MW at $t = 1$ s. The autonomous control is enabled at $t = 2$ s, targeting to keep the power of DC line 3-2 constant. The voltage reference of the droop controlled VSC-2 is adaptive to realize the autonomous control of DC line power regulation.

The DC line powers are shown in Figures 3-5 (a) and (b). It is observed that the power of DC line 3-2 increased from 192.2 MW to 262.3 MW following the power variation of VSC-3 at $t = 1$ s. After the autonomous control is activated at $t = 2$ s, the power of DC line 3-2 is recovered to 193.7 MW, which is very close to its original value with an error of 0.78%. Additionally, the DC powers and voltages of VSC stations are shown in Figures 3-6 (a) and (b) respectively. It is noted that the transient responses of the autonomous control settle down quickly with minor overshoots in the DC powers and voltages. This is due to the fact that a smooth change of the voltage reference is implemented using an integrator block in Figure 3-2.

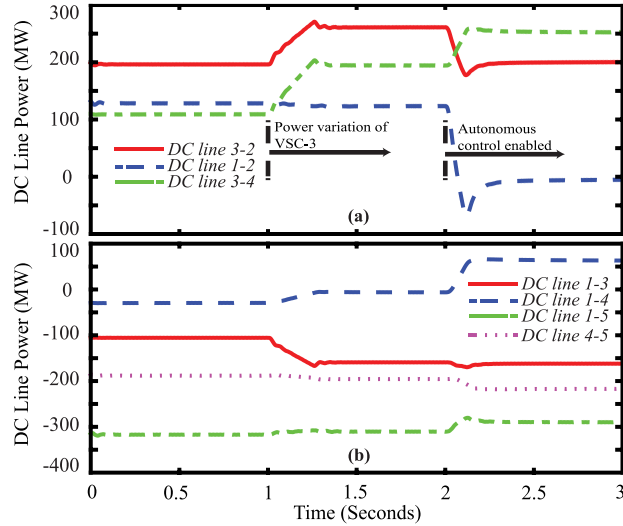


Figure 3-5 DC line powers under VSC-3 power variation.

(a) powers of DC lines 3-2, 1-2 and 3-4; (b) powers of DC lines 1-3, 1-4, 1-5 and 4-5.

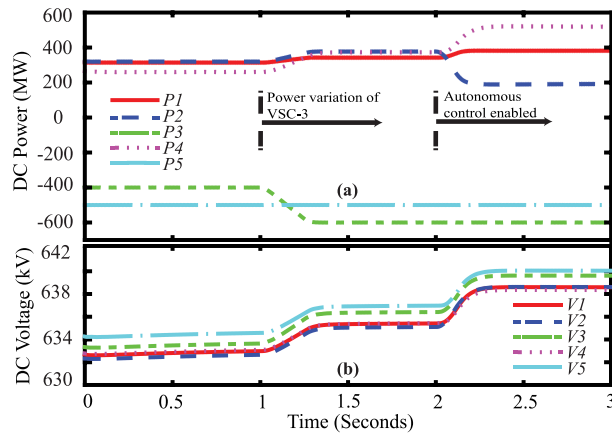


Figure 3-6 DC powers and voltages of VSCs under VSC-3 power variation.

(a) DC powers of the VSCs; (b) DC voltages of the VSCs.

3.3.3 Multiple DC Line Power Regulation under Converter Outage

In Case C, the proposed autonomous control approach is used to regulate two DC line powers simultaneously under a large system disturbance, i.e. converter outage. It is assumed that VSC-5 is forced into outage at $t = 0.5s$. The proposed DC line power regulation method is activated at $t = 1.5s$. According to the degree of freedom discussed in Subsection 3.2.5, at least two adaptive droop controlled VSCs are required to regulate two DC line powers. Therefore, the voltage references of droop controlled VSCs-1 and 2 are set to be adaptive. The powers of DC line 3-2 and 1-4 are kept constant. It is seen in Figures 3-7 (a) and (b) that noticeable drops of the powers of DC lines

3-2 and 1-4 occur when VSC-5 is tripped at $t = 0.5s$. After the proposed control is activated at $t = 1.5s$, the powers of the DC lines 3-2 and 1-4 are both recovered close to their original values with the minor errors of 0.31% and 0.54% respectively. It is also observed in Figures 3-7 and 8 that the DC line powers, converter powers, and node voltages experience minor transients after the autonomous control is activated since a smooth change of the voltage reference is implemented.

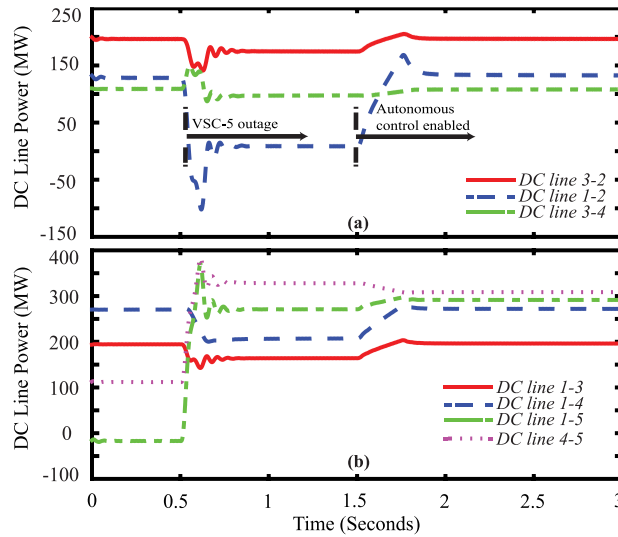


Figure 3-7 DC line powers under converter outage.

(a) powers of DC lines 3-2, 1-2 and 3-4; (b) powers of DC lines 1-3, 1-4, 1-5 and 4-5.

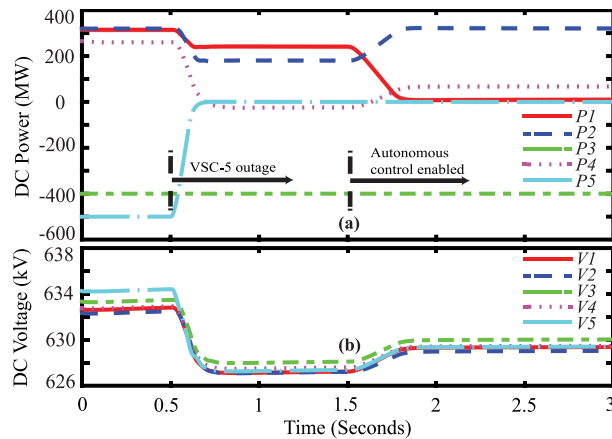


Figure 3-8 DC powers and voltages of VSCs under converter outage.

(a) DC powers of the VSCs; (b) DC voltages of the VSCs.

3.3.4 Multiple DC Line Power Regulation under Converter Outage

In this case study, the power generation of the offshore wind farm connected to VSC-5 increases from -500 MW to -750 MW at $t=0.5$ s. The proposed DC line power flow control method is activated at $t=1.5$ s. The DC line current and power limits for all the DC lines are given in Table 3.6. It is noted that the DC line power limits are calculated from their current limits using (25) and the nominal DC voltage of 640 kV.

The dynamic simulation results of the power variation, before and after the proposed autonomous control is activated, are illustrated in Figures 3-9 and 10. It is observed from Figure 3-9 that, following the power increase of VSC-5, the power of DC line 5-1 increases from 313.5 MW to 456.6 MW and the power of DC line 5-4 varies from 186.5 MW to 293.4 MW. It is noted that DC line 5-1 exceeds its DC line power limit (430 MW), while DC line 5-4 still has some extra capacity, given its power limit of 350 MW.

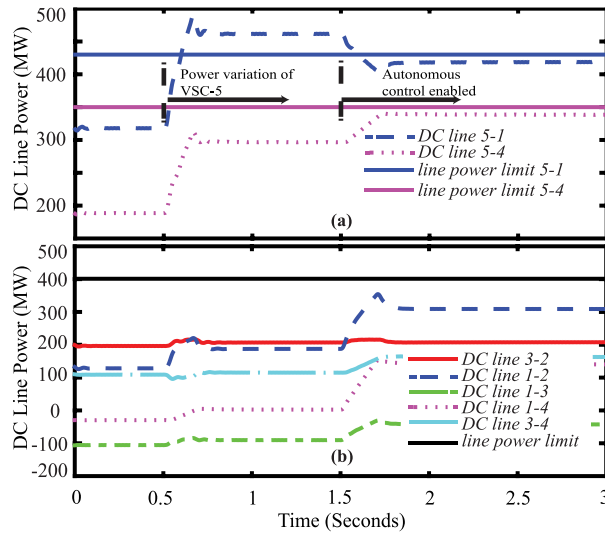


Figure 3-9 DC line powers under power increase of VSC-5.

(a) powers of DC lines 5-1 and 5-4; (b) powers of DC lines 3-2, 1-2, 1-3, 1-4 and 3-4.

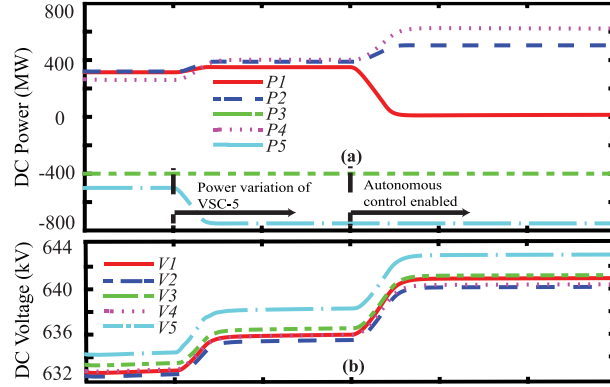


Figure 3-10 DC powers and voltages under power increase of VSC-5.

(a) DC powers of the VSCs; (b) DC voltages of the VSCs.

Table 3.6 DC Line Current and Power Limits

DC Line	3-2	1-2	1-4	5-1	3-4	5-4
Current Limit (A)	625	625	625	672	625	547
Power Limit (MW)	400	400	400	430	400	350

After the proposed DC line power control method is activated at $t = 1.5s$, it is observed in Figure 3-9 (a) that DC line powers 5-1 and 5-4 are shared nearly proportionally based on their power limits. Due to linearization in the proposed approach, the line power sharing errors of lines 5-1 and 5-4 are 0.70% and 0.86% respectively. Thus, all the DC line powers are within their power limits, as shown in Figures 3-9 (a) and (b). The DC power and voltage profiles are shown in Figures 3-10 (a) and (b) respectively. It is observed in Figure 3-10 (a) that the converter DC powers are all within their rated values given in Table 3.3 after the autonomous control is activated.

3.3.5 Disconnection of One DC Line

In this case, the DC line 3-4 is disconnected at $t = 0.5s$. The autonomous control is enabled at $t = 1.5s$, targeting to keep the power of DC line 3-2 constant. The voltage reference of the droop controlled VSC-2 is adaptive to realize the autonomous control of DC line power regulation. The DC line powers are shown in Figures 3-11 (a) and (b). It is observed that the power of DC line 3-2 increases from 192.2 MW to 251.3 MW due to the line disconnection. After the autonomous

control is activated, the power of DC line 3-2 is recovered to 198.3 MW, which is very close to its original value with a minor error of 3.17%. Moreover, the DC powers and voltages of VSC stations are within their limits, as shown in Figures 3-12 (a) and (b) respectively.

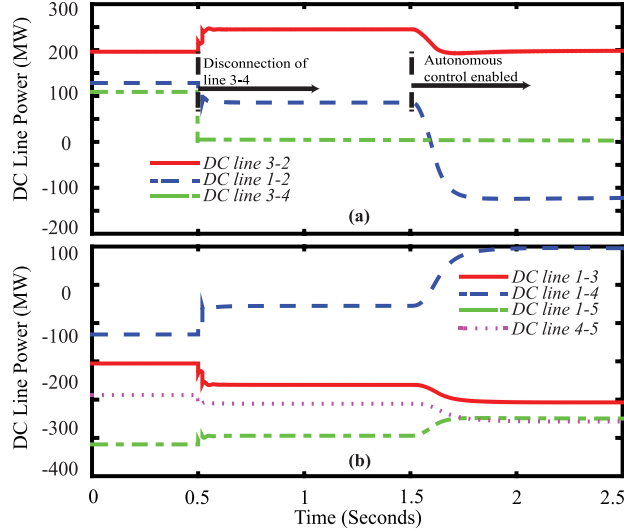


Figure 3-11 DC line powers under disconnection of line 3-4.

(a) powers of DC lines 3-2, 1-2, and 3-4; (b) powers of DC lines 1-3, 1-4, 1-5, and 4-5.

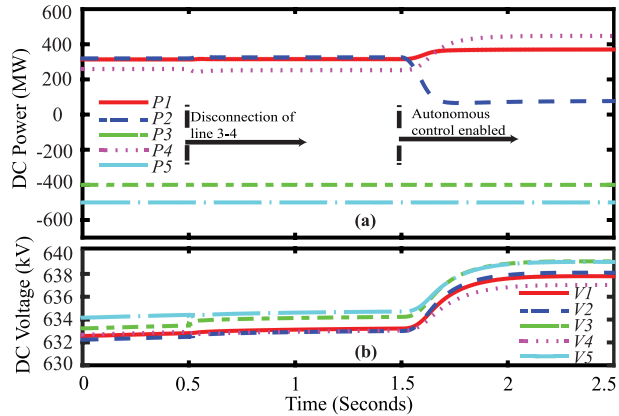


Figure 3-12 DC powers and voltages under disconnection of line 3-4.

(a) DC powers of the VSCs; (b) DC voltages of the VSCs.

3.4 Summary

In this chapter, a DC line power flow regulation method is proposed based on an improved HVDC grid analytical model and the adaptive droop control method. The proposed method can autonomously regulate the targeted DC line powers to the predefined values or share the powers

among DC lines proportionally without solving DC grid nonlinear power flow equations. The proposed control strategy can operate under various contingencies including converter outage, power variation, and DC grid topology change. Since the droop reference voltage is adaptive, the proposed autonomous control does not influence the stability of the DC grid. The proposed DC line power flow regulation strategy is validated under various contingencies using the study system of a five-terminal MTDC grid. The simulation results show that the proposed approach can regulate multiple DC line powers or share the DC line powers proportionally with minor errors.

4 Converter Power Sharing and Average Voltage Regulation in MTDC System

Based on the improved power flow methods proposed in Section II and the linearized model developed in Section III, this chapter discusses the converter power sharing and average voltage regulation in MTDC system. Autonomous³ and distributed⁴ control methods are proposed to regulate average DC voltage and share the converter power burden proportionally, using the adaptive droop control strategy. Then, a combined hierarchical and autonomous DC grid control scheme for proportional power sharing⁵ is proposed.

4.1 Autonomous Controls of Average Voltage and Converter Power Sharing in MTDC Grid

In this subsection, two autonomous control methods are proposed to regulate average DC voltage and share the power mismatch proportionally.

4.1.1 Steady-State Operation of MTDC System

In the following, the steady-state model of the VSC-MTDC system under the LVDC strategy is introduced. The generalized DC voltage droop control equation is represented as:

$$P_i - P_i^* + R_i(V_i - V_i^*) = 0 \quad (4.1)$$

where P_i and P_i^* are the actual and reference values of the AC-side power injection from the i^{th} VSC ($i \in \{1, \dots, n\}$ and n denotes the number of DC nodes), respectively; V_i and V_i^* are the actual and reference DC voltages, respectively; R_i is the droop coefficient of the i^{th} VSC in actual value, which can be calculated by

$$R_i = P_i^r k_i / V^r \quad (4.2)$$

³ **Yuanshi Zhang**, Liwei Wang and Wei Li, “Autonomous Controls of Average Voltage and Converter Power Sharing in MTDC Grid”, submitted to *IEEE Transactions on Power System*.

⁴ **Yuanshi Zhang**, Amin Shotorbani, Liwei Wang, and Wei Li, “Distributed Voltage Regulation and Automatic Power Sharing in Multi-Terminal HVDC Grids”, published in *IEEE Transactions on Power Systems*, vol. 35, no. 5, 2020.

⁵ **Yuanshi Zhang**, Amin M. Shotorbani, Liwei Wang and Wei Li, “A Combined Hierarchical and Autonomous DC Grid Control for Proportional Power Sharing with Minimized Voltage Variation and Transmission Loss”, submitted to *IEEE Transactions on Power Delivery*.

where k_i is the droop coefficient in per-unit; V^r and P_i^r are the nominal voltage and power rating. It is noted that R_i is positive for a VSC in droop control mode and $R_i = 0$ for a VSC in real power control mode. Additionally, if a DC node is not connected to a VSC, R_i and P_i^* are both set to zero.

The DC power equation is given by

$$P_{dc,i} = V_i \left(\sum_{j=1}^n G_{ij} V_j \right) \quad (4.3)$$

where G_{ij} is self- or mutual-conductance between node i and node j . The vector format of (4.3) is written by

$$\mathbf{P} = \mathbf{V} \otimes (\mathbf{G}\mathbf{V}) \quad (4.4)$$

where $\mathbf{P} = [P_i]_{n \times 1}$, $\mathbf{V} = [V_i]_{n \times 1}$ and $\mathbf{G} = [G_{ij}]_{n \times n}$. The symbol \otimes is an entry-wise matrix multiplication operator.

The relation between P_i and $P_{dc,i}$ is given by

$$P_i = P_{dc,i} + P_{C,Loss,i} \quad (4.5)$$

where $P_{C,Loss,i}$ is the converter loss, which can be calculated by a function of DC current $I_{dc,i}$ given as

$$P_{C,Loss,i} = a_i + b_i * I_{dc,i} + c_i * I_{dc,i}^2 \quad (4.6)$$

where a_i , b_i and c_i are constant, linear, quadratic coefficients of $I_{dc,i}$. $I_{dc,i}$ is given by

$$I_{dc,i} = \sum_{k=1}^n G_{ik} V_k \quad (4.7)$$

If there are x DC lines and n DC nodes in the MTDC system, the $x \times n$ matrix \mathbf{T} is defined as incidence matrix [57]. An element of \mathbf{T} , i.e. T_{pq} , equals to -1 , 0 or 1 . $T_{pq} = -1$ or 1 denotes that the defined line current of the p^{th} line enters or leaves the node q , while $T_{pq} = 0$ indicates that the p^{th} line is not connected to the node q . Therefore, DC line voltage vector \mathbf{U}_L can be expressed by

$$\mathbf{U}_L = \mathbf{T}\mathbf{V} \quad (4.8)$$

The DC grid transmission loss is given by

$$P_{G,Loss} = \mathbf{U}_L^T \otimes (\text{diag}(\mathbf{Y}_L) \mathbf{U}_L) \quad (4.9)$$

where \mathbf{Y}_L is the DC line conductance vector [57]. The average voltage of DC grid, defined as V_{avg} , is given by

$$V_{avg} = \frac{\sum_{i=1}^n V_i}{n} \quad (4.10)$$

4.1.2 Autonomous Controls of Average Voltage Regulation and Proportional Power Sharing

In order to regulate average DC voltage and realize proportional power sharing, the voltage reference of the droop controlled VSC is set to be adaptive to provide additional degree of freedom, while the droop coefficient and power reference are both unchanged. In this section, two novel algorithms are proposed to obtain the adaptive voltage reference autonomously. The first method is based on DC grid lossy model with LVDC strategy, while a modified common voltage droop control strategy is proposed as an alternative method to reduce the errors involved in the DC grid lossless model.

4.1.2.1 Proposed Method I

The proposed Method I adopts the DC grid lossy model with the LVDC strategy. It is assumed that the initial steady-state operating point of the i^{th} VSC ($i \in \{1, \dots, n\}$) is given by (4.1). Following unscheduled contingencies, let the variations of AC power and DC voltage of the i^{th} VSC be ΔP_i and ΔV_i respectively. ΔV_i^* and ΔP_i^* are the voltage and power reference variations respectively. The post-contingency operating point of the i^{th} droop controlled VSC station can be derived from (4.1) by

$$P_i + \Delta P_i - P_i^* - \Delta P_i^* + R_i(V_i + \Delta V_i - V_i^* - \Delta V_i^*) = 0 \quad (4.11)$$

Subtracting (4.11) from (4.1) yields

$$\Delta P_i = \Delta P_i^* + (\Delta V_i^* - \Delta V_i) R_i \mathbf{Y} \mathbf{V}(t) = \mathbf{I}_h(t - \Delta t) \quad (4.12)$$

It is noted that for the droop controlled VSCs, $\Delta P_i^* = 0$, while R_i and ΔV_i^* are both zero for the real power controlled VSCs.

The vector form of (4.12) is expressed as

$$\Delta \mathbf{P} = \Delta \mathbf{P}^* + \text{diag}(\mathbf{R})(\Delta \mathbf{V}^* - \Delta \mathbf{V}) \quad (4.13)$$

From (4.5), the variation of converter power injection to the AC grid is given by

$$\Delta \mathbf{P} = \Delta \mathbf{P}_{dc} + \Delta \mathbf{P}_{C,Loss} \quad (4.14)$$

where $\Delta \mathbf{P}_{dc}$ and $\Delta \mathbf{P}_{C,Loss}$ are the variations of converter power injection to DC grid and converter loss, respectively.

The post-contingency operating condition of VSC loss formula (4.6) is given by

$$P_{C,Loss,i} + \Delta P_{C,Loss,i} = a_i + b_i(I_{dc,i} + \Delta I_{dc,i}) + c_i(I_{dc,i} + \Delta I_{dc,i})^2 \quad (4.15)$$

Subtracting (4.14) from (4.6) and neglecting the quadratic variation term $c_i \Delta I_{dc,i}^2$ yield

$$\Delta P_{C,Loss,i} = (b_i + 2c_i) \Delta I_{dc,i} \quad (4.16)$$

The variation of DC current vector $\Delta I_{dc,i}$ can be obtained from (4.7) by

$$\Delta I_{dc,i} = \sum_{k=1}^n G_{ik} \Delta V_k \quad (4.17)$$

Substituting (4.17) into (4.16) and rewriting into vector form, one can obtain

$$\Delta \mathbf{P}_{C,Loss} = (\mathbf{b} + 2\mathbf{c}) \otimes (\mathbf{G} \Delta \mathbf{V}) \quad (4.18)$$

where $\mathbf{b} = [b_i]_{n \times 1}$ and $\mathbf{c} = [c_i]_{n \times 1}$.

The relation between the DC voltage variation $\Delta \mathbf{V}$ and DC power variation $\Delta \mathbf{P}_{dc}$ can be linearized by [34]

$$\Delta \mathbf{P}_{dc} = \mathbf{J} \Delta \mathbf{V} \quad (4.19)$$

where \mathbf{J} is the Jacobian matrix of the MTDC system.

Substituting (4.18) and (4.19) into (4.14) yields

$$\Delta \mathbf{P} = [(\mathbf{b} + 2\mathbf{c}) \otimes \mathbf{G} + \mathbf{J}] \Delta \mathbf{V} \quad (4.20)$$

By equating $\Delta \mathbf{P}$ in (4.13) and (4.20), the DC node voltage variation can be derived by

$$\Delta \mathbf{V} = [\mathbf{J} + (\mathbf{b} + 2\mathbf{c}) \otimes \mathbf{G} + \text{diag}(\mathbf{R})]^{-1} (\Delta \mathbf{P}^* + \text{diag}(\mathbf{R}) \Delta \mathbf{V}^*) \quad (4.21)$$

According to the power balance principle, one can obtain

$$\sum_{j=1}^m \Delta P_j + \Delta P_{\Sigma}^* + \sum_{i=1}^n \Delta P_{C,Loss,i} + \Delta P_{G,Loss} = 0 \quad (4.22)$$

where m denotes the number of droop controlled VSCs and $j \in \{1, \dots, m\}$; $\Delta P_{G,Loss}$ is the variation of DC grid loss; ΔP_{Σ}^* is the total power burden caused by unscheduled contingencies including fluctuation of renewable power generation and converter outage. It is noted that $\Delta P_{\Sigma}^* = \sum_{i=1}^n \Delta P_i^*$. Thus, (4.22) denotes that the power burden ΔP_{Σ}^* (together with the loss variations) caused by the contingencies are shared by the VSCs in LVDC strategy. Considering (4.16) and (4.17), $\sum_{i=1}^n \Delta P_{C,Loss,i}$ in (4.22) is given by

$$\sum_{i=1}^n \Delta P_{C,Loss,i} = \sum_{i=1}^n [(b_i + 2c_i) \sum_{k=1}^n G_{ik} \Delta V_k] \quad (4.23)$$

The post-contingency DC grid loss is obtained from (4.9) by

$$P_{G,Loss} + \Delta P_{G,Loss} = (\mathbf{U}_L + \Delta \mathbf{U}_L)^T \otimes (\text{diag}(\mathbf{Y}_L)(\mathbf{U}_L + \Delta \mathbf{U}_L)) \quad (4.24)$$

Subtracting (4.24) from (4.9) and neglecting the quadratic variation term give

$$\Delta P_{G,Loss} = 2\Delta \mathbf{U}_L^T \otimes (\text{diag}(\mathbf{Y}_L)\mathbf{U}_L) \quad (4.25)$$

From (4.8), $\Delta \mathbf{U}_L$ can be obtained by

$$\Delta \mathbf{U}_L = \mathbf{T}\Delta \mathbf{V} \quad (4.26)$$

Substituting (4.26) and (4.8) into (4.25) yields

$$\Delta P_{G,Loss} = 2(\mathbf{T}\Delta \mathbf{V})^T \otimes (\text{diag}(\mathbf{Y}_L)\mathbf{T}\mathbf{V}) \quad (4.27)$$

It is defined that

$$\Delta P_{\Sigma}^* + \sum_{i=1}^n \Delta P_{C,Loss,i} + \Delta P_{G,Loss} = P_{mis} \quad (4.28)$$

As can be seen from (4.23) and (4.27), $\sum_{i=1}^n \Delta P_{C,Loss,i}$ and $\Delta P_{G,Loss}$ are both functions of $\Delta \mathbf{V}$.

Moreover, ΔP_{Σ}^* is a known value, so that P_{mis} in (4.28) is also a function of $\Delta \mathbf{V}$.

The available headroom [28] of the j^{th} droop-controlled converter is expressed by

$$H_j = P_j^r - P_j \quad (4.29)$$

where H_j is the available headroom and P_j^r is the rated power of the VSC station.

If the power mismatch P_{mis} is shared according to the headroom H_j among the VSCs in LVDC, the relation between ΔP_j and P_{mis} is obtained by

$$\Delta P_j = -P_{mis} H_j / \left(\sum_{j=1}^m H_j \right) \quad (4.30)$$

For the j^{th} droop-controlled converter in LVDC ($j \in \{1, \dots, m\}$), (4.12) can be rewritten as

$$\Delta P_j = (\Delta V_j^* - \Delta V_j) R_j \quad (4.31)$$

Equating ΔP_j in (4.30) and (4.31) yields the relation between ΔV_j and ΔV_j^* as

$$\Delta V_j = \frac{P_{mis} H_j}{R_j \sum_{j=1}^m H_j} + \Delta V_j^* \quad (4.32)$$

It is noted that if all the 1th to $m-1$ th VSCs satisfy the power sharing constraint (4.30), the power mismatch ΔP_m of the m^{th} VSC in LVDC is automatically shared according to its headroom. Therefore, only $m-1$ number of equality constraints are needed for the power sharing control. If all the voltage references ΔV_j^* are set to be adaptive, there is one degree of freedom left to regulate the average DC voltage. The following expression of post-contingency DC average voltage regulation is written as

$$\Delta V_{avg} = \frac{\sum_{i=1}^n \Delta V_i}{n} = V_{avg,sch} - V_{avg,pre} \quad (4.33)$$

where ΔV_{avg} is the average voltage variation; $V_{avg,sch}$ and $V_{avg,pre}$ are the scheduled and initial average DC voltages.

Considering (4.32) and (4.33), the equation set to realize power sharing control and average voltage regulation is given by

$$\begin{bmatrix} \Delta V_1 \\ \vdots \\ \Delta V_{m-1} \\ \frac{\sum_{i=1}^n \Delta V_i}{n} \end{bmatrix} = \begin{bmatrix} \frac{P_{mis} H_1}{R_1 \sum_{j=1}^m H_j} + \Delta V_1^* \\ \vdots \\ \frac{P_{mis} H_{m-1}}{R_{m-1} \sum_{j=1}^m H_j} + \Delta V_{m-1}^* \\ V_{avg,sch} - V_{avg,pre} \end{bmatrix} \quad (4.34)$$

Finally, the DC voltage reference variation vector $\Delta \mathbf{V}^*$ can be calculated by combining (4.21) and (4.34).

4.1.2.2 Proposed Method II

In the ideal DC grid lossless model [61], [57], the DC voltages are assumed to be identical. Thus, (4.31) can be rewritten as

$$\Delta P_j = (\Delta V_j^* - \Delta V) R_j \quad (4.35)$$

where ΔV is the identical voltage variation.

This DC lossless model for the MTDC grid in LVDC strategy is a useful tool to estimate the power distribution of the MTDC system following a disturbance. However, it may involve large errors in post-contingency DC power and voltage estimation as the DC voltage in (4.25) is assumed to be identical [61], [57]. In [57], the authors point out that the ideal lossless model results in large errors when calculating the changes in DC voltages and powers. In addition, the errors are affected by the values of droop coefficients, line resistances, and types of the contingency.

The CVDC is expressed as

$$P_j - P_j^* + R_j(V_c - V_c^*) = 0 \quad (4.36)$$

where V_c is the common voltage feedback signal while V_c^* is its reference value [28], [39], [63]. It is noted that the common voltage V_c can be selected as the voltage of a certain pilot DC bus or a combination of several DC buses. In this subsection, V_c is assumed to be the DC grid average voltage to facilitate the average voltage regulation.

Using the CVDC can avoid the large errors involved in the LVDC strategy with the DC grid lossless model, because a common voltage feedback signal removes the local voltage dependence of the power sharing following a contingency [31]. The relationship between power variation ΔP_j and common voltage variation ΔV_c is given by

$$\Delta P_j = (\Delta V_c^* - \Delta V_c) R_j \quad (4.37)$$

Comparing (4.35) and (4.37), setting V_j^* of all the droop- controlled converters to be adaptive in (35) can provide m degree of freedom, while setting V_c^* to be adaptive in (4.37) can only provide one degree of freedom. Thus, the disadvantage of the CVDC is that it lacks degree of freedom for the adaptive droop control.

In this subsection, a modified common voltage droop control (MCVDC) is proposed, which is given by

$$P_j - P_j^* + R_j(V_c - V_j^*) = 0 \quad (4.38)$$

The relationship between power variation and common voltage variation in the MCVDC is given by

$$\Delta P_j = (\Delta V_j^* - \Delta V_c)R_j \quad (4.39)$$

Comparing (4.39) with (4.35) and (4.37), it can be seen that the MCVDC avoids the large errors involved in the DC grid lossless model with LVDC and at the same time provides as much degree of freedom as the LVDC.

As the proposed Method II adopts the DC grid lossless model, the variations of converter and DC grid losses are neglected. Thus, (4.22) can be rewritten as

$$\sum_{j=1}^m \Delta P_j + \Delta P_{\Sigma}^* = 0 \quad (4.40)$$

Substituting (4.39) into (4.40) gives

$$\Delta V_c = \left(\sum_{j=1}^m \Delta V_j^* R_j + \Delta P_{\Sigma}^* \right) / \left(\sum_{j=1}^m R_j \right) \quad (4.41)$$

Substituting (4.41) into (4.39) yields

$$\Delta P_j = \left[\Delta V_j^* - \left(\sum_{j=1}^m \Delta V_j^* R_j + \Delta P_{\Sigma}^* \right) / \sum_{j=1}^m R_j \right] R_j \quad (4.42)$$

Equating (4.30) and (4.42) yields the following equation system:

$$\begin{bmatrix} \Delta V_1^* \\ \Delta V_2^* \\ \vdots \\ \Delta V_m^* \end{bmatrix} = \begin{bmatrix} \left(\sum_{j=1}^m \Delta V_j^* R_j + \Delta P_{\Sigma}^* \right) / \sum_{j=1}^m R_j \\ \left(\sum_{j=1}^m \Delta V_j^* R_j + \Delta P_{\Sigma}^* \right) / \sum_{j=1}^m R_j \\ \vdots \\ \left(\sum_{j=1}^m \Delta V_j^* R_j + \Delta P_{\Sigma}^* \right) / \sum_{j=1}^m R_j \end{bmatrix} - \begin{bmatrix} \frac{\Delta P_{\Sigma}^* H_1}{R_1 (\sum_{j=1}^m H_j)} \\ \frac{\Delta P_{\Sigma}^* H_2}{R_2 (\sum_{j=1}^m H_j)} \\ \vdots \\ \frac{\Delta P_{\Sigma}^* H_m}{R_m (\sum_{j=1}^m H_j)} \end{bmatrix} \quad (4.43)$$

It is observed from the right hand side of (4.43) that the same term $(\sum_{j=1}^m \Delta V_j^* R_j + \Delta P_{\Sigma}^*) / \sum_{j=1}^m R_j$ is included in every equation. Therefore, (4.43) can be simplified by subtracting j^{th} row

($j \in \{1, \dots, m-1\}$) from $j+1^{\text{th}}$ row and m^{th} row from the 1^{st} row in (4.11), which yields the equivalent equation set

$$\begin{bmatrix} \Delta V_1^* - \Delta V_2^* \\ \Delta V_2^* - \Delta V_3^* \\ \vdots \\ -\Delta V_1^* + \Delta V_m^* \end{bmatrix} = - \begin{bmatrix} \frac{\Delta P_\Sigma^*}{\sum_{j=1}^m H_j} \left(\frac{H_1}{R_1} - \frac{H_2}{R_2} \right) \\ \frac{\Delta P_\Sigma^*}{\sum_{j=1}^m H_j} \left(\frac{H_2}{R_2} - \frac{H_3}{R_3} \right) \\ \vdots \\ \frac{\Delta P_\Sigma^*}{\sum_{j=1}^m H_j} \left(\frac{H_m}{R_m} - \frac{H_1}{R_1} \right) \end{bmatrix} \quad (4.44)$$

Extracting the coefficient matrix of (4.44) yields

$$\begin{bmatrix} 1 & -1 & 0 & \cdots & 0 \\ 0 & 1 & -1 & \cdots & 0 \\ & \vdots & & \ddots & \vdots \\ -1 & 0 & 0 & \cdots & 1 \end{bmatrix}_{m \times m} \quad (4.45)$$

As the rank of the $m \times m$ matrix (4.45) is $m-1$, matrix (4.45) is not a full rank matrix. Thus, there are non-unique solutions of (4.44). In other words, one degree of freedom exists in (4.44). Therefore, we can utilize this additional degree of freedom to regulate the DC average voltage. It is noted that the average DC voltage is selected to be the common voltage feedback signal V_c . Combining (4.33) and (4.41) gives

$$\frac{\sum_{j=1}^m \Delta V_j^* R_j + \Delta P_\Sigma^*}{\sum_{j=1}^m R_j} = V_{avg,sch} - V_{avg,pre} \quad (4.46)$$

Substituting (4.46) into (4.43), one can get the equation set with a unique solution as

$$\begin{bmatrix} \Delta V_1^* \\ \Delta V_2^* \\ \vdots \\ \Delta V_m^* \end{bmatrix} = \begin{bmatrix} V_{avg,sch} - V_{avg,pre} \\ V_{avg,sch} - V_{avg,pre} \\ \vdots \\ V_{avg,sch} - V_{avg,pre} \end{bmatrix} - \begin{bmatrix} \frac{\Delta P_\Sigma^* H_1}{R_1 (\sum_{j=1}^m H_j)} \\ \frac{\Delta P_\Sigma^* H_2}{R_2 (\sum_{j=1}^m H_j)} \\ \vdots \\ \frac{\Delta P_\Sigma^* H_m}{R_m (\sum_{j=1}^m H_j)} \end{bmatrix} \quad (4.47)$$

4.1.2.3 Control Scheme Diagram

The control diagram of the proposed autonomous power sharing and average voltage regulation based on adaptive voltage droop control is shown in Figure 4-1. The physical layer is composed of offshore wind farms (OWFs), wind farm VSCs (WFVSCs), AC grids, grid-side VSCs

(GSVSCs) and the MTDC system. The primary control layer consists of outer power control, inner current control (ICC) and the pulse width modulation (PWM). It is assumed that the WFVSCs are in real power control and AC voltage magnitude control modes for the d -axis and q -axis controls, respectively. The GSVSCs are in adaptive droop control and reactive power control modes for the d -axis and q -axis controls, respectively. The reference values of the d -axis and q -axis currents, i.e. i_d^* and i_q^* , are transmitted from the outer power controls to the ICCs.

It is noted that the adaptive droop voltage reference V^* is obtained from the proposed autonomous control layer and is calculated using either the proposed Method I or II, as shown Figure 4-1 by the switch position I or II, respectively. In the autonomous control layer, the output voltage reference variation ΔV^* is smoothed by an integral controller before transmitting to the primary layer to avoid large transient.

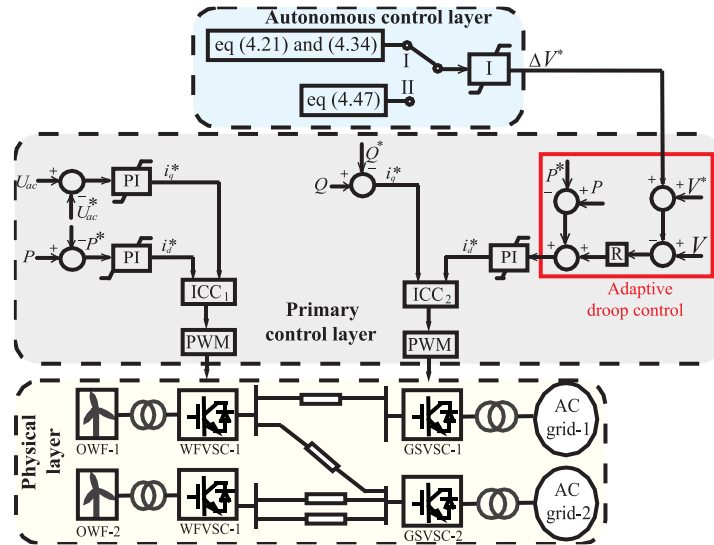


Figure 4-1 Control scheme diagram of the proposed autonomous control strategy.

4.1.2.4 Discussion

In order to compare the power sharing accuracy of the proposed Methods I and II, the power sharing error, i.e. P_{err} , is defined as

$$P_{err} = \left\| \Delta \mathbf{P} - \left(-\frac{\mathbf{H} P_{mis}^{ref}}{\sum_{j=1}^m H_j} \right) \right\|_1 / P^r \quad (4.48)$$

where P^r is the nominal power of the GSVSCs (since all the GSVSCs in the case study have the same power rating); \mathbf{H} is vector of the available headroom ($\mathbf{H} = [H_1, \dots, H_m]$). It is noted that P_{mis}^{ref}

is obtained by the accurate MTDC grid power flow result following the method proposed in [33] and is used as the benchmark in this work.

The average voltage regulation error V_{err} is given by

$$V_{err} = |V_{avg,sch} - V_{avg,post}|/V^r \quad (4.49)$$

where $V_{avg,sch}$ and $V_{avg,post}$ are the scheduled average voltage and post-contingency average voltage, respectively.

The errors, P_{err} and V_{err} , of the proposed Method I are due to the linearization of MTDC power flow in (4.19), while the errors of the proposed Method II are caused by neglecting the converter and grid loss variations in (4.40).

It is noted that the computational burden of the proposed Method II is much smaller than that of the proposed Method I since the proposed Method II adopts the DC grid lossless model and void calculating the Jacobian matrix \mathbf{J} and variations of DC grid and converter losses. However, the proposed Method II needs the communication among different VSC stations as the common voltage feedback signal V_c is used in the proposed MCVDC strategy.

Four types of contingencies are considered in this work, i.e. real power variation caused by the OWF power generation intermittency, real-power-controlled converter outage, droop-controlled converter outage, and DC line disconnection. It is straightforward to set $\Delta\mathbf{P}^*$ in (4.21) and ΔP_{Σ}^* in (4.22) for the first two types of disturbances. For the droop-controlled converter outage, the tripped converter is assumed to be a real power controlled converter (i.e., $R_i = 0$) at the initial steady state to keep $\text{diag}(\mathbf{R})$ in (4.21) unchanged before and after the contingency.

In the following, the method to set $\Delta\mathbf{P}^*$ and ΔP_{Σ}^* following DC line disconnection is discussed in detail. Assume that the line is disconnected at the initial state and two dummy generators are added at two ends of the disconnected line, respectively. The real power of the dummy generators is the same as the original line power injections. Thus, the topology change caused by a line disconnection is converted to real power variations of the two DC nodes. The corresponding elements in $\Delta\mathbf{P}^*$ are the negative values of the line power injections while ΔP_{Σ}^* equals to the initial copper loss of the disconnected transmission line.

4.1.3 Case Studies

4.1.3.1 System Configuration

A five-terminal VSC-MTDC system with OWFs is used to verify the proposed autonomous controls of average DC voltage regulation and power sharing, as shown in Figure 4-2. The MTDC system is implemented using MATLAB/Simulink Simscape/Specialized Technology Blockset and OPAL-RT RT-LAB libraries. Two OWFs and three AC grids represented by ideal voltage sources behind the impedances are connected to the MTDC system at VSCs-3 and 5 and VSCs-1, 2, and 4. The WFVSCs are under real power control mode, while the GSVSCs are under adaptive droop control mode. The VSC stations are represented by average-value model [5], [62] of modular multilevel converter (MMC).

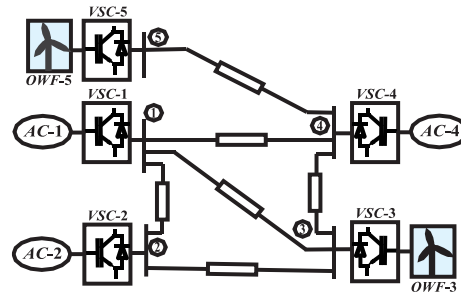


Figure 4-2 Single line diagram of the test system.

The DC cables are simulated using distributed parameter transmission line model in RT-LAB/ARTEMiS Blockset. The DC cable length and parameters as well as VSC station parameters are given in Tables 4.1, 2 and 4. The VSCs-1 and 2 are implemented using MMC with half-bridge submodules, while the other VSCs are implemented using MMC with full-bridge submodules. The converter loss coefficients in (4.6) are given in Table 4.4. Positive direction is assumed when real power is transmitted from DC grid to AC grid. The upper and lower DC voltage limits are 380 kV and 420 kV, respectively.

The performance of the autonomous controls of the proposed Methods I and II is verified using wind farm generation variation in Case A. Cases B demonstrates that the proposed autonomous controls can realize proportional power sharing and average voltage regulation under GSVSC outage. In Case C, the performance of the proposed autonomous control methods is verified under $N - 2$ contingency.

Table 4.1 DC Cable Length

Line	1-2	1-3	1-4	1-5	2-3	3-4	4-5
<i>Length (km)</i>	160	400	250	320	320	320	500

Table 4.2 DC Cable Parameter

Parameter	R(Ω/km)	L(mH/km)	C($\mu F/km$)
<i>Value</i>	0.0200	0.1463	0.2662

Table 4.3 VSC Station Parameter

VSC Station Number	1	2	3	4	5
Nominal Voltage V_i^r (kV)	400	400	400	400	400
Rated Power P_i^r (MW)	500	500	800	500	900
Droop Coefficient k_i (IN P.U.) [29]	0.1	0.0668	0	0.04	0
Power Reference P_i^* (MW)	400	500	-400	600	-500

Table 4.4 Converter Loss Coefficients (in P.U.) [33]

Submodule Type	a_{dc}	b_{dc}	c_{dc}
Half-bridge	8.800	4.000	0.473
Full-bridge		6.700	0.956

$\times 10^{-3}$

4.1.3.2 Case A : Variation of OWF Generation

Case A demonstrates that the proposed autonomous controls can share power proportionally and regulate DC average voltage to the nominal value under wind power generation variation. In Case A, the power generation of the OWF connected to VSC-5 increases from -500 MW to -850 MW at $t = 0.5$ s. The autonomous controls are activated at $t = 1$ s.

The DC powers, voltages and average voltage of VSCs under the proposed Methods I and II are given in Figures 4-3 and 4-4, respectively. It is observed from Figures 4-3 and 4-4 that the autonomous controls in Methods I and II produce similar results with small errors (shown in Table 4.5). From Figures 4-3 (a) and 4-4 (a), one can see that following the power increase of VSC-5, the power sharing of the VSCs-1, 2 and 4 under the fixed droop is not desirable as VSC-4 approaches the rated power and VSC-1 still has relatively large headroom. After the proposed autonomous controls are activated at $t = 1$ s, the active powers of the GSVSCs are shared proportionally to their headrooms. On the other hand, it can be seen from Figures 4-3 (b) and 4-4 (b) that the DC voltage profile increases following the power variation of the VSC-5. Especially, the voltage of the VSC-5 is near the upper voltage limit. As shown in Figures 4-3 (c) and 4-4 (c), the voltage profile increase is mitigated after the autonomous controls are enabled to regulate the average voltage to the nominal value. It is observed from Table 4.5 that V_{err} and P_{err} of the proposed Method II are smaller than those of the proposed Method I, indicating the proposed Method II is more accurate than the proposed Method I. This is because the error due to neglecting the converter and grid loss variations in (4.40) of the proposed Method II is smaller than the linearization error of MTDC power flow in (4.19) of the proposed Method I.

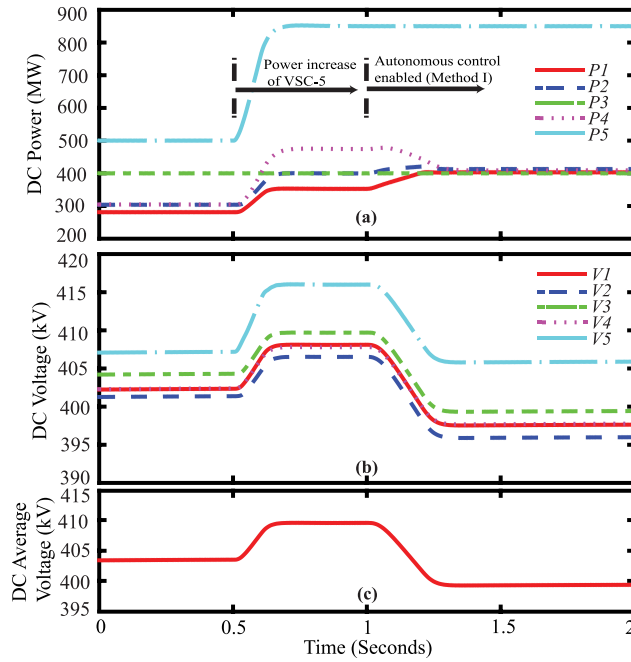


Figure 4-3 DC powers, voltages and average voltage of VSCs when VSC-5 power increases under the proposed Method I.

(a) DC powers of the VSCs; (b) DC voltages of the VSCs; (c) DC average voltage of VSCs.

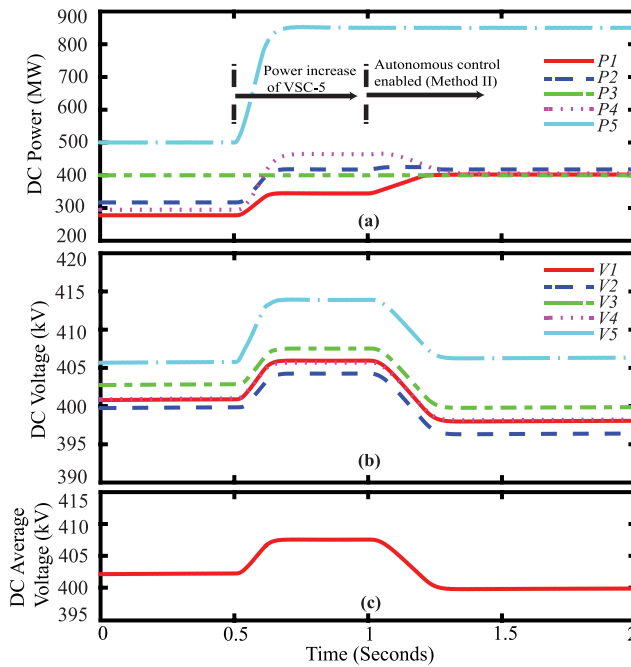


Figure 4-4 DC powers, voltages and average voltage of VSCs when VSC-5 power increases under the proposed Method II.

(a) DC powers of the VSCs; (b) DC voltages of the VSCs; (c) DC average voltage of VSCs.

Table 4.5 Comparison of Methods I and II under Power Variation

Method	I	II
V_{err} (%)	0.12	0.05
P_{err} (%)	1.86	0.82

4.1.3.3 Case B: GSVSC Outage

In Case B, the proposed autonomous control methods are applied to share power proportionally and regulate average DC voltage under a large system disturbance, i.e. GSVSC outage. In this case, VSC-2 is under forced outage at $t = 0.5$ s. The proposed autonomous controls are activated at $t = 1$ s. It is seen from Table 4.6 that the proposed Methods I and II can both realize the desirable power sharing control and voltage regulation with small errors. Similar to Case A, Method II is more accurate than Method I. Due to space limitation, only the DC powers, voltages and average voltage of VSCs of the proposed Method II are shown in Figure 4-5.

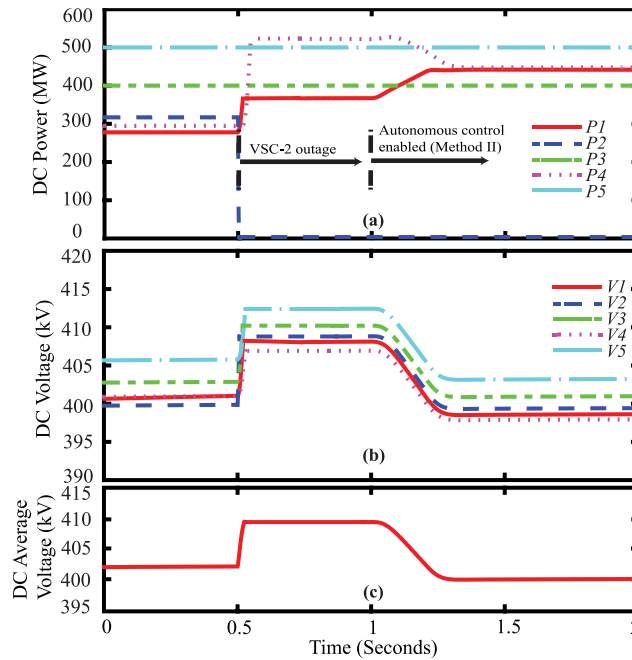


Figure 4-5 DC powers, voltages and average voltage of VSCs when VSC-2 is forced outage under the proposed Method II.

(a) DC powers of the VSCs; (b) DC voltages of the VSCs; (c) DC average voltage of VSCs.

Table 4.6 Comparison of Methods I and II under Converter Outage

Method	I	II
V_{err} (%)	0.11	0.03
P_{err} (%)	1.62	0.68

It is observed in Figure 4-5 (a) that the DC power of VSC-4 is overloaded following the VSC-2 outage while VSC-1 still has plenty of headroom. After the autonomous control is activated, the power burden caused by VSC-2 outage is proportionally shared by VSCs-1 and 4 according to their headrooms. It is seen in Figures 4-5 (b) and (c) that noticeable voltage increase occurs in the DC voltage profile when VSC-2 is tripped at $t = 0.5s$. After the proposed control is enabled at $t = 1s$, the increase of DC voltage profile is mitigated while the average DC voltage is regulated to the nominal value.

4.1.3.4 Case C: $N - 2$ Contingency

In Case C, the performance of the proposed autonomous control methods is validated under $N - 2$ contingency. VSC-1 is under forced outage at $t = 0.5s$. Moreover, the DC line 1-2 is tripped at $t = 0.5s$. The proposed autonomous control method is activated at $t = 1.5s$. From P_{err} and V_{err} listed in Table 4.7, it is observed that, both of the proposed methods are verified with small errors under $N - 2$ contingency. The DC powers, voltages and average voltage of VSCs under the proposed Method II are shown in Figure 4-6. It is observed from Figures 4-6 (a) and (b) that, VSCs-4 and 5 experience overload and overvoltage under the fixed droop control. After the autonomous control is activated at $t = 1.5s$, the DC power is shared proportionally while the average voltage is regulated close to the nominal value. Thus, overloading and overvoltage of the VSC stations are avoided by the proposed autonomous control methods.

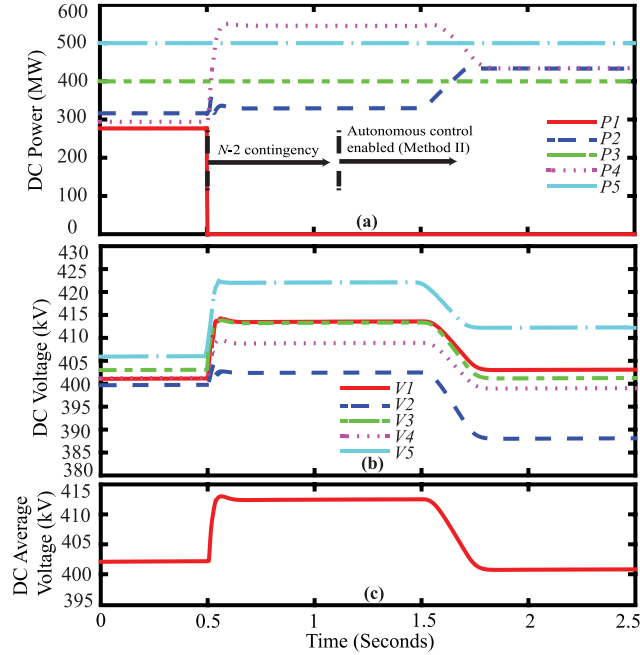


Figure 4-6 DC powers, voltages and average voltage of VSCs following N-2 contingency under the proposed Method II.

(a) DC powers of the VSCs; (b) DC voltages of the VSCs; (c) DC average voltage of VSCs.

Table 4.7 Comparison of Methods I and II under N-2 Contingency

Method	I	II
V_{err} (%)	0.19	0.13
P_{err} (%)	1.90	0.83

4.1.4 Summary

In this subsection, two autonomous control methods are proposed to regulate average DC voltage and share converter power burden proportionally, using adaptive droop control strategy. The proposed Method I utilizes the DC grid lossy model with the LVDC scheme, while the proposed Method II adopts an MCVDC strategy in the DC grid. The performance of the proposed autonomous control methods is verified using dynamic simulations under various disturbances, i.e., power variation, converter outage, and DC cable disconnection. Moreover, both $N - 1$ and $N - 2$ contingencies are included in the simulation studies. From the simulation results, it is observed that the proposed methods can realize average DC voltage regulation and power sharing

simultaneously with very small errors. The proposed Method II is more accurate than the proposed Method I although it requires the communication of common voltage signal among the VSC stations.

4.2 A Combined Hierarchical and Autonomous DC Grid Control for Proportional Power Sharing

This subsection presents a combined control scheme that consists of two complementary control strategies, namely hierarchical control and autonomous control to handle contingencies in a multi-terminal high voltage direct current (MTDC) system. The combined control framework is shown in Figure 4-7, with a two-layer hierarchical control scheme complemented by an autonomous control scheme. The hierarchical control is the normal operating strategy which requires communication to exchange information between the secondary and primary layers to properly configure the adaptive-droop voltage reference, as shown in Figure 4-7. However, during sudden operating point changes or critical contingencies, e.g. communication loss or rapid active power variation caused by renewable energy sources, e.g., wind power generation [65], the hierarchical control may not be able to update the adaptive voltage reference timely. Therefore, the autonomous control proposed in this section can be applied to enhance the overall control reliability and flexibility. The proposed autonomous power-sharing control can realize proper power sharing among the converters and regulate the DC-grid voltage profile within acceptable limits without the solution of DC power flow and the use of communication system. It comprises two parts, i.e., open-loop control and feedback control **which will be discussed in the subsection.**

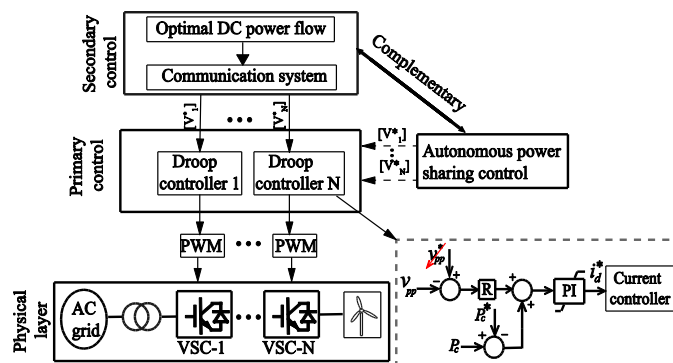


Figure 4-7 Combined control framework for an MTDC system.

4.2.1 Autonomous Power-Sharing Control in MTDC

4.2.1.1 Open-Loop Autonomous Power Sharing Control

Without loss of generality, two types of DC nodes are assumed in droop-controlled DC grid, i.e., active-power-controlled and droop-controlled nodes which can be represented by the unified power-voltage droop equation as

$$P_{c,i} - P_{c,i}^* + R_i(V_{pp,i} - V_{pp,i}^*) = 0 \quad (4.50)$$

where $P_{c,i}$ and $P_{c,i}^*$ are the actual and reference real powers injected to VSC from AC grid, respectively; $V_{pp,i}$ and $V_{pp,i}^*$ are the actual and reference pole-pole DC voltages, respectively; R_i is the real value droop coefficient, which can be defined as

$$P_{c,i} - P_{c,i}^* + R_i(V_{pp,i} - V_{pp,i}^*) = 0 \quad (4.51)$$

where P_i^r and v_i^r are the rated power and voltage of the i^{th} VSC, k_i is the per-unit droop coefficient for the i^{th} VSC.

It is assumed that the initial steady-state operating point of the i^{th} droop-controlled VSC is depicted as (4.50). As the DC system will reach to another steady-state operating point after a contingency, the post-contingency steady-state real power difference, DC voltage difference, and DC voltage reference difference are denoted by $\Delta P_{c,i}$, $\Delta V_{pp,i}$ and $\Delta V_{pp,i}^*$. It is assumed that the droop power reference $P_{c,i}^*$ and the droop coefficient R_i are kept constant. The post-contingency steady-state operating point can be expressed in terms of the initial steady-state condition as

$$P_{c,i} + \Delta P_{c,i} - P_{c,i}^* + R_i(V_{pp,i} + \Delta V_{pp,i} - \Delta V_{pp,i}^* - \Delta V_{pp,i}^*) = 0 \quad (4.52)$$

Since the virtual resistance of the droop constant reduces the sensitivity of the power sharing to DC line resistances [65], for the open-loop control, the ideal DC lossless model [34] is adopted for the droop-controlled nodes. That is to say, the DC voltages of droop controlled nodes are assumed to be identical. Therefore, we can use a unified ΔV_{pp} in place of $\Delta V_{pp,i}$ in (4.52). Subtracting (4.52) from (4.50), we can get

$$\Delta P_{c,i} = (\Delta V_{pp,i}^* - \Delta V_{pp}) R_i \quad (4.53)$$

According to the real power balance, we can obtain

$$\sum_{i=1}^n \Delta P_{c,i} + \Delta P^* + \Delta P_{loss} \quad (4.54)$$

where ΔP_{loss} is the transmission loss difference of prior- and post-contingency; ΔP^* is the variation of power reference.

There are mainly three types of contingencies considered in this subsection. The first one is power variation of active-power- controlled converter, which applies to the cases of power increase or decrease of offshore wind farms or loads. The second one is outage of active-power-controlled VSC. The third one is outage of droop-controlled VSC. For the first and second types, let the power difference of the active-power-controlled VSC before and after contingencies be ΔP^* . For the droop-controlled converter, we also use ΔP^* to represent the actual real power of the converter before the outage.

Substituting (4.53) into (4.54) and neglecting ΔP_{loss} , ΔV_{pp} can be expressed as

$$\Delta V_{pp} = \left(\sum_{i=1}^n (\Delta V_{pp,i}^* R_i) + \Delta P^* \right) / \sum_{i=1}^n R_i \quad (4.55)$$

Substituting (4.55) into (4.53), one can obtain

$$\Delta P_{c,i} = \left[\Delta V_{pp,i}^* - \left(\sum_{i=1}^n (\Delta V_{pp,i}^* R_i) + \Delta P^* \right) / \sum_{i=1}^n R_i \right] R_i \quad (4.56)$$

The autonomous control can realize equal power sharing locally even two types of communication, i.e., communication between the secondary and primary control layers, communication among different droop-controlled VSCs in the primary control layer, are both lost. Before the autonomous control is activated, ΔP^* can be estimated locally by each droop controlled VSC as the power mismatch $\Delta P_{c,i}$ is proportional to droop coefficient R_i when the identical voltage difference $\Delta V_{pp,pre}$ is assumed for the fixed droop control. Then, ΔP^* can be estimated locally as

$$\Delta P^* = -\Delta V_{pp,pre} \left(\sum_{i=1}^n R_i \right) \quad (4.57)$$

If ΔP^* is distributed equally among the remaining n droop-controlled VSC, one can expect the post-contingency power-sharing difference $\Delta P_{c,i}$ to be equal to the reference value of post-contingency power-sharing difference $\Delta P_{c,i}^{ref}$ as

$$\Delta P_{c,i} = \Delta P_{c,i}^{ref} = -\Delta P^*/n \quad (4.58)$$

Substituting (4.58) into (4.56) and rewriting it into matrix form:

$$\begin{bmatrix} \Delta V_{pp,1}^* \\ \Delta V_{pp,2}^* \\ \vdots \\ \Delta V_{pp,n}^* \end{bmatrix} - \begin{bmatrix} \left(\Delta P^* + \sum_{i=1}^n (\Delta V_{pp,i}^* R_i) \right) / \sum_{i=1}^n R_i \\ \left(\Delta P^* + \sum_{i=1}^n (\Delta V_{pp,i}^* R_i) \right) / \sum_{i=1}^n R_i \\ \vdots \\ \left(\Delta P^* + \sum_{i=1}^n (\Delta V_{pp,i}^* R_i) \right) / \sum_{i=1}^n R_i \end{bmatrix} = -\frac{\Delta P^*}{n} \begin{bmatrix} \frac{1}{R_1} \\ \frac{1}{R_2} \\ \vdots \\ \frac{1}{R_n} \end{bmatrix} \quad (4.59)$$

It is observed from (4.59) that the left-hand side of each equation contains $(\Delta P^* + \sum_{i=1}^n (\Delta V_{pp,i}^* R_i)) / \sum_{i=1}^n R_i$. Therefore, we can simplify (4.59) by subtracting its i^{th} row ($i \in \{1, \dots, n-1\}$) from $i+1^{\text{th}}$ row and n^{th} row with the first row of (4.59) as

$$\begin{bmatrix} \Delta V_{pp,1}^* - \Delta V_{pp,2}^* \\ \Delta V_{pp,2}^* - \Delta V_{pp,3}^* \\ \vdots \\ -\Delta V_{pp,1}^* + \Delta V_{pp,n}^* \end{bmatrix} = -\frac{\Delta P^*}{n} \begin{bmatrix} \frac{1}{R_1} - \frac{1}{R_2} \\ \frac{1}{R_2} - \frac{1}{R_3} \\ \vdots \\ \frac{1}{R_n} - \frac{1}{R_1} \end{bmatrix} \quad (4.60)$$

The coefficient matrix of the left side of (4.60) can be written as

$$\begin{bmatrix} 1 & -1 & 0 & \cdots & 0 \\ 0 & 1 & -1 & \cdots & 0 \\ \vdots & \vdots & \vdots & \ddots & \vdots \\ -1 & 0 & 0 & \cdots & 1 \end{bmatrix}_n \quad (4.61)$$

Obviously, the rank of (4.61) is $n-1$, which is not a full rank matrix. Therefore, (4.60) has infinite numbers of solutions and thus has one degree of freedom. To obtain a unique solution, we can define

$$\Delta P^* + \sum_{i=1}^n (\Delta V_{pp,i}^* R_i) = P_v \begin{bmatrix} 1 & -1 & 0 & \cdots & 0 \\ 0 & 1 & -1 & \cdots & 0 \\ & \vdots & & \ddots & \vdots \\ -1 & 0 & 0 & \cdots & 1 \end{bmatrix}_n \quad (4.62)$$

From (4.55), it can be seen that P_v has a proportional relationship with the voltage difference ΔV_{pp} . Therefore, P_v can be used for DC voltage regulation. If the DC voltage profile before contingency is within a user-defined boundary $[V_{min}, V_{max}]$, P_v is set to zero to reduce DC voltage variation after contingencies. On the other hand, if DC voltage profile before the contingency is close or even out of the voltage boundary, P_v can be adjusted to regulate the DC voltage after the contingency to be within the boundary.

Assume that $|V_{pp,l} - V_{nominal}| = \|[V_{pp,i} - V_{nominal}]_n\|_\infty$ where $V_{nominal}$ is the nominal DC voltage and $l \in \{1, \dots, n\}$. According to (4.55), P_{set} can be configured as

$$P_v = \begin{cases} -\|[V_{pp,i} - V_{nominal}]_n\|_\infty \sum_{i=1}^n R_i, & V_{pp,l} - V_{nominal} > 0 \\ \|[V_{pp,i} - V_{nominal}]_n\|_\infty \sum_{i=1}^n R_i, & otherwise \end{cases} \quad (4.63)$$

Therefore, (4.59) can be solved as

$$\begin{bmatrix} \Delta V_{pp,1}^* \\ \Delta V_{pp,2}^* \\ \vdots \\ \Delta V_{pp,n}^* \end{bmatrix} = \begin{bmatrix} \frac{P_v}{\sum_{i=1}^n R_i} - \frac{\Delta P^*}{nR_1} \\ \frac{P_v}{\sum_{i=1}^n R_i} - \frac{\Delta P^*}{nR_2} \\ \vdots \\ \frac{P_v}{\sum_{i=1}^n R_i} - \frac{\Delta P^*}{nR_n} \end{bmatrix} \quad (4.64)$$

When the communication between the secondary and primary control layers is lost but there is still communication among different VSC stations in the primary control layer, it is possible to realize proportional power sharing according to available headroom. The available headroom [29] is defined as

$$H_i = P_i^r - P_{c,i} \quad (4.65)$$

where P_i^r is the rated power of the i^{th} VSC.

Similar to (4.58), the post-contingency power-sharing difference $\Delta P_{c,i}$ should be equal to the reference value of post-contingency power-sharing difference $\Delta P_{c,i}^{ref}$ as

$$\Delta P_{c,i} = \Delta P_{c,i}^{ref} = -\Delta P^* H_i / \sum_{i=1}^n H_i H_i = P_i^r - P_{c,i} \quad (4.66)$$

Following similar derivation of (4.59)–(4.64), we can get

$$\begin{bmatrix} \Delta V_{pp,1}^* \\ \Delta V_{pp,2}^* \\ \vdots \\ \Delta V_{pp,n}^* \end{bmatrix} = \begin{bmatrix} \frac{P_v}{\sum_{i=1}^n R_i} - \frac{\Delta P^* H_1}{\sum_{i=1}^n H_i R_1} \\ \frac{P_v}{\sum_{i=1}^n R_i} - \frac{\Delta P^* H_2}{\sum_{i=1}^n H_i R_2} \\ \vdots \\ \frac{P_v}{\sum_{i=1}^n R_i} - \frac{\Delta P^* H_n}{\sum_{i=1}^n H_i R_n} \end{bmatrix} \quad (4.67)$$

It is noted that the proposed proportional power sharing control does not require the communication between the secondary and primary layers. But it needs the communication among different droop-controlled converters in the primary control layer to calculate the headrooms before contingencies.

4.2.1.2 Feedback-Control-Based Autonomous Power Sharing

As the open-loop control assumes DC voltages of droop-controlled converters to be identical, it involves small errors to achieve accurate power sharing. A feedback control is proposed along with the open-loop control to improve the accuracy and reliability of the autonomous power sharing control.

Figure 4-8 shows the feedback control to adapt the voltage reference setpoint of the droop-controlled converter. $\Delta V_{pp,i}^*$ is the adjustable voltage reference calculated by (4.64) or (4.67) in the open-loop control. $V_{pp-FB,i}^*$ is the droop voltage reference setpoint from the feedback control and is formulated as

$$V_{pp-FB,i}^* = (\Delta P_{c,i}^{ref} - \Delta P_{c,i}^{mea}) \left(K_p + \frac{K_i}{s} \right) + \Delta V_{pp,i}^* \quad (4.68)$$

where $\Delta P_{c,i}^{ref}$ is the reference value of post-contingency power-sharing difference, given in (4.58) or (4.66) where $\Delta P_{c,i}^{mea}$ is the measured post-contingency power-sharing difference.

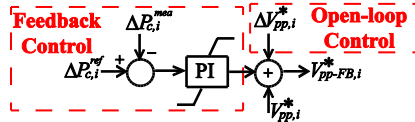


Figure 4-8 Autonomous control framework.

4.2.2 Autonomous Power-Sharing Control in MTDC

The autonomous power sharing control can achieve equal or proportional power sharing without the formulation and solution of global DC power flow which greatly reduces the computational cost and communication requirement. However, the autonomous power sharing control cannot realize optimal operations of DC grid, e.g., minimization of DC grid loss. On other hand, the hierarchical control can be used to achieve optimal DC power flow. Three optimization objectives (i.e. proportional power sharing, minimization of DC-grid loss and total DC voltage variation after contingency) are taken into account in the secondary control layer. Adaptive droop control strategy is utilized in the primary control layer. The three optimization targets can be realized separately, pairwise or simultaneously using linear scalarization method [24].

4.2.2.1 Hierarchical Control Framework

In this subsection, the hierarchical control scheme, shown in Figure 4-9, is elaborated in this section. The proposed hierarchical control consists of the primary and the secondary control layers. In the primary control layer, the voltage reference of a droop-controlled outer loop is adaptive. The voltage reference setpoint of a droop controller is obtained from the secondary control layer. In the secondary layer, the proposed DC power flow considering three optimization objectives (i.e. proportional power sharing, minimizations of DC-grid loss and total DC voltage variation after contingency) is implemented. The proposed optimal DC power flow calculates the voltage reference setpoints of the droop-controlled VSCs which are sent to the primary control layer via the communication system.

4.2.2.2 Optimization Targets

Three optimization targets can be considered separately, pairwise or simultaneously according to the operation requirements by the system operator. During contingencies, power sharing is normally considered to be the most important as undesirable power sharing may cause converter overloading, leading to detrimental effects on the VSCs and even unstable operation of the entire MTDC system. Therefore, proportional power sharing is realized by equality constraints

embedded in optimal DC power flow. Minimizations of DC-grid loss and the DC voltage variation are set to be the optimization objectives of the proposed optimal DC power flow, so that economic and secure operations of the MTDC system can be realized.

The degree of freedom is the difference between the amount of the variables and amount of equations in an optimization algorithm. The degree of freedom must be a non-negative number to ensure that the algorithm is solvable. Obviously, there is no additional degree of freedom in the conventional DC power flow under constant droop control scheme. If voltage reference setpoint $V_{pp,i}^*$ is set to be variable, one additional degree of freedom will be obtained for each droop-controlled VSC equation in adaptive droop control scheme. Now it is assumed that there are n number of droop-controlled VSCs after the contingency. Then, the total number of degree of freedom is also n .

Here, $n - 1$ number of constraints are added to the equation set of optimal DC power flow to realize equal power sharing, which can be written as

$$\begin{bmatrix} P_{c,post,1} - P_{c,pre,1} = P_{c,post,2} - P_{c,pre,2} \\ P_{c,post,2} - P_{c,pre,2} = P_{c,post,3} - P_{c,pre,3} \\ \vdots \\ P_{c,post,n-1} - P_{c,pre,n-1} = P_{c,post,n} - P_{c,pre,n} \end{bmatrix} \quad (4.69)$$

where $P_{c,pre,i}$ and $P_{c,post,i}$ are the active power before and after the contingency.

It is also desirable to share the power mismatch proportionally according to the available headroom. Then, (4.69) can be reformulated as

$$\begin{bmatrix} \frac{P_{c,post,1} - P_{c,pre,1}}{H_1} = \frac{P_{c,post,2} - P_{c,pre,2}}{H_2} \\ \frac{P_{c,post,2} - P_{c,pre,2}}{H_2} = \frac{P_{c,post,3} - P_{c,pre,3}}{H_3} \\ \vdots \\ \frac{P_{c,post,n-1} - P_{c,pre,n-1}}{H_{n-1}} = \frac{P_{c,post,n} - P_{c,pre,n}}{H_n} \end{bmatrix} \quad (4.70)$$

where the available headroom H_i is defined in (4.65). From the analysis above, it is noted that there is one additional degree of freedom in the DC power flow for which system optimization can be applied to minimize DC-grid transmission losses or DC voltage variation.

Since high efficiency of DC-grid power transmission is very desirable, minimization of DC-grid loss is chosen to be one of the objectives of the optimal DC power flow. The optimization problem is mathematically modeled as

$$\left\{ \begin{array}{l} \min(P_{loss}) = \sum_{i=1}^m \sum_{j=i+1}^m G_{ij} (V_{pp,i} - V_{pp,j})^2 \\ s. t. \mathbf{f}_1(\mathbf{P}_c, \mathbf{V}_{dc}) = \mathbf{0} \\ \mathbf{f}_2(\mathbf{P}_c) = \mathbf{0} \\ \mathbf{g}(\mathbf{P}_c, \mathbf{V}_{dc}) \leq \mathbf{0} \end{array} \right. \quad (4.71)$$

where G_{ij} is the conductance of the transmission line between nodes i and j ; m is the number of DC nodes existing in MTDC system and assuming that $i, j \in \{1, \dots, m\}$; $\mathbf{f}_1(\mathbf{P}_c, \mathbf{V}_{dc})$ is the DC power flow equation; $\mathbf{f}_2(\mathbf{P}_c)$ stands for the power sharing constraint (4.69) or (4.70); $\mathbf{g}(\mathbf{P}_c, \mathbf{V}_{dc})$ represents the inequalities, which include DC voltage limits, convert limits and DC current limits.

A contingency in DC grid brings DC voltage variation at post-contingency steady state. Smaller voltage variation will result in less impact on the DC grid. Optimal objective function is set up to optimize the RMS value of the DC voltage variation by

$$\min(V_{variation}) = \sqrt{\frac{1}{m} \sum_{i=1}^m (V_{pp,post,i} - V_{pp,pre,i})^2} \quad (4.72)$$

where $V_{pp,pre,i}$ and $V_{pp,post,i}$ are the DC voltage for the i^{th} node before and after the contingency.

Two optimization objectives have been introduced in the optimal DC power flow, i.e. minimizations of the DC-grid loss and the total DC voltage variation. Equal or proportional power sharing can be realized with either one of the objective functions in the optimal DC power flow. However, achieving one optimization target may have an adverse effect on the other one. In other words, when one optimization objective is realized by adaptive droop control, the other objective function may be worse than that of the fixed droop control. Therefore, it is desirable to take both objectives into consideration. If the two objective functions are combined, a tradeoff will be made between minimizations of the DC-grid loss and the total DC voltage variation, leading to multi-objective optimization.

In this work, linear scalarization [66] is adopted to deal with the abovementioned multi-objective problem. If the weighting factor is defined as w , the objective function can be expressed as

$$f_{obj} = w * \min(P_{loss}) + (1 - w) * \min(V_{variation}) \quad (4.73)$$

It is noted that w is selected by the system operator according to the actual optimization requirement. If the value of w increases, DC-grid loss will be reduced but with larger total DC voltage variation, and vice versa.

4.2.3 Case Studies

A five-terminal MTDC system [34], shown in Figure 4-9, is implemented in Matlab/Simulink/SimPowerSystems Toolbox for electro-magnetic transient (EMT) simulation to verify the proposed combined hierarchical and autonomous control strategy. VSCs-1, -2 and -4 are operated in droop control mode with the initial voltage reference to be the nominal voltage, i.e., 640 kV while VSCs-3 and -5 are in real power control mode with their droop coefficients to be zero. The AC grid is represented by AC Thevenin equivalent circuits. The proposed optimization problem (4.71) and (4.72) is implemented in Matlab using the nonlinear programming solver *fmincon* to find the optimal solution of constrained nonlinear multivariable functions.

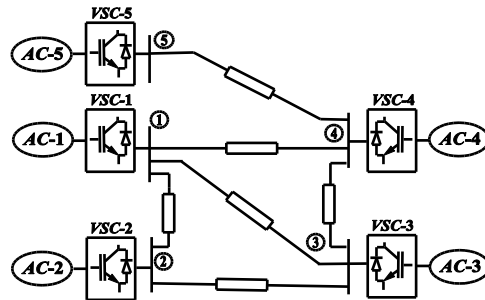


Figure 4-10 Five-terminal MTDC system.

4.2.3.1 Autonomous Power Sharing Control

In this case, the droop-controlled VSC-2 is forced outage at $t = 0.2$. Assuming that the communication between secondary layer and primary layer is lost. Thus, the hierarchical control strategy cannot work due to communication failure. In this situation, the autonomous control proposed is activated to proportionally share the power mismatch according to the available headrooms among the remaining droop controlled VSCs, i.e. VSCs-1 and -4. It is noted that equal power sharing among the VSCs can be regarded as a special case of proportional power sharing. Thus, the proportional power sharing is shown in the following study.

From Figure 4- 10 (a), it is observed that, after the outage of VSC-2, the DC power of VSC-4 exceeds its rated power (650MW), while there is still much surplus headroom for VSC-1. Thus, it is desirable if VSC-1 can share more power burden from VSC-4. It can be seen from Figure 4- 10 (b) that, the autonomous control is activated immediately following the VSC-2 outage. The power mismatch is shared nearly proportionally according to the available headrooms between VSCs-1 and -4. The DC powers of the VSCs are all within their rated values. The accurate power sharing result is used as benchmark in comparison with the results of the autonomous control and the fixed control in Table 4.8. It can be seen in Table 4.8 that the ratio of the power variation against its headroom ($\Delta P_{c,i}/H_i$) is not desirable under the fixed droop control, while $\Delta P_{c,i}/H_i$ is very close to the accurate result under autonomous control with feedback control

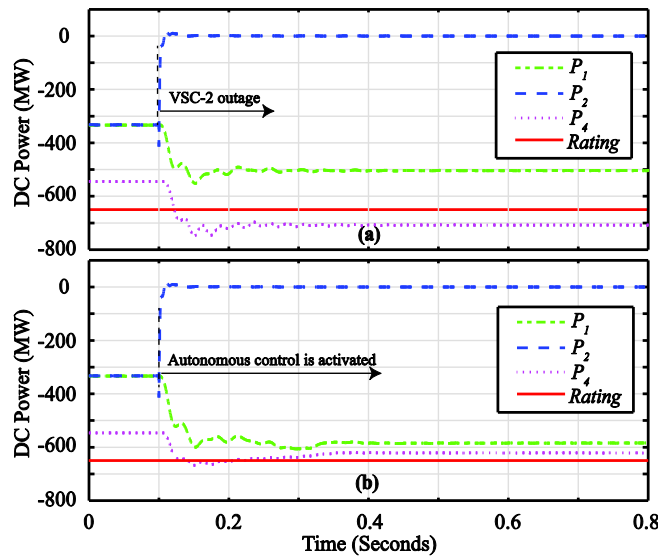


Figure 4-11 DC power of the droop-controlled VSCs under outage of VSC-2.

(a) Fixed droop control; (b) Autonomous control.

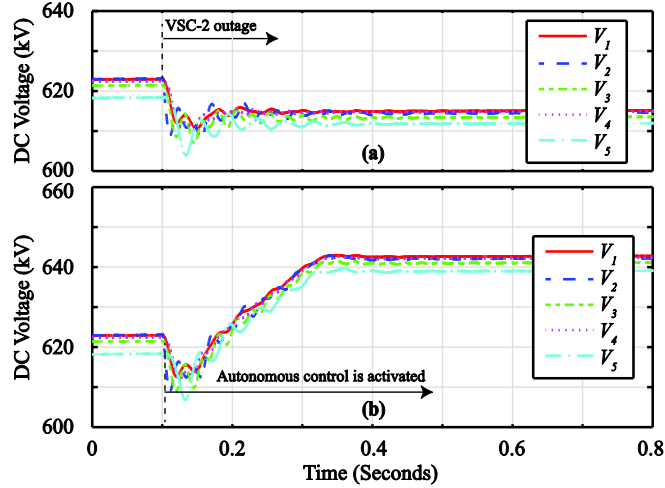


Figure 4-12 DC voltage of VSCs under outage of VSC-2.

(a) Fixed droop control; (b) Autonomous control.

It is assumed that the DC voltage boundary is within $\pm 2\%$ of the nominal DC voltage, i.e., $[0.98 \times 640 \text{ kV}, 1.02 \times 640 \text{ kV}]$. The DC voltage profile under the fixed droop control is shown in Figure 4- 11 (a) where the lowest DC voltage before the contingency is observed to be less than $0.97 \times 640 \text{ kV}$, below the lower boundary. The DC voltages further decrease after VSC-2 outage. On the other hand, Figure 4- 11 (b) illustrates that the DC voltages of all the VSCs are regulated around the nominal value under the autonomous control.

Table 4.8 Proportional Power Sharing Results of Autonomous Controls

VSC No.	Fixed Droop	Autonomous Control (open-loop)	Autonomous Control (feedback)	Accurate Result
	$\Delta P_{c,i}/H_i$	$\Delta P_{c,i}/H_i$	$\Delta P_{c,i}/H_i$	$\Delta P_{c,i}/H_i$
1	0.529	0.780	0.774	0.773
4	1.510	0.765	0.771	0.773

4.2.3.2 Hierarchical Power Sharing Control with Minimized Voltage Variation and Transmission Loss

The real power of VSC-5 increases by 250 MW, to its rated power. Proportional power sharing is achieved simultaneously with the other two objectives, i.e., minimizations of DC-grid loss and the total DC voltage variation. This operating scenario is selected because, when one realizes one of them by adaptive droop control strategy, the other one may be even worse than the results of fixed

droop control. The results of linear scalarization algorithm to solve this multi-objective optimization problem are demonstrated in this case.

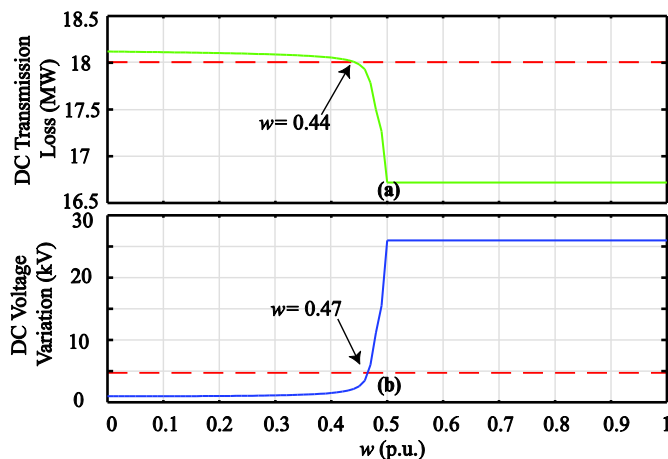


Figure 4-13 Relationships of DC-grid loss and DC voltage variation with w .

(a) DC-grid loss; (b) DC voltage variation.

Figure 4-12 (a) shows the relationship of DC-grid loss and the weighting factor w . The DC-grid loss keeps reducing and finally comes to a nearly constant value of around 16.7 MW when w goes from zero to one. In contrast, Figure 4-12 (b) witnesses an opposite tendency of the DC voltage variation. The red dashed lines in Figures 4-12 (a) and (b) stand for the DC-grid loss and voltage variation under fixed droop control, respectively. In order to make both the values of objectives smaller than those under fixed droop control, the desired value range of w is obtained as

$$0.44 < w < 0.47 \quad (4.74)$$

4.2.1 Summary

In this subsection, a combined control scheme composed of autonomous control and hierarchical control is proposed for the MTDC system. The autonomous control enables equal or proportional power sharing while regulating the voltage profile to the nominal value without communication system. However, it cannot realize optimization targets since optimal power flow is not used in the autonomous control. On the other hand, the hierarchical control can achieve accurate power sharing with various optimization targets, e.g., minimizations of voltage deviation and transmission loss, it requires communication system between the secondary and primary layers. Therefore, the two control schemes can operate in a complementary fashion in a generalized control framework.

A five-terminal MTDC system modeled in Matlab/Simulink demonstrates the effectiveness of the proposed control strategies. From the results of the case studies, it can be observed that the two control schemes can both realize desirable power sharing among the droop controlled VSCs. However, the autonomous control acts much faster than the hierarchical control as it does not require solving DC power flow and the communication system between primary and secondary layers. The hierarchical control is employed as the normal control strategy since it can realize various optimization targets in addition to desirable power sharing. During communication loss or rapid power variation caused by renewable energy sources, autonomous control is adopted to share the power mismatch among the droop controlled VSCs.

5 Concluding Chapter

5.1 Conclusion

Sustainable energy future calls for the development of large-scale onshore and offshore wind power generation. Offshore wind farms are growing rapidly due to the advantages of less wind variation and space restriction. Generally, offshore wind farms are located far away from the main AC grid. Therefore, a VSC MTDC system seems a more suitable solution than a high-voltage AC system because of its distinct advantages and flexible control capabilities. In the MTDC grid, the VSC stations use one of the three main control schemes: constant power mode, constant DC voltage mode, and the droop control mode. In the constant DC voltage control mode, when a converter outage occurs in the voltage control station, the stability of the MTDC grid is deteriorated significantly. In this case, the droop control scheme seems more reliable than the constant DC voltage control mode since the droop-controlled buses share the function of the DC slack bus, greatly alleviating the impact of converter outage. However, all variants of droop controls result in the deviation of the voltage from the nominal value in the steady state. On the other hand, system operators need to regulate the average voltage of the DC buses, especially for an MTDC grid with large power flow and long transmission distance. Another challenge of operating the MTDC grid is to automatically share the power demands among the converter stations after transients, in order to minimize the influence on the adjoining AC system. The objectives introduced in subsection 1.3 are achieved throughout this thesis as described in the following:

The **Objective 1**, which proposes two improved sequential power flow algorithms for AC-MTDC grid under DC power-voltage droop control, is accomplished in Chapter 2. The second proposed algorithm is based on the first one with higher efficiency and negligible errors. Compared to the conventional sequential power flow methods, it is shown that the proposed algorithms have much less computational burden than the existing approaches while maintaining their calculation accuracy under two types of system contingencies in the interconnected AC-MTDC grid consisting of an *IEEE* New England 39-bus AC grid integrated with a six-terminal MTDC grid. Additionally, based on the proposed AC-DC power flow methods, an optimization algorithm to minimize the total loss of the AC-DC grid or the DC voltage deviation after the change of operating conditions is proposed. The adaptive droop control strategy is used to achieve the optimization targets by dynamically adjusting the active power references of the droop-controlled MMC stations. The two

optimal targets can also be realized together with compromise by employing the linear scalarization method. The results of static and dynamic simulation studies verify the validity and feasibility of the proposed adaptive droop control based optimal power flow method. The static simulations show that two optimal targets, achieved by the proposed adaptive droop control strategy, are smaller than 100 random samples. The dynamic simulations demonstrate that the proposed optimization method can reduce 11.3% of system loss and 50% DC voltage deviation compared with the fixed droop control. The proposed OPF algorithm is based on the adaptive droop control scheme in which the OPF decision variables are the power references of the droop controlled converters. Therefore, the adaptive droop control method can realize the optimization targets without the negative impact on the stability of the AC-DC grid assuming that the system operating points experience small changes. The proposed power flow algorithms for AC-DC sequential power flow approach can also be applied to the unified power flow approach as well as the microgrid.

The **Objective 2**, which proposes a new method to regulate DC line power flow based on the adaptive DC voltage droop control strategy, is achieved in Chapter 3, where a DC line power flow regulation method is proposed based on an improved HVDC grid analytical model and the adaptive droop control method. The proposed method can autonomously regulate the targeted DC line powers to the predefined values or share the powers among DC lines proportionally without solving DC grid nonlinear power flow equations. The proposed control strategy can operate under various contingencies including converter outage, power variation, and DC grid topology change. The proposed DC line power flow regulation strategy is validated under various contingencies using the study system of a five-terminal MTDC grid. The simulation results, which are implemented using MATLAB/Simulink Simscape Blockset and OPAL-RT RT-LAB libraries show that the proposed approach can regulate multiple DC line powers or share the DC line powers proportionally with minor errors.

The **Objective 3**, which proposes novel autonomous control methods to regulate average DC voltage and share the power burden proportionally using the adaptive droop control strategy, is accomplished in Chapter 4. Firstly, two autonomous control methods are proposed to regulate average DC voltage and share converter power burden proportionally, using adaptive droop control strategy. The proposed Method I utilizes the DC grid lossy model with the LVDC scheme, while

the proposed Method II adopts an MCVDC strategy in the DC grid. The performance of the proposed autonomous control methods is verified using dynamic simulations under various disturbances, i.e., power variation, converter outage, and DC cable disconnection. Moreover, both $N - 1$ and $N - 2$ contingencies are included in the simulation studies. From the simulation results, it is observed that the proposed methods can realize average DC voltage regulation and power sharing simultaneously with very small errors. The proposed Method II is more accurate than the proposed Method I although it requires the communication of a common voltage signal among the VSC stations. Lastly, a combined control scheme composed of autonomous control and hierarchical control is proposed for the MTDC system. The autonomous control enables equal or proportional power sharing while regulating the voltage profile to the nominal value without communication system. However, it cannot realize optimization targets since optimal power flow is not used in the autonomous control. On the other hand, the hierarchical control can achieve accurate power sharing with various optimization targets, e.g., minimizations of voltage deviation and transmission loss, it requires communication system between the secondary and primary layers. Therefore, the two control schemes can operate in a complementary fashion in a generalized control framework.

5.2 Future Work

Based on the existing research, the following potential works are listed below to be realized in the future.

- **Frequency Support by Adaptive Droop Control Method**

Integrating wind turbines decreases the inherent inertia of the AC-MTDC grid, which will have adverse impact on the frequency stability of the interconnected AC-DC system. By incorporating the frequency deviation into the d-axis of the VSC inner current control loop, the adaptive droop control method can participate in frequency support for the weak-connected AC grids.

- **DC Line Flow Control with Insufficient Degree of Freedom**

The autonomous DC line flow method realized by adaptive droop control method proposed in Chapter 3 is based on the assumption that sufficient degree of freedom is provided by adaptive voltage references. In other words, the number of VSC stations utilizing the adaptive droop control scheme is greater than the controlled DC line powers. However, the proposed method cannot work

when there is insufficient degree of freedom. In this case, besides the voltage references, the droop coefficients/slopes also need to be adaptive. However, varying the droop slopes will affect the stability of the MTDC system. Thus, small signal stability and transient analyses of the AC-MTDC system are required to be performed for the adaptive droop control using droop slopes.

Bibliography

- [1] E. Prieto-Araujo, F. D. Bianchi, A. Junyent-Ferre, and O. Gomis-Bellmunt, “Methodology for droop control dynamic analysis of multiterminal VSC-HVDC grids for offshore wind farms,” *IEEE Trans. Power Del.*, vol. 26, no. 4, pp. 2476–2485, Oct. 2011.
- [2] N. R. Chaudhuri, R. Majumder, and B. Chaudhuri, “System frequency support through multi-terminal DC (MTDC) grids,” *IEEE Trans. Power Syst.*, vol. 28, no. 1, pp. 347–356, Feb. 2013.
- [3] C. Li et al., “Offshore wind farms integration and frequency support control utilizing hybrid multi-terminal HVDC transmission,” in *Proc. IEEE Ind. Appl. Soc. Annu. Meet.*, 2013, pp. 1–9.
- [4] S. Debnath, J. Qin, B. Bahrani, M. Saedifard, and P. Barbosa, “Operation, control, and applications of the modular multilevel converter: A review,” *IEEE Trans. Power Electron.*, vol. 30, no. 1, pp. 37–53, Jan. 2015.
- [5] H. Saad, K. Jacobs, W. Lin, and D. Jovcic, “Modelling of MMC including half-bridge and full-bridge submodules for EMT study,” in *Proc. Power Systems Computation Conference*, 2016, pp. 1–7.
- [6] H. Saad, S. Denetiere, J. Mahseredjian, P. Delarue, X. Guillaud, J. Peralta, and S. Nguefeu, “Modular multilevel converter models for electromagnetic transients,” *IEEE Trans. Power Del.*, vol. 29, no. 3, pp. 1481–1489, Jun. 2014.
- [7] V. Nasirian, A. Davoudi, F. Lewis, and J. Guerrero, “Distributed adaptive droop control for DC distribution systems,” *IEEE Trans. Energy Convers.*, vol. 29, no. 4, pp. 944–956, Dec. 2014.
- [8] K. Rouzbehi, A. Miranian, J. I. Candela, A. Luna, and P. Rodriguez, “A generalized voltage droop strategy for control of multiterminal DC grids,” *IEEE Trans. Ind. Appl.*, vol. 51, no. 1, pp. 607–618, Jan./Feb. 2015.
- [9] C. Dierckxsens, K. Srivastava, M. Reza, S. Cole, J. Beerten, and R. Belmans, “A distributed DC voltage control method for VSC MTDC systems,” *Elect. Power Syst. Res.*, vol. 82, no. 1, pp. 54–58, Oct. 2012.
- [10] T. M. Haileselassie and K. Uhlen, “Precise control of power flow in multiterminal VSC-HVDCs using DC voltage droop control,” in *Proc. IEEE Power Energy Soc. Gen. Meeting*, 2012, pp. 1–9.
- [11] X. Chen, L. Wang, H. Sun, and Y. Chen, “Fuzzy logic based adaptive droop control in multi-terminal HVDC for wind power integration,” *IEEE Trans. Energy Convers.*, vol. 32, no. 3, pp. 1200–1208, Sep. 2017.
- [12] J. Beerten, S. Cole, and R. Belmans, “Generalized steady-state VSC MTDC model for sequential AC/DC power flow algorithms,” *IEEE Trans. Power Syst.*, vol. 27, pp. 821–829, 2012.
- [13] W. Y. Wang and M. Barnes, “Power flow algorithms for multi-terminal VSC-HVDC with

- droop control,” *IEEE Trans. Power Syst.*, vol. 29, no. 4, pp. 1721–1730, Jul. 2014.
- [14] J. Beerten, D. V. Hertem, and R. Belmans, “VSC MTDC systems with a distributed DC voltage control—A power flow approach,” in *Proc. IEEE Trondheim PowerTech*, Jun. 2011, pp. 1–6.
- [15] M. Baradar and M. Ghandhari, “A multi-option unified power flow approach for hybrid AC/DC grids incorporating multi-terminal VSCHVDC,” *IEEE Trans. Power Syst.*, vol. 28, no. 3, pp. 2376–2383, Aug. 2013.
- [16] J. Lei, T. An, Z. Du, and Z. Yuan, “A general unified AC/DC power flow algorithm with MTDC,” *IEEE Trans. Pow. Syst.*, vol. 32, no. 4, pp. 2837–2846, Jul. 2017.
- [17] S. Khan and S. Bhowmick, “A generalized power flow model of VSC based hybrid AC-DC systems integrated with offshore wind farms”, *IEEE Trans. Sustain. Energy*, vol. 10, no. 4, pp. 1775-1783, Oct. 2019.
- [18] K. Rouzbehi, A. Miranian, A. Luna, and P. Rodriguez, “DC voltage control and power-sharing in multi-terminal DC grids based on optimal DC power flow and voltage-droop strategy,” *IEEE J. Emerging Sel. Topics Power Electron.*, vol. 2, no. 4, pp. 1–10, Dec. 2014.
- [19] J. Khazaei, Z. Miao, L. Piyasinghe, and L. Fan, “Minimizing DC system loss in multi-terminal HVDC systems through adaptive droop control,” *Elect. Power Syst. Res.*, vol. 126, pp. 78–86, 2015.
- [20] S. Rodrigues, R. T. Pinto, P. Bauer, and J. Pierik, “Optimal power flow control of VSC-based multiterminal DC network for offshore wind integration in the north sea,” *IEEE J. Emerg. Sel. Topics Power Electron.*, vol. 1, no. 4, pp. 260–268, Dec. 2013.
- [21] R. Wiget and G. Andersson, “Optimal power flow for combined AC and multi-terminal HVDC grids based on VSC converters,” in *Proc. IEEE Power Energy Soc. General Meeting*, San Diego, CA, USA, Jul. 2012, pp. 1–8.
- [22] S. Bahrami, F. Therrien, V. W. S. Wong and J. Jatskevich, "Semidefinite relaxation of optimal power flow for AC–DC grids," *IEEE Trans. Power Syst.*, vol. 32, no. 1, pp. 289-304, Jan. 2017.
- [23] M. K. Kim, “Multi-objective optimization operation with corrective control actions for meshed AC/DC grids including multi-terminal VSCHVDC,” *Int. J. Electr. Power Energy Syst.*, vol. 93, pp. 178–193, Dec. 2017.
- [24] H. Ergun, J. Dave, D. Van Hertem and F. Geth, "Optimal power flow for AC–DC grids: formulation, convex relaxation, linear approximation, *IEEE Trans. Power Syst.*, vol. 34, no. 4, pp. 2980-2990, July 2019.
- [25] M. Hotz and W. Utschick, "hynet: An optimal power flow framework for hybrid AC/DC power systems," *IEEE Trans. Power Syst.*, vol. 35, no. 2, pp. 1036-1047, March 2020.
- [26] N. Meyer-Huebner, M. Suriyah and T. Leibfried, "Distributed optimal power flow in hybrid AC–DC grids," *IEEE Trans. Power Syst.*, vol. 34, no. 4, pp. 2937-2946, July 2019.
- [27] Z. Yang, H. Zhong, A. Bose, Q. Xia, and C. Kang, “Optimal power flow in AC–DC grids

- with discrete control devices,” *IEEE Trans. Power Syst.*, vol. 33, no. 2, pp. 1461–1472, Mar. 2018.
- [28] N. R. Chaudhuri and B. Chaudhuri, “Adaptive droop control for effective power sharing in multi-terminal DC (MTDC) grids,” *IEEE Trans. Power Syst.*, vol. 28, no. 1, pp. 21–29, Feb. 2013.
- [29] A. Yogarathinam and N. R. Chaudhuri, “Stability-constrained adaptive droop for power sharing in AC-MTDC grids,” *IEEE Trans. Power Syst.*, vol. 34, no. 3, pp. 1955–1965, May 2019.
- [30] Y. Wang, W. Wen, C. Wang, H. Liu, X. Zhan, and X. Xiao, “Adaptive voltage droop control of multiterminal VSC-HVDC systems for DC voltage deviation and power sharing,” *IEEE Trans. Power Del.*, pp. 169–176, 2018.
- [31] J. Beerten and R. Belmans, “Analysis of power sharing and voltage deviations in droop-controlled DC grids,” *IEEE Trans. Power Syst.*, vol. 28, no. 4, pp. 4588–4597, Nov. 2013.
- [32] Y. Li, Y. Li, G. Li, D. Zhao, and C. Chen, “Two-stage multi-objective OPF for AC/DC grids with VSC-HVDC: Incorporating decisions analysis into optimization process,” *Energy*, vol. 147, pp. 286–296, Mar. 2018.
- [33] J. Beerten, S. Cole, and R. Belmans, “Implementation aspects of a sequential AC/DC power flow computation algorithm for multi-terminal VSC HVDC systems,” *Proc. IET ACDC ’10*, London, U.K., Oct., 2010.
- [34] T. M. Haileselassie and K. Uhlen, “Impact of DC Line voltage drops on power flow of MTDC using droop control,” *IEEE Trans. Power Syst.*, vol. 27, no. 3, pp. 1441–1449, Aug. 2012.
- [35] B. Berggren, K. Lindén, and R. Majumder, “DC grid control through the pilot voltage droop concept—methodology for establishing droop constants,” *IEEE Trans. Power Syst.*, vol. 30, no. 5, pp. 2312–2320, Sep. 2015.
- [36] J. M. Guerrero, J. C. Vasquez, J. Matas, L. G. de Vicuña, and M. Castilla, “Hierarchical control of droop-controlled AC and DC microgrids—a general approach toward standardization,” *IEEE Trans. Ind. Electron.*, vol. 58, no. 1, pp. 158–172, Jan. 2011.
- [37] P.-H. Huang, P.-C. Liu, W. Xiao, and M. S. El Moursi, “A novel droop based average voltage sharing control strategy for DC microgrids,” *IEEE Trans. Smart Grid*, vol. 5, no. 5, pp. 1096–1106, Sep. 2014.
- [38] R. Teixeira Pinto, P. Bauer, S. F. Rodrigues, E. J. Wiggelinkhuizen, J. Pierik, and B. Ferreira, “A novel distributed direct-voltage control strategy for grid integration of offshore wind energy systems through MTDC network,” *IEEE Trans. Ind. Electron.*, vol. 60, no. 6, pp. 2429–2441, Jun. 2013.
- [39] B. Berggren, R. Majumder, C. Sao, and K. Linden, Method and Control Device for Controlling Power Flow Within a dc Power Transmission Network, WIPO International Publication Number WO 2012/000549.
- [40] P. Rault, F. Colas, X. Guillaud, and S. Nguéfeu, “Method for small signal stability analysis

- of VSC-MTDC grids,” in *Proc. IEEE Power Energy Soc. Gen. Meet.*, San Diego, CA, USA, Jul. 2012, pp. 1–7.
- [41] W. Du, Q. Fu, and H. F. Wang, “Comparing AC dynamic transients propagated through VSC HVDC connection with master slave control vs DC voltage droop control,” *IEEE Trans. Sustain. Energy*, vol. 9, no. 3, pp. 1285–1297, July 2018.
- [42] C. Gavriluta, I. Candela, A. Luna, A. Gomez-Exposito, and P. Rodriguez, “Hierarchical control of HV-MTDC systems with droop-based primary and OPF-based secondary,” *IEEE Trans. Smart Grid*, vol. 6, no. 3, pp. 1502–1510, May 2015.
- [43] R. Eriksson, “On the centralized nonlinear control of HVDC systems using Lyapunov theory,” *IEEE Trans. Power Del.*, vol. 28, no. 2, pp. 1156–1163, Apr. 2013.
- [44] Y. Wen, J. Zhan, C. Chung, and W. Li, “Frequency stability enhancement of integrated AC/VSC-MTDC systems with massive infeed of offshore wind generation,” *IEEE Trans. Power Syst.*, pp. 1–10, Jan. 2018.
- [45] P. Wang, N. Deng, and X.-P. Zhang, “Droop control for a multi-line current flow controller in meshed multi-terminal HVDC grid under large DC disturbances,” *IEEE Power Energy Technol. Syst. J.*, vol. 5, no. 2, pp. 35–46, Jun. 2018.
- [46] K. Rouzbehi, J. I. Candela, A. Luna, G. B. Gharehpetian, and P. Rodriguez, “Flexible control of power flow in multiterminal dc grids using dc–dc converter,” *IEEE J. Emerg. Sel. Topics Power Electron.*, vol. 4, no. 3, pp. 1135–1144, Sep. 2016.
- [47] Q. Mu, J. Liang, Y. Li, and X. Zhou, “Power flow control devices in dc grids,” in *Proc. IEEE Power Energy Soc. Gen. Meeting*, 2012, pp. 1–7.
- [48] E. Veilleux and B.-T. Ooi, “Multiterminal HVDC with thyristor powerflow controller,” *IEEE Trans. Power Del.*, vol. 27, no. 3, pp. 1205–1212, Jul. 2012.
- [49] D. Jovicic, M. Hajian, H. Zhang, and G. Asplund, “Power flow control in DC transmission grids using mechanical and semiconductor based DC/DC devices,” in *Proc. IEEE ACDC*, Dec. 2012, pp. 1–6.
- [50] J. Yang, Z. He, H. Pang, and G. Tang, “The hybrid-cascaded dc-dc converters suitable for HVDC applications,” *IEEE Trans. Power Electron.*, vol. 30, no. 10, pp. 5358–5363, Oct. 2015.
- [51] J. Sau-Bassols, E. Prieto-Araujo, and O. Gomis-Bellmunt, “Modelling and control of an interline current flow controller for meshed HVDC grids,” *IEEE Trans. Power Del.*, vol. 32, no. 1, pp. 11–22, Feb. 2017.
- [52] W. Chen et al., “A novel interline DC power-flow controller (IDCPFC) for meshed HVDC grids,” *IEEE Trans. Power Del.*, vol. 31, no. 4, pp. 1719–1727, Aug. 2016.
- [53] M. Ranjram and P. W. Lehn, “A multiport power-flow controller for DC transmission grids,” *IEEE Trans. Power Del.*, vol. 31, no. 1, pp. 389–396, Feb. 2016.
- [54] S. Balasubramaniam, C. E. Ugalde-Loo, J. Liang, T. Joseph, R. King, and A. Adamczyk, “Experimental validation of dual H-bridge current flow controllers for meshed HVdc

- grids,” *IEEE Trans. Power Del.*, vol. 33, no. 1, pp. 381–392, Feb. 2018.
- [55] K. Rouzbehi, S. S. H. Yazdi, and N. S. Shariati, “Power flow control in multi-terminal HVDC grids using a serial-parallel DC power flow controller,” *IEEE Access*, vol. 6, pp. 56934–56944, 2018.
- [56] Mehdi Abbasipour, et al. "Power injection model of IDC-PFC for NR-based and technical constrained MT-HVDC grids power flow studies" Elsevier, *Electric Power Systems Research*, 2020.
- [57] L. Xiao, Z. Xu, T. An, and Z. Bian, “Improved analytical model for the study of steady state performance of droop-controlled VSC-MTDC systems,” *IEEE Trans. Power Syst.*, vol. 32, no. 3, pp. 2083–2093, May 2017.
- [58] C. Gavriluta, J. I. Candela, J. Rocabert, A. Luna, and P. Rodriguez, “Adaptive droop for control of multiterminal DC bus integrating energy storage,” *IEEE Trans. Power Del.*, vol. 30, no. 1, pp. 16–24, Feb. 2015.
- [59] M. A. Abdelwahed and E. F. El-Saadany, “Power sharing control strategy of multiterminal VSC-HVDC transmission systems utilizing adaptive voltage droop,” *IEEE Trans. Sustain. Energy*, vol. 8, no. 2, pp. 605–615, Apr. 2017.
- [60] R. Eriksson, J. Beerten, M. Ghandhari, and R. Belmans, “Optimizing DC voltage droop settings for AC/DC system interactions,” *IEEE Trans. Power Del.*, vol. 29, no. 1, pp. 362–369, Feb. 2014.
- [61] Y. Wang, W. Wen, C. Wang, H. Liu, X. Zhan and X. Xiao, "Adaptive Voltage Droop Method of Multiterminal VSC-HVDC Systems for DC Voltage Deviation and Power Sharing," *IEEE Trans. Power Del.*, vol. 34, no. 1, pp. 169-176, Feb. 2019.
- [62] X. Meng, J. Han, L. M. Bieber, L. Wang, W. Li and J. Belanger, "A universal blocking-module-based average value model of modular multilevel converters with different types of submodules," *IEEE Trans. Energy Convers.*, vol. 35, no. 1, pp. 53-66, March 2020, doi: 10.1109/TEC.2019.2944332.
- [63] W. Wang, Y. Li, Y. Cao, U. Häger, and C. Rehtanz, "Adaptive droop control of VSC-MTDC system for frequency support and power sharing," *IEEE Trans. Power Syst.* vol. 33, no. 2, pp. 1264-1274, 2018.
- [64] V. Nasirian, S. Moayedi, A. Davoudi, and F. L. Lewis, “Distributed cooperative control of DC microgrids,” *IEEE Trans. Power Electron.*, vol. 30, no. 4, pp. 2288–2303, Apr. 2015.
- [65] K. Rouzbehi, A. Miranian, A. Luna, and P. Rodriguez, “DC voltage control and power sharing in multiterminal DC grids based on optimal DC power flow and voltage-droop strategy,” *IEEE J. Emerg. Sel. Topics Power Electron.*, vol. 2, no. 4, pp. 1171–1180, Dec. 2014.
- [66] S. Boyd and L. Vandenberghe, *Convex Optimization*. Cambridge, MA: Cambridge Univ. Press, 2004.